Processes at solid surfaces

25

In this chapter we see how solids grow at their surfaces and how the details of the structure and composition of solid surfaces can be determined experimentally. A major part of the material concerns the extent to which a surface is covered and the variation of the extent of coverage with the pressure and temperature. This material is used to discuss how surfaces affect the rate and course of chemical change by acting as the site of catalysis. Reactions at surfaces include the processes that lie at the heart of electrochemistry. Therefore, we revisit in this chapter some of the topics treated in Chapter 7, but focus on the dynamics of electrode processes rather than the equilibrium properties treated there. Finally, we analyse the kinetics of reactions that are responsible for power production in fuel cells and for corrosion.

Processes at solid surfaces govern the viability of industry both constructively, as in catalysis, and destructively, as in corrosion. Chemical reactions at solid surfaces may differ sharply from reactions in the bulk, for reaction pathways of much lower activation energy may be provided, and hence result in catalysis. The concept of a solid surface has been extended in recent years with the availability of microporous materials as catalysts.

An important kinetic problem examined in this chapter is the rate at which oxidizable or reducible species—in short, **electroactive species**—can donate or accept electrons on the surfaces of electrodes. In Chapter 24 we explored the dynamics of electron transfer in homogeneous systems. In heterogeneous systems, the rates of processes that occur at the interface between the phases, such as an electrode immersed in an ionic solution, are very important. A measure of this rate is the **current density**, j, the charge flux through a region (the electric current divided by the area of the region). We shall discuss the properties that control the current density and its consequences.

We shall see that acronyms are widely used in surface studies; for convenience, a list of the acronyms used in this chapter is given in Table 25.7 at the end of the chapter.

The growth and structure of solid surfaces

In this section we see how surfaces are extended and crystals grow. The attachment of particles to a surface is called **adsorption**. The substance that adsorbs is the **adsorbate** and the underlying material that we are concerned with in this section is the **adsorbent** or **substrate**. The reverse of adsorption is **desorption**.

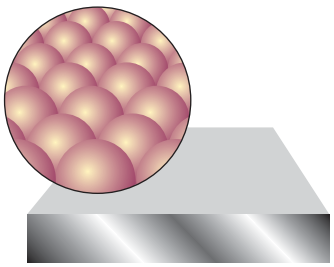

Fig. 25.1 A schematic diagram of the flat surface of a solid. This primitive model is largely supported by scanning tunnelling microscope images (see *Impact* I9.1).

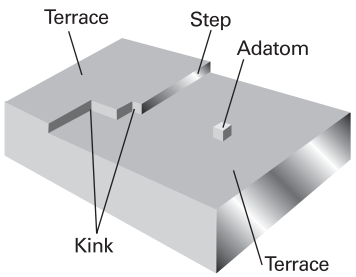

Fig. 25.2 Some of the kinds of defects that may occur on otherwise perfect terraces. Defects play an important role in surface growth and catalysis.

25.1 Surface growth

A simple picture of a perfect crystal surface is as a tray of oranges in a grocery store (Fig. 25.1). A gas molecule that collides with the surface can be imagined as a ping-pong ball bouncing erratically over the oranges. The molecule loses energy as it bounces, but it is likely to escape from the surface before it has lost enough kinetic energy to be trapped. The same is true, to some extent, of an ionic crystal in contact with a solution. There is little energy advantage for an ion in solution to discard some of its solvating molecules and stick at an exposed position on the surface.

The picture changes when the surface has defects, for then there are ridges of incomplete layers of atoms or ions. A common type of surface defect is a **step** between two otherwise flat layers of atoms called **terraces** (Fig. 25.2). A step defect might itself have defects, for it might have kinks. When an atom settles on a terrace it bounces across it under the influence of the intermolecular potential, and might come to a step or a corner formed by a kink. Instead of interacting with a single terrace atom, the molecule now interacts with several, and the interaction may be strong enough to trap it. Likewise, when ions deposit from solution, the loss of the solvation interaction is offset by a strong Coulombic interaction between the arriving ions and several ions at the surface defect.

Not all kinds of defect result in sustained surface growth. As the process of settling into ledges and kinks continues, there comes a stage when an entire lower terrace has been covered. At this stage the surface defects have been eliminated, and growth will cease. For continuing growth, a surface defect is needed that propagates as the crystal grows. We can see what form of defect this must be by considering the types of **dislocations**, or discontinuities in the regularity of the lattice, that exist in the bulk of a crystal. One reason for their formation may be that the crystal grows so quickly that its particles do not have time to settle into states of lowest potential energy before being trapped in position by the deposition of the next layer.

A special kind of dislocation is the **screw dislocation** shown in Fig. 25.3. Imagine a cut in the crystal, with the atoms to the left of the cut pushed up through a distance of one unit cell. The unit cells now form a continuous spiral around the end of the cut, which is called the **screw axis**. A path encircling the screw axis spirals up to the top of the crystal, and where the dislocation breaks through to the surface it takes the form of a spiral ramp.

The surface defect formed by a screw dislocation is a step, possibly with kinks, where growth can occur. The incoming particles lie in ranks on the ramp, and successive ranks reform the step at an angle to its initial position. As deposition continues the step rotates around the screw axis and is not eliminated. Growth may therefore continue indefinitely. Several layers of deposition may occur, and the edges of the spirals might be cliffs several atoms high. Propagating spiral edges can also give rise to flat terraces (Fig. 25.4). Terraces are formed if growth occurs simultaneously at neighbouring left- and right-handed screw dislocations (Fig. 25.5). Successive tables of atoms may form as counter-rotating defects collide on successive circuits, and the terraces formed may then fill up by further deposition at their edges to give flat crystal planes.

The rapidity of growth depends on the crystal plane concerned, and the slowest growing faces dominate the appearance of the crystal. This feature is explained in Fig. 25.6, where we see that, although the horizontal face grows forward most rapidly, it grows itself out of existence, and the slower-growing faces survive.

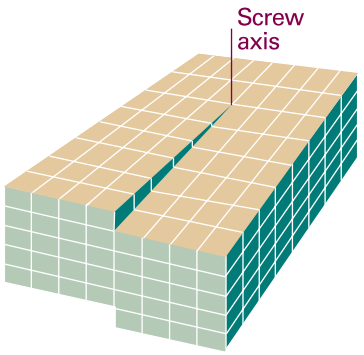

Fig. 25.3 A screw dislocation occurs where one region of the crystal is pushed up through one or more unit cells relative to another region. The cut extends to the screw axis. As atoms lie along the step the dislocation rotates round the screw axis and is not annihilated.

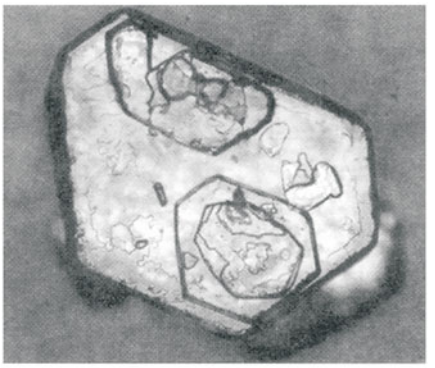

Fig. 25.4 The spiral growth pattern is sometimes concealed because the terraces are subsequently completed by further deposition. This accounts for the appearance of this cadmium iodide crystal. (H.M. Rosenberg, *The solid state*. Clarendon Press, Oxford (1978).)

25.2 Surface composition

Under normal conditions, a surface exposed to a gas is constantly bombarded with molecules and a freshly prepared surface is covered very quickly. Just how quickly can be estimated using the kinetic model of gases and the expression (eqn 21.14) for the collision flux:

$$Z_W = \frac{p}{(2\pi mkT)^{1/2}} \qquad (25.1a)$$

A practical form of this equation is

$$Z_W = \frac{Z_0(p/\text{Pa})}{\{(T/\text{K})(M/(\text{g mol}^{-1})\}^{1/2}} \quad \text{with} \quad Z_0 = 2.63 \times 10^{24}\ \text{m}^{-2}\ \text{s}^{-1} \qquad (25.1b)$$

where M is the molar mass of the gas. For air ($M \approx 29$ g mol^{-1}) at 1 atm and 25°C the collision flux is 3×10^{27} m^{-2} s^{-1}. Because 1 m^2 of metal surface consists of about 10^{19} atoms, each atom is struck about 10^8 times each second. Even if only a few collisions leave a molecule adsorbed to the surface, the time for which a freshly prepared surface remains clean is very short.

The obvious way to retain cleanliness is to reduce the pressure. When it is reduced to 10^{-4} Pa (as in a simple vacuum system) the collision flux falls to about 10^{18} m^{-2} s^{-1}, corresponding to one hit per surface atom in each 0.1 s. Even that is too brief in most experiments, and in **ultrahigh vacuum** (UHV) techniques pressures as low as 10^{-7} Pa (when $Z_W = 10^{15}$ m^{-2} s^{-1}) are reached on a routine basis and as low as 10^{-9} Pa (when $Z_W = 10^{13}$ m^{-2} s^{-1}) are reached with special care. These collision fluxes correspond to each surface atom being hit once every 10^5 to 10^6 s, or about once a day.

The layout of a typical UHV apparatus is such that the whole of the evacuated part can be heated to 150–250°C for several hours to drive gas molecules from the walls. All the taps and seals are usually of metal so as to avoid contamination from greases. The sample is usually in the form of a thin foil, a filament, or a sharp point. Where there is interest in the role of specific crystal planes the sample is a single crystal with a freshly cleaved face. Initial surface cleaning is achieved either by heating it electrically or by

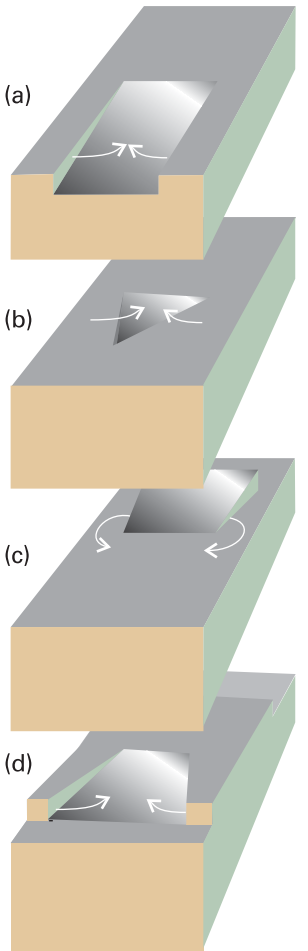

Fig. 25.5 Counter-rotating screw dislocations on the same surface lead to the formation of terraces. Four stages of one cycle of growth are shown here. Subsequent deposition can complete each terrace.

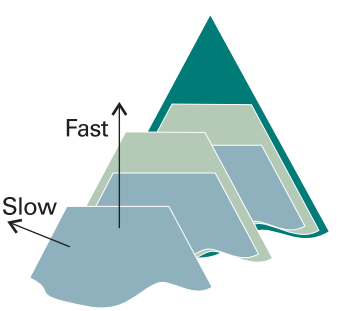

Fig. 25.6 The slower-growing faces of a crystal dominate its final external appearance. Three successive stages of the growth are shown.

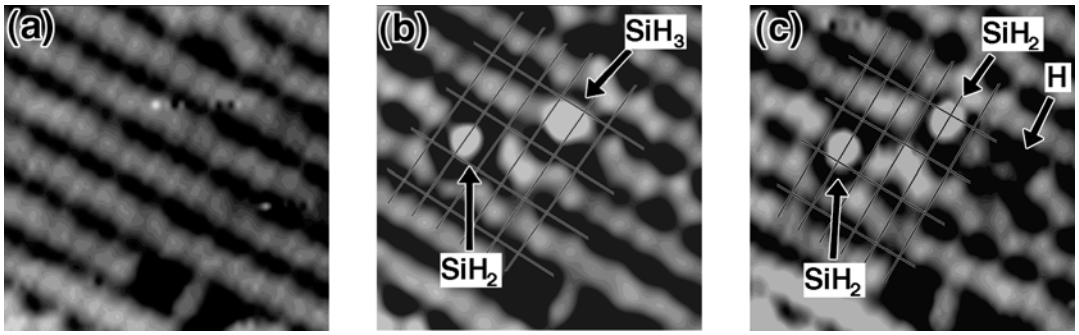

Fig. 25.7 Visualization by STM of the reaction $SiH_3 \rightarrow SiH_2 + H$ on a 4.7 nm × 4.7 nm area of a Si(001) surface. (a) The Si(001) surface before exposure to Si_2H_6(g). (b) Adsorbed Si_2H_6 dissociates into SiH_2(surface), on the left of the image, and SiH_3(surface), on the right. (c) After 8 min, SiH_3(surface) dissociates to SiH_2(surface) and H(surface). (Reproduced with permission from Y. Wang, M.J. Bronikowski, and R.J. Hamers, *Surface Science* **64**, 311 (1994).)

bombarding it with accelerated gaseous ions. The latter procedure demands care because ion bombardment can shatter the surface structure and leave it an amorphous jumble of atoms. High temperature annealing is then required to return the surface to an ordered state.

We have already discussed three important techniques for the characterization of surfaces: scanning electron microscopy (*Impact* I8.1), which is often used to observe terraces, steps, kinks, and dislocations on a surface, and scanning probe microscopy (*Impact* I9.1), which reveals the atomic details of structure of the surface and of adsorbates and can be used to visualize chemical reactions as they happen on surfaces (Fig. 25.7). In the following sections, we describe additional techniques that comprise the toolbox of a surface scientist.

(a) Ionization techniques

Surface composition can be determined by a variety of ionization techniques. The same techniques can be used to detect any remaining contamination after cleaning and to detect layers of material adsorbed later in the experiment. Their common feature is that the **escape depth** of the electrons, the maximum depth from which ejected electrons come, is in the range 0.1–1.0 nm, which ensures that only surface species contribute.

One technique that may be used is photoelectron spectroscopy (Section 11.4), which in surface studies is normally called **photoemission spectroscopy**. X-rays or hard ultraviolet ionizing radiation of energy in the range 5–40 eV may be used, giving rise to the techniques denoted XPS and UPS, respectively.

In XPS, the energy of the incident photon is so great that electrons are ejected from inner cores of atoms. As a first approximation, core ionization energies are insensitive to the bonds between atoms because they are too tightly bound to be greatly affected by the changes that accompany bond formation, so core ionization energies are characteristic of the individual atom. Consequently, XPS gives lines characteristic of the elements present on a surface. For instance, the *K*-shell ionization energies of the second row elements are

Li	Be	B	C	N	O	F
50	110	190	280	400	530	690 eV

Detection of one of these values (and values corresponding to ejection from other inner shells) indicates the presence of the corresponding element (Fig. 25.8). This

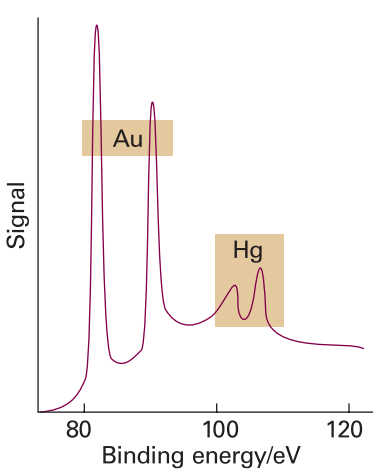

Fig. 25.8 The X-ray photoelectron emission spectrum of a sample of gold contaminated with a surface layer of mercury. (M.W. Roberts and C.S. McKee, *Chemistry of the metal–gas interface*, Oxford (1978).)

application is responsible for the alternative name **electron spectroscopy for chemical analysis** (ESCA). The technique is very useful for studying the surface state of heterogeneous catalysts, the differences between surface and bulk structures, and the processes that can cause damage to high-temperature superconductors and semiconductor wafers.

UPS, which examines electrons ejected from valence shells, is more suited to establishing the bonding characteristics and the details of valence shell electronic structures of substances on the surface. Its usefulness is its ability to reveal which orbitals of the adsorbate are involved in the bond to the substrate. For instance, the principal difference between the photoemission results on free benzene and benzene adsorbed on palladium is in the energies of the π electrons. This difference is interpreted as meaning that the C_6H_6 molecules lie parallel to the surface and are attached to it by their π orbitals.

In **secondary-ion mass spectrometry** (SIMS), the surface is ionized by bombardment with other ions and the secondary ions that emerge from the surface are detected by a mass spectrometer. Among the advantages of SIMS are the ability to detect adsorbed H and He atoms, which are not easily probed by XPS, and the high sensitivity of the mass spectrometer detector. A disadvantage is that SIMS analysis erodes the part of the sample that is bombarded. However, it is possible to control the degree of erosion to one or two monolayers by controlling the bombardment parameters.

(b) Vibrational spectroscopy

Several kinds of vibrational spectroscopy have been developed to study adsorbates and to show whether dissociation has occurred. Measurement of transmitted radiation is not practical in surfaces, which are typically too opaque to infrared or visible radiation. One technique that circumvents this problem is **reflection–absorption infrared spectroscopy** (RAIRS), in which the Fourier-transform IR absorption spectrum of the adsorbate is obtained by comparing the intensity of the incident infrared beam with the intensity of infrared radiation reflected by the surface.

Raman spectroscopy is better suited for studies of surfaces because it involves the detection of scattered radiation, but spectral bands are typically very weak. However, **surface-enhanced Raman scattering** (SERS) is viable for surface studies: the strong enhancement of the Raman spectrum of the adsorbate can increase intensities by a factor as big as 10^6. The effect is due in part to local accumulations of electron density at the features of the roughened surface and at regions where bonding occurs. The SERS effect is also observed when molecules adsorb to colloidal particles of gold and silver, with the surface of the colloid fostering the enhancement of the Raman spectrum. Disadvantages of SERS include weak enhancement observed on flat single crystal surfaces and the fact that the technique works for only certain metals.

(c) Electron spectroscopy

A hybrid version of photoemission spectroscopy and vibrational spectroscopy is **electron energy loss spectroscopy** (EELS, or HREELS, where HR denotes high resolution) in which the energy loss suffered by a beam of electrons is monitored when they are reflected from a surface. As in Raman spectroscopy, the spectrum of energy loss can be interpreted in terms of the vibrational spectrum of the adsorbate. High resolution and sensitivity are attainable, and the technique is sensitive to light elements (to which X-ray techniques are insensitive). Very tiny amounts of adsorbate can be detected, and one report estimated that about 48 atoms of phosphorus were detected in one sample. As an example, Fig. 25.9 shows the EELS result for CO on the (111) face of a platinum crystal as the extent of surface coverage increases. The main peak arises

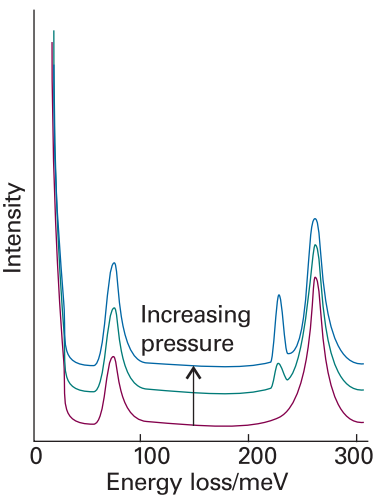

Fig. 25.9 The electron energy loss spectrum of CO adsorbed on Pt(111). The results for three different pressures are shown, and the growth of the additional peak at about 200 meV (1600 cm^{-1}) should be noted. (Based on spectra provided by Professor H. Ibach.)

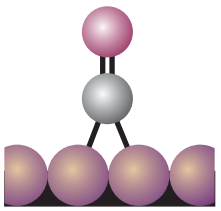

1 Bridge site

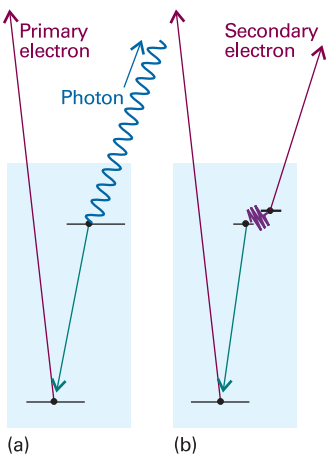

Fig. 25.10 When an electron is expelled from a solid (a) an electron of higher energy may fall into the vacated orbital and emit an X-ray photon to produce X-ray fluorescence. Alternatively, (b) the electron falling into the orbital may give up its energy to another electron, which is ejected in the Auger effect.

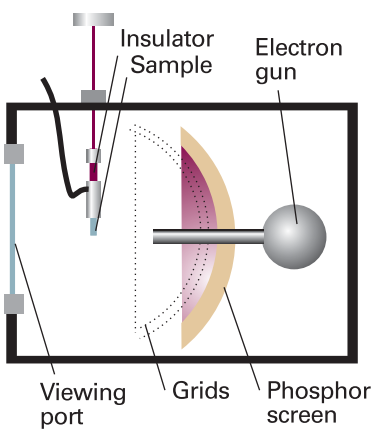

Fig. 25.11 A schematic diagram of the apparatus used for a LEED experiment. The electrons diffracted by the surface layers are detected by the fluorescence they cause on the phosphor screen.

from CO attached perpendicular to the surface by a single Pt atom. As the coverage increases the neighbouring smaller peak increases in intensity. This peak is due to CO at a bridge site, attached to two Pt atoms, as in (**1**).

A very important technique, which is widely used in the microelectronics industry, is **Auger electron spectroscopy** (AES). The **Auger effect** is the emission of a second electron after high energy radiation has expelled another. The first electron to depart leaves a hole in a low-lying orbital, and an upper electron falls into it. The energy this releases may result either in the generation of radiation, which is called **X-ray fluorescence** (Fig. 25.10a) or in the ejection of another electron (Fig. 25.10b). The latter is the secondary electron of the Auger effect. The energies of the secondary electrons are characteristic of the material present, so the Auger effect effectively takes a fingerprint of the sample. In practice, the Auger spectrum is normally obtained by irradiating the sample with an electron beam of energy in the range 1–5 keV rather than electromagnetic radiation. In **scanning Auger electron microscopy** (SAM), the finely focused electron beam is scanned over the surface and a map of composition is compiled; the resolution can reach below about 50 nm.

(d) Surface-extended X-ray absorption fine structure spectroscopy

The technique known as **surface-extended X-ray absorption fine structure spectroscopy** (SEXAFS) uses intense X-radiation from synchrotron sources (*Further information* 13.1). Oscillations in X-ray absorbance are observed on the high-frequency side of the absorption edge (the start of an X-ray absorption band) of a substance. These oscillations arise from a quantum mechanical interference between the wavefunction of a photoejected electron and parts of that electron's wavefunction that are scattered by neighbouring atoms. If the waves interfere destructively, then the photoelectron appears with lower probability and the X-ray absorption is correspondingly less. If the waves interfere constructively, then the photoelectron amplitude is higher, and the photoelectron has a higher probability of appearing; correspondingly, the X-ray absorption is greater. The oscillations therefore contain information about the number and distances of the neighbouring atoms. Such studies show that a solid's surface is much more plastic than had previously been thought, and that it undergoes **reconstruction**, or structural modification, in response to adsorbates that are present.

(e) Low-energy electron diffraction

One of the most informative techniques for determining the arrangement of the atoms close to the surface is **low energy electron diffraction** (LEED). This technique is like X-ray diffraction (Chapter 20) but uses the wave character of electrons, and the sample is now the surface of a solid. The use of low energy electrons (with energies in the range 10–200 eV, corresponding to wavelengths in the range 100–400 pm) ensures that the diffraction is caused only by atoms on and close to the surface. The experimental arrangement is shown in Fig. 25.11, and typical LEED patterns, obtained by photographing the fluorescent screen through the viewing port, are shown in Fig. 25.12.

A LEED pattern portrays the two-dimensional structure of the surface. By studying how the diffraction intensities depend on the energy of the electron beam it is also possible to infer some details about the vertical location of the atoms and to measure the thickness of the surface layer, but the interpretation of LEED data is much more complicated than the interpretation of bulk X-ray data. The pattern is sharp if the surface is well-ordered for distances long compared with the wavelength of the incident electrons. In practice, sharp patterns are obtained for surfaces ordered to depths of about 20 nm and more. Diffuse patterns indicate either a poorly ordered surface or the presence of impurities. If the LEED pattern does not correspond to the pattern

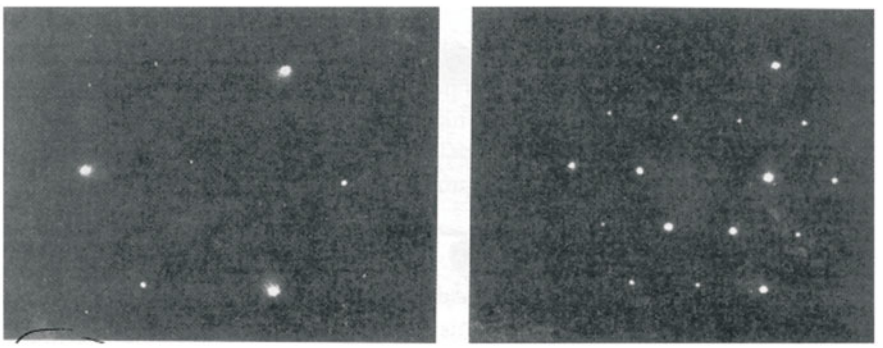

Fig. 25.12 LEED photographs of (a) a clean platinum surface and (b) after its exposure to propyne, $CH_3C{\equiv}CH$. (Photographs provided by Professor G.A. Somorjai.)

expected by extrapolation of the bulk surface to the surface, then either a reconstruction of the surface has occurred or there is order in the arrangement of an adsorbed layer.

The results of LEED experiments show that the surface of a crystal rarely has exactly the same form as a slice through the bulk. As a general rule, it is found that metal surfaces are simply truncations of the bulk lattice, but the distance between the top layer of atoms and the one below is contracted by around 5 per cent. Semiconductors generally have surfaces reconstructed to a depth of several layers. Reconstruction occurs in ionic solids. For example, in lithium fluoride the Li^+ and F^- ions close to the surface apparently lie on slightly different planes. An actual example of the detail that can now be obtained from refined LEED techniques is shown in Fig. 25.13 for $CH_3C{-}$ adsorbed on a (111) plane of rhodium.

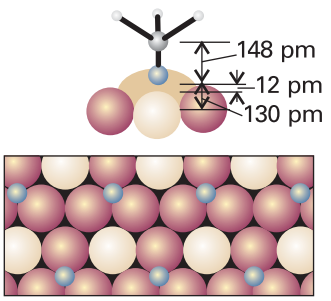

Fig. 25.13 The structure of a surface close to the point of attachment of $CH_3C{-}$ to the (110) surface of rhodium at 300 K and the changes in positions of the metal atoms that accompany chemisorption.

The presence of terraces, steps, and kinks in a surface shows up in LEED patterns, and their surface density (the number of defects in a region divided by the area of the region) can be estimated. The importance of this type of measurement will emerge later. Three examples of how steps and kinks affect the pattern are shown in Fig. 25.14. The samples used were obtained by cleaving a crystal at different angles to a plane of

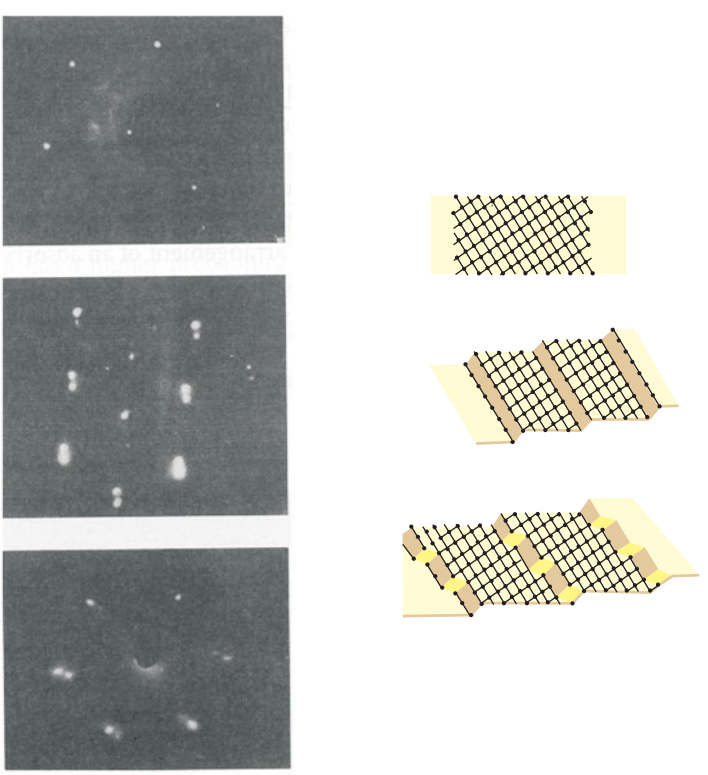

Fig. 25.14 LEED patterns may be used to assess the defect density of a surface. The photographs correspond to a platinum surface with (top) low defect density, (middle) regular steps separated by about six atoms, and (bottom) regular steps with kinks. (Photographs provided by Professor G.A. Samorjai.)

atoms. Only terraces are produced when the cut is parallel to the plane, and the density of steps increases as the angle of the cut increases. The observation of additional structure in the LEED patterns, rather than blurring, shows that the steps are arrayed regularly.

(f) Molecular beam techniques

Whereas many important studies have been carried out simply by exposing a surface to a gas, modern work is increasingly making use of **molecular beam scattering** (MBS). One advantage is that the activity of specific crystal planes can be investigated by directing the beam on to an orientated surface with known step and kink densities (as measured by LEED). Furthermore, if the adsorbate reacts at the surface the products (and their angular distributions) can be analysed as they are ejected from the surface and pass into a mass spectrometer. Another advantage is that the time of flight of a particle may be measured and interpreted in terms of its residence time on the surface. In this way a very detailed picture can be constructed of the events taking place during reactions at surfaces.

The extent of adsorption

The extent of surface coverage is normally expressed as the **fractional coverage**, θ:

$$\theta = \frac{\text{number of adsorption sites occupied}}{\text{number of adsorption sites available}} \qquad [25.2]$$

The fractional coverage is often expressed in terms of the volume of adsorbate adsorbed by $\theta = V/V_\infty$, where V_∞ is the volume of adsorbate corresponding to complete monolayer coverage. The **rate of adsorption**, $\mathrm{d}\theta/\mathrm{d}t$, is the rate of change of surface coverage, and can be determined by observing the change of fractional coverage with time.

Among the principal techniques for measuring $\mathrm{d}\theta/\mathrm{d}t$ are flow methods, in which the sample itself acts as a pump because adsorption removes particles from the gas. One commonly used technique is therefore to monitor the rates of flow of gas into and out of the system: the difference is the rate of gas uptake by the sample. Integration of this rate then gives the fractional coverage at any stage. In **flash desorption** the sample is suddenly heated (electrically) and the resulting rise of pressure is interpreted in terms of the amount of adsorbate originally on the sample. The interpretation may be confused by the desorption of a compound (for example, WO_3 from oxygen on tungsten). **Gravimetry**, in which the sample is weighed on a microbalance during the experiment, can also be used. A common instrument for gravimetric measurements is the **quartz crystal microbalance** (QCM), in which the mass of a sample laid on the surface of a quartz crystal is related to changes in the latter's mechanical properties. The key principle behind the operation of a QCM is the ability of a quartz crystal to vibrate at a characteristic frequency when an oscillating electric field is applied. The vibrational frequency decreases when material is spread over the surface of the crystal and the change in frequency is proportional to the mass of material. Masses as small as a few nanograms ($1\ \mathrm{ng} = 10^{-9}\ \mathrm{g}$) can be measured reliably in this way.

25.3 Physisorption and chemisorption

Molecules and atoms can attach to surfaces in two ways. In **physisorption** (an abbreviation of 'physical adsorption'), there is a van der Waals interaction (for example, a dispersion or a dipolar interaction) between the adsorbate and the substrate. Van der Waals interactions have a long range but are weak, and the energy released when a

particle is physisorbed is of the same order of magnitude as the enthalpy of condensation. Such small energies can be absorbed as vibrations of the lattice and dissipated as thermal motion, and a molecule bouncing across the surface will gradually lose its energy and finally adsorb to it in the process called **accommodation**. The enthalpy of physisorption can be measured by monitoring the rise in temperature of a sample of known heat capacity, and typical values are in the region of 20 kJ mol^{-1} (Table 25.1). This small enthalpy change is insufficient to lead to bond breaking, so a physisorbed molecule retains its identity, although it might be distorted by the presence of the surface.

In **chemisorption** (an abbreviation of 'chemical adsorption'), the molecules (or atoms) stick to the surface by forming a chemical (usually covalent) bond, and tend to find sites that maximize their coordination number with the substrate. The enthalpy of chemisorption is very much greater than that for physisorption, and typical values are in the region of 200 kJ mol^{-1} (Table 25.2). The distance between the surface and the closest adsorbate atom is also typically shorter for chemisorption than for physisorption. A chemisorbed molecule may be torn apart at the demand of the unsatisfied valencies of the surface atoms, and the existence of molecular fragments on the surface as a result of chemisorption is one reason why solid surfaces catalyse reactions.

Except in special cases, chemisorption must be exothermic. A spontaneous process requires $\Delta G < 0$. Because the translational freedom of the adsorbate is reduced when it is adsorbed, ΔS is negative. Therefore, in order for $\Delta G = \Delta H - T\Delta S$ to be negative, ΔH must be negative (that is, the process is exothermic). Exceptions may occur if the adsorbate dissociates and has high translational mobility on the surface. For example, H_2 adsorbs endothermically on glass because there is a large increase of translational entropy accompanying the dissociation of the molecules into atoms that move quite freely over the surface. In its case, the entropy change in the process $H_2(g) \rightarrow 2\,H(glass)$ is sufficiently positive to overcome the small positive enthalpy change.

The enthalpy of adsorption depends on the extent of surface coverage, mainly because the adsorbate particles interact. If the particles repel each other (as for CO on palladium) the adsorption becomes less exothermic (the enthalpy of adsorption less negative) as coverage increases. Moreover, LEED studies show that such species settle on the surface in a disordered way until packing requirements demand order. If the adsorbate particles attract one another (as for O_2 on tungsten), then they tend to cluster together in islands, and growth occurs at the borders. These adsorbates also show order–disorder transitions when they are heated enough for thermal motion to overcome the particle–particle interactions, but not so much that they are desorbed.

Synoptic table 25.1* Maximum observed enthalpies of physisorption

Adsorbate	$\Delta_{ad}H^{\ominus}$/(kJ mol^{-1})
CH_4	−21
H_2	−84
H_2O	−59
N_2	−21

* More values are given in the *Data section*.

Synoptic table 25.2* Enthalpies of chemisorption, $\Delta_{ad}H^{\ominus}$/(kJ mol^{-1})

Adsorbate	Adsorbent (substrate)		
	Cr	Fe	Ni
CH_4	−427	−285	−243
CO		−192	
H_2	−188	−134	
NH_3		−188	−155

* More values are given in the *Data section*.

25.4 Adsorption isotherms

The free gas and the adsorbed gas are in dynamic equilibrium, and the fractional coverage of the surface depends on the pressure of the overlying gas. The variation of θ with pressure at a chosen temperature is called the **adsorption isotherm**.

(a) The Langmuir isotherm

The simplest physically plausible isotherm is based on three assumptions:

1 Adsorption cannot proceed beyond monolayer coverage.

2 All sites are equivalent and the surface is uniform (that is, the surface is perfectly flat on a microscopic scale).

3 The ability of a molecule to adsorb at a given site is independent of the occupation of neighbouring sites (that is, there are no interactions between adsorbed molecules).

The dynamic equilibrium is

$$A(g) + M(surface) \rightleftharpoons AM(surface)$$

with rate constants k_a for adsorption and k_d for desorption. The rate of change of surface coverage due to adsorption is proportional to the partial pressure p of A and the number of vacant sites $N(1-\theta)$, where N is the total number of sites:

$$\frac{d\theta}{dt} = k_a pN(1-\theta) \tag{25.3a}$$

The rate of change of θ due to desorption is proportional to the number of adsorbed species, $N\theta$:

$$\frac{d\theta}{dt} = -k_d N\theta \tag{25.3b}$$

At equilibrium there is no net change (that is, the sum of these two rates is zero), and solving for θ gives the **Langmuir isotherm**:

$$\theta = \frac{Kp}{1+Kp} \qquad K = \frac{k_a}{k_d} \tag{25.4}$$

Example 25.1 *Using the Langmuir isotherm*

The data given below are for the adsorption of CO on charcoal at 273 K. Confirm that they fit the Langmuir isotherm, and find the constant K and the volume corresponding to complete coverage. In each case V has been corrected to 1.00 atm (101.325 kPa).

p/kPa	13.3	26.7	40.0	53.3	66.7	80.0	93.3
V/cm^3	10.2	18.6	25.5	31.5	36.9	41.6	46.1

Method From eqn 25.4,

$$Kp\theta + \theta = Kp$$

With $\theta = V/V_\infty$, where V_∞ is the volume corresponding to complete coverage, this expression can be rearranged into

$$\frac{p}{V} = \frac{p}{V_\infty} + \frac{1}{KV_\infty}$$

Hence, a plot of p/V against p should give a straight line of slope $1/V_\infty$ and intercept $1/KV_\infty$.

Answer The data for the plot are as follows:

p/kPa	13.3	26.7	40.0	53.3	66.7	80.0	93.3
$(p/\text{kPa})/(V/\text{cm}^3)$	1.30	1.44	1.57	1.69	1.81	1.92	2.02

The points are plotted in Fig. 25.15. The (least squares) slope is 0.00900, so $V_\infty = 111$ cm^3. The intercept at $p = 0$ is 1.20, so

$$K = \frac{1}{(111\ \text{cm}^3) \times (1.20\ \text{kPa cm}^{-3})} = 7.51 \times 10^{-3}\ \text{kPa}^{-1}$$

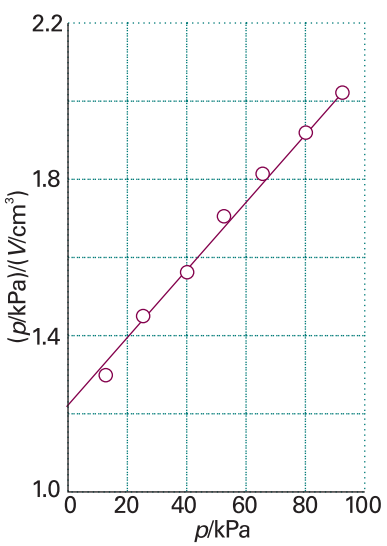

Fig. 25.15 The plot of the data in Example 25.1. As illustrated here, the Langmuir isotherm predicts that a straight line should be obtained when p/V is plotted against p.

Self-test 25.1 Repeat the calculation for the following data:

p/kPa	13.3	26.7	40.0	53.3	66.7	80.0	93.3
V/cm^3	10.3	19.3	27.3	34.1	40.0	45.5	48.0

[128 cm^3, 6.69×10^{-3} kPa^{-1}]

For adsorption with dissociation, the rate of adsorption is proportional to the pressure and to the probability that both atoms will find sites, which is proportional to the square of the number of vacant sites,

$$\frac{d\theta}{dt} = k_a p\{N(1-\theta)\}^2 \tag{25.5a}$$

The rate of desorption is proportional to the frequency of encounters of atoms on the surface, and is therefore second-order in the number of atoms present:

$$\frac{d\theta}{dt} = -k_d(N\theta)^2 \tag{25.5b}$$

The condition for no net change leads to the isotherm

$$\theta = \frac{(Kp)^{1/2}}{1+(Kp)^{1/2}} \tag{25.6}$$

The surface coverage now depends more weakly on pressure than for non-dissociative adsorption.

The shapes of the Langmuir isotherms with and without dissociation are shown in Figs. 25.16 and 25.17. The fractional coverage increases with increasing pressure, and approaches 1 only at very high pressure, when the gas is forced on to every available site of the surface. Different curves (and therefore different values of K) are obtained at different temperatures, and the temperature dependence of K can be used to determine the **isosteric enthalpy of adsorption**, $\Delta_{ad}H^{\ominus}$, the standard enthalpy of adsorption at a fixed surface coverage. To determine this quantity we recognize that K is essentially an equilibrium constant, and then use the van 't Hoff equation (eqn 7.23) to write:

$$\left(\frac{\partial \ln K}{\partial T}\right)_\theta = \frac{\Delta_{ad}H^{\ominus}}{RT^2} \tag{25.7}$$

Example 25.2 *Measuring the isosteric enthalpy of adsorption*

The data below show the pressures of CO needed for the volume of adsorption (corrected to 1.00 atm and 273 K) to be 10.0 cm^3 using the same sample as in Example 25.1. Calculate the adsorption enthalpy at this surface coverage.

T/K	200	210	220	230	240	250
p/kPa	4.00	4.95	6.03	7.20	8.47	9.85

Method The Langmuir isotherm can be rearranged to

$$Kp = \frac{\theta}{1-\theta}$$

Therefore, when θ is constant,

$$\ln K + \ln p = \text{constant}$$

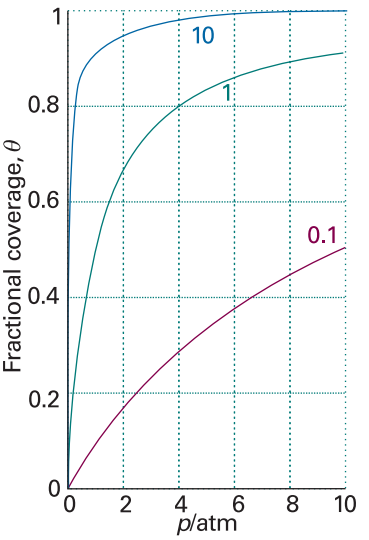

Fig. 25.16 The Langmuir isotherm for dissociative adsorption, $X_2(g) \rightarrow 2\,X(surface)$, for different values of K.

Exploration Using eqn 25.4, generate a family of curves showing the dependence of $1/\theta$ on $1/p$ for several valuesof K.

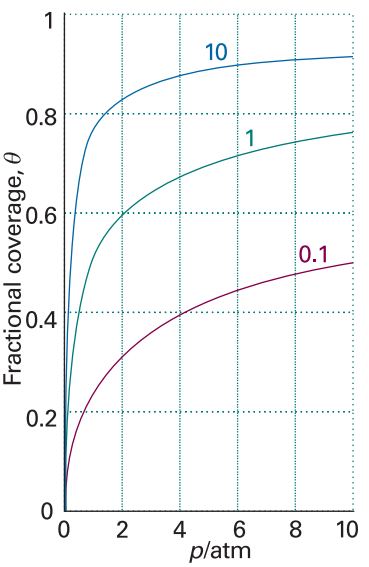

Fig. 25.17 The Langmuir isotherm for non-dissociative adsorption for different values of K.

Exploration Using eqn 25.6, generate a family of curves showing the dependence of $1/\theta$ on $1/p$ for several valuesof K. Taking these results together with those of the previous *Exploration*, discuss how plots of $1/\theta$ against $1/p$ can be used to distinguish between adsorption with and without dissociation.

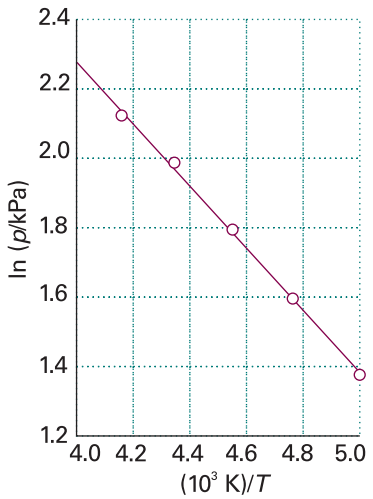

Fig. 25.18 The isosteric enthalpy of adsorption can be obtained from the slope of the plot of ln p against $1/T$, where p is the pressure needed to achieve the specified surface coverage. The data used are from Example 25.2.

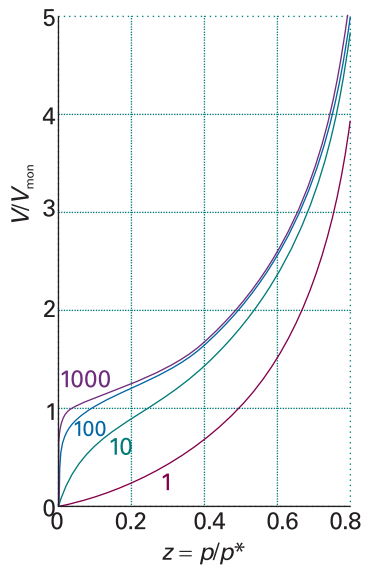

Fig. 25.19 Plots of the BET isotherm for different values of c. The value of V/V_{mon} rises indefinitely because the adsorbate may condense on the covered substrate surface.

Exploration Using eqn 25.8, generate a family of curves showing the dependence of $zV_{mon}/(1-z)V$ on z for different values of c.

It follows from eqn 25.7 that

$$\left(\frac{\partial \ln p}{\partial T}\right)_\theta = -\left(\frac{\partial \ln K}{\partial T}\right)_\theta = -\frac{\Delta_{ad}H^\ominus}{RT^2}$$

With $d(1/T)/dT = -1/T^2$, this expression rearranges to

$$\left(\frac{\partial \ln p}{\partial (1/T)}\right)_\theta = \frac{\Delta_{ad}H^\ominus}{R}$$

Therefore, a plot of ln p against $1/T$ should be a straight line of slope $\Delta_{ad}H^\ominus/R$.

Answer We draw up the following table:

T/K	200	210	220	230	240	250
$10^3/(T/\text{K})$	5.00	4.76	4.55	4.35	4.17	4.00
$\ln(p/\text{kPa})$	1.39	1.60	1.80	1.97	2.14	2.29

The points are plotted in Fig. 25.18. The slope (of the least squares fitted line) is −0.904, so

$$\Delta_{ad}H^\ominus = -(0.904 \times 10^3\ \text{K}) \times R = -7.52\ \text{kJ mol}^{-1}$$

The value of K can be used to obtain a value of $\Delta_{ad}G^\ominus$, and then that value combined with $\Delta_{ad}H^\ominus$ to obtain the standard entropy of adsorption. The expression for $(\partial \ln p/\partial T)_\theta$ in this example is independent of the model for the isotherm.

Self-test 25.2 Repeat the calculation using the following data:

T/K	200	210	220	230	240	250
p/kPa	4.32	5.59	7.07	8.80	10.67	12.80

[−9.0 kJ mol^{-1}]

(b) The BET isotherm

If the initial adsorbed layer can act as a substrate for further (for example, physical) adsorption, then, instead of the isotherm levelling off to some saturated value at high pressures, it can be expected to rise indefinitely. The most widely used isotherm dealing with multilayer adsorption was derived by Stephen Brunauer, Paul Emmett, and Edward Teller, and is called the **BET isotherm**:

$$\frac{V}{V_{mon}} = \frac{cz}{(1-z)\{1-(1-c)z\}} \qquad \text{with} \quad z = \frac{p}{p^\star} \tag{25.8}$$

In this expression, $p^\star$ is the vapour pressure above a layer of adsorbate that is more than one molecule thick and which resembles a pure bulk liquid, V_{mon} is the volume corresponding to monolayer coverage, and c is a constant which is large when the enthalpy of desorption from a monolayer is large compared with the enthalpy of vaporization of the liquid adsorbate:

$$c = e^{(\Delta_{des}H^\ominus - \Delta_{vap}H^\ominus)/RT} \tag{25.9}$$

Figure 25.19 illustrates the shapes of BET isotherms. They rise indefinitely as the pressure is increased because there is no limit to the amount of material that may condense when multilayer coverage may occur. A BET isotherm is not accurate at all pressures, but it is widely used in industry to determine the surface areas of solids.

Example 25.3 *Using the BET isotherm*

The data below relate to the adsorption of N_2 on rutile (TiO_2) at 75 K. Confirm that they fit a BET isotherm in the range of pressures reported, and determine V_{mon} and c.

p/kPa	0.160	1.87	6.11	11.67	17.02	21.92	27.29
V/mm^3	601	720	822	935	1046	1146	1254

At 75 K, $p^* = 76.0$ kPa. The volumes have been corrected to 1.00 atm and 273 K and refer to 1.00 g of substrate.

Method Equation 25.8 can be reorganized into

$$\frac{z}{(1-z)V} = \frac{1}{cV_{mon}} + \frac{(c-1)z}{cV_{mon}}$$

It follows that $(c-1)/cV_{mon}$ can be obtained from the slope of a plot of the expression on the left against z, and cV_{mon} can be found from the intercept at $z = 0$. The results can then be combined to give c and V_{mon}.

Answer We draw up the following table:

p/kPa	0.160	1.87	6.11	11.67	17.02	21.92	27.29
$10^3 z$	2.11	24.6	80.4	154	224	288	359
$10^4 z/(1-z)(V/\text{mm}^3)$	0.035	0.350	1.06	1.95	2.76	3.53	4.47

These points are plotted in Fig. 25.20. The least squares best line has an intercept at 0.0398, so

$$\frac{1}{cV_{mon}} = 3.98 \times 10^{-6}\ \text{mm}^{-3}$$

The slope of the line is 1.23×10^{-2}, so

$$\frac{c-1}{cV_{mon}} = (1.23 \times 10^{-2}) \times 10^3 \times 10^{-4}\ \text{mm}^{-3} = 1.23 \times 10^{-3}\ \text{mm}^{-3}$$

The solutions of these equations are $c = 310$ and $V_{mon} = 811$ mm^3. At 1.00 atm and 273 K, 811 mm^3 corresponds to 3.6×10^{-5} mol, or 2.2×10^{19} atoms. Because each atom occupies an area of about 0.16 nm^2, the surface area of the sample is about 3.5 m^2.

Self-test 25.3 Repeat the calculation for the following data:

p/kPa	0.160	1.87	6.11	11.67	17.02	21.92	27.29
V/cm^3	235	559	649	719	790	860	950

[370, 615 cm^3]

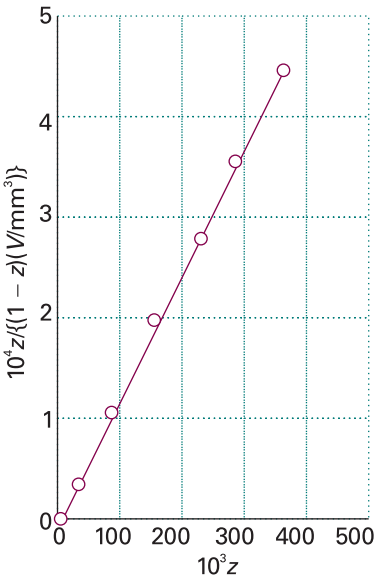

Fig. 25.20 The BET isotherm can be tested, and the parameters determined, by plotting $z/(1-z)V$ against $z = p/p^*$. The data are from Example 25.3.

When $c \gg 1$, the BET isotherm takes the simpler form

$$\frac{V}{V_{mon}} = \frac{1}{1-z} \qquad (25.10)$$

This expression is applicable to unreactive gases on polar surfaces, for which $c \approx 10^2$ because $\Delta_{des}H^\ominus$ is then significantly greater than $\Delta_{vap}H^\ominus$ (eqn 25.9). The BET isotherm

fits experimental observations moderately well over restricted pressure ranges, but it errs by underestimating the extent of adsorption at low pressures and by overestimating it at high pressures.

(c) Other isotherms

An assumption of the Langmuir isotherm is the independence and equivalence of the adsorption sites. Deviations from the isotherm can often be traced to the failure of these assumptions. For example, the enthalpy of adsorption often becomes less negative as θ increases, which suggests that the energetically most favourable sites are occupied first. Various attempts have been made to take these variations into account. The **Temkin isotherm**,

$$\theta = c_1 \ln(c_2 p) \tag{25.11}$$

where c_1 and c_2 are constants, corresponds to supposing that the adsorption enthalpy changes linearly with pressure. The **Freundlich isotherm**

$$\theta = c_1 p^{1/c_2} \tag{25.12}$$

corresponds to a logarithmic change. This isotherm attempts to incorporate the role of substrate–substrate interactions on the surface (see Problem 25.24).

Different isotherms agree with experiment more or less well over restricted ranges of pressure, but they remain largely empirical. Empirical, however, does not mean useless for, if the parameters of a reasonably reliable isotherm are known, reasonably reliable results can be obtained for the extent of surface coverage under various conditions. This kind of information is essential for any discussion of heterogeneous catalysis.

25.5 The rates of surface processes

The rates of surface processes may be studied by techniques described in Section 25.2 and *Impact* I25.1. Another technique, **second harmonic generation** (SHG), is very important for the study of all types of surfaces, including thin films and liquid–gas interfaces. We saw in Section 20.10 that second harmonic generation is the conversion of an intense, pulsed laser beam to radiation with twice its initial frequency as it passes though a material. In addition to a number of crystals, surfaces are also suitable materials for SHG. Because pulsed lasers are the excitation sources, time-resolved measurements of the kinetics and dynamics of surface processes are possible over timescales as short as femtoseconds.

Figure 25.21 shows how the potential energy of a molecule varies with its distance from the substrate surface. As the molecule approaches the surface its energy falls as it becomes physisorbed into the **precursor state** for chemisorption. Dissociation into fragments often takes place as a molecule moves into its chemisorbed state, and after an initial increase of energy as the bonds stretch there is a sharp decrease as the adsorbate–substrate bonds reach their full strength. Even if the molecule does not fragment, there is likely to be an initial increase of potential energy as the molecule approaches the surface and the bonds adjust.

In most cases, therefore, we can expect there to be a potential energy barrier separating the precursor and chemisorbed states. This barrier, though, might be low, and might not rise above the energy of a distant, stationary particle (as in Fig. 25.21a). In this case, chemisorption is not an activated process and can be expected to be rapid. Many gas adsorptions on clean metals appear to be non-activated. In some cases the barrier rises above the zero axis (as in Fig. 25.21b); such chemisorptions are activated and slower than the non-activated kind. An example is H_2 on copper, which has an activation energy in the region of 20–40 kJ mol^{-1}.

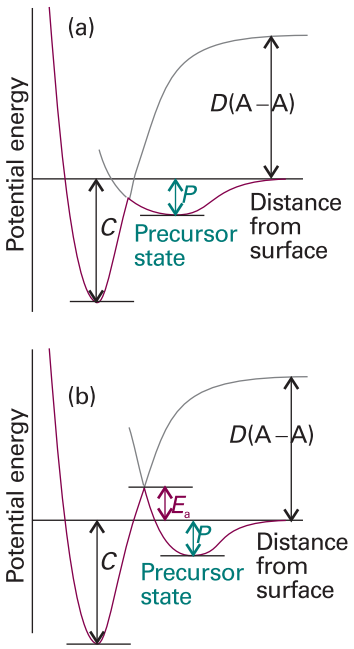

Fig. 25.21 The potential energy profiles for the dissociative chemisorption of an A_2 molecule. In each case, P is the enthalpy of (non-dissociative) physisorption and C that for chemisorption (at $T = 0$). The relative locations of the curves determines whether the chemisorption is (a) not activated or (b) activated.

One point that emerges from this discussion is that rates are not good criteria for distinguishing between physisorption and chemisorption. Chemisorption can be fast if the activation energy is small or zero, but it may be slow if the activation energy is large. Physisorption is usually fast, but it can appear to be slow if adsorption is taking place on a porous medium.

(a) The rate of adsorption

The rate at which a surface is covered by adsorbate depends on the ability of the substrate to dissipate the energy of the incoming particle as thermal motion as it crashes on to the surface. If the energy is not dissipated quickly, the particle migrates over the surface until a vibration expels it into the overlying gas or it reaches an edge. The proportion of collisions with the surface that successfully lead to adsorption is called the **sticking probability**, s:

$$s = \frac{\text{rate of adsorption of particles by the surface}}{\text{rate of collision of particles with the surface}} \qquad [25.13]$$

The denominator can be calculated from the kinetic model, and the numerator can be measured by observing the rate of change of pressure.

Values of s vary widely. For example, at room temperature CO has s in the range 0.1–1.0 for several d-metal surfaces, but for N_2 on rhenium $s < 10^{-2}$, indicating that more than a hundred collisions are needed before one molecule sticks successfully. Beam studies on specific crystal planes show a pronounced specificity: for N_2 on tungsten, s ranges from 0.74 on the (320) faces down to less than 0.01 on the (110) faces at room temperature. The sticking probability decreases as the surface coverage increases (Fig. 25.22). A simple assumption is that s is proportional to $1 - \theta$, the fraction uncovered, and it is common to write

$$s = (1 - \theta)s_0 \qquad (25.14)$$

where s_0 is the sticking probability on a perfectly clean surface. The results in the illustration do not fit this expression because they show that s remains close to s_0 until the coverage has risen to about 6×10^{13} molecules cm^{-2}, and then falls steeply. The explanation is probably that the colliding molecule does not enter the chemisorbed state at once, but moves over the surface until it encounters an empty site.

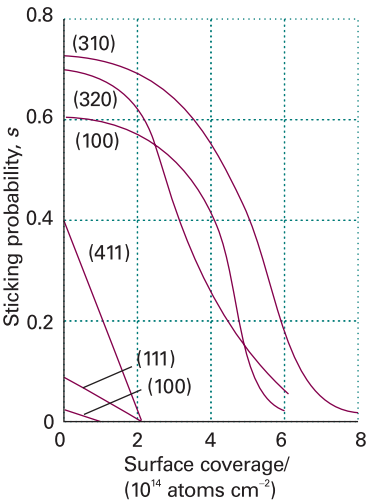

Fig. 25.22 The sticking probability of N_2 on various faces of a tungsten crystal and its dependence on surface coverage. Note the very low sticking probability for the (110) and (111) faces. (Data provided by Professor D.A. King.)

(b) The rate of desorption

Desorption is always activated because the particles have to be lifted from the foot of a potential well. A physisorbed particle vibrates in its shallow potential well, and might shake itself off the surface after a short time. The temperature dependence of the first-order rate of departure can be expected to be Arrhenius-like, with an activation energy for desorption, E_d, comparable to the enthalpy of physisorption:

$$k_d = Ae^{-E_d/RT} \qquad (25.15)$$

Therefore, the half-life for remaining on the surface has a temperature dependence

$$t_{1/2} = \frac{\ln 2}{k_d} = \tau_0 e^{E_d/RT} \qquad \tau_0 = \frac{\ln 2}{A} \qquad (25.16)$$

(Note the positive sign in the exponent.) If we suppose that $1/\tau_0$ is approximately the same as the vibrational frequency of the weak particle–surface bond (about 10^{12} Hz) and $E_d \approx 25$ kJ mol^{-1}, then residence half-lives of around 10 ns are predicted at room temperature. Lifetimes close to 1 s are obtained only by lowering the temperature to about 100 K. For chemisorption, with $E_d = 100$ kJ mol^{-1} and guessing that $\tau_0 = 10^{-14}$ s

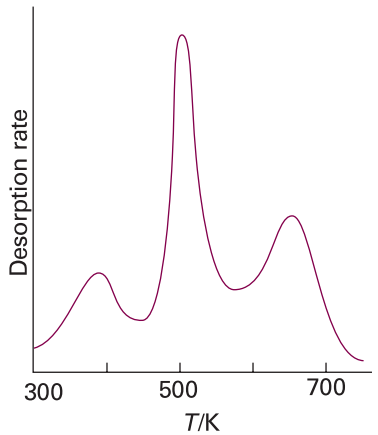

Fig. 25.23 The flash desorption spectrum of H_2 on the (100) face of tungsten. The three peaks indicate the presence of three sites with different adsorption enthalpies and therefore different desorption activation energies. (P.W. Tamm and L.D. Schmidt, *J. Chem. Phys.* **51**, 5352 (1969).)

(because the adsorbate–substrate bond is quite stiff), we expect a residence half-life of about 3×10^3 s (about an hour) at room temperature, decreasing to 1 s at about 350 K.

The desorption activation energy can be measured in several ways. However, we must be guarded in its interpretation because it often depends on the fractional coverage, and so may change as desorption proceeds. Moreover, the transfer of concepts such as 'reaction order' and 'rate constant' from bulk studies to surfaces is hazardous, and there are few examples of strictly first-order or second-order desorption kinetics (just as there are few integral-order reactions in the gas phase too).

If we disregard these complications, one way of measuring the desorption activation energy is to monitor the rate of increase in pressure when the sample is maintained at a series of temperatures, and to attempt to make an Arrhenius plot. A more sophisticated technique is **temperature programmed desorption** (TPD) or **thermal desorption spectroscopy** (TDS). The basic observation is a surge in desorption rate (as monitored by a mass spectrometer) when the temperature is raised linearly to the temperature at which desorption occurs rapidly, but once the desorption has occurred there is no more adsorbate to escape from the surface, so the desorption flux falls again as the temperature continues to rise. The TPD spectrum, the plot of desorption flux against temperature, therefore shows a peak, the location of which depends on the desorption activation energy. There are three maxima in the example shown in Fig. 25.23, indicating the presence of three sites with different activation energies.

In many cases only a single activation energy (and a single peak in the TPD spectrum) is observed. When several peaks are observed they might correspond to adsorption on different crystal planes or to multilayer adsorption. For instance, Cd atoms on tungsten show two activation energies, one of 18 kJ mol^{-1} and the other of 90 kJ mol^{-1}. The explanation is that the more tightly bound Cd atoms are attached directly to the substrate, and the less strongly bound are in a layer (or layers) above the primary overlayer. Another example of a system showing two desorption activation energies is CO on tungsten, the values being 120 kJ mol^{-1} and 300 kJ mol^{-1}. The explanation is believed to be the existence of two types of metal–adsorbate binding site, one involving a simple M—CO bond, the other adsorption with dissociation into individually adsorbed C and O atoms.

(b) Mobility on surfaces

A further aspect of the strength of the interactions between adsorbate and substrate is the mobility of the adsorbate. Mobility is often a vital feature of a catalyst's activity, because a catalyst might be impotent if the reactant molecules adsorb so strongly that they cannot migrate. The activation energy for diffusion over a surface need not be the same as for desorption because the particles may be able to move through valleys between potential peaks without leaving the surface completely. In general, the activation energy for migration is about 10–20 per cent of the energy of the surface–adsorbate bond, but the actual value depends on the extent of coverage. The defect structure of the sample (which depends on the temperature) may also play a dominant role because the adsorbed molecules might find it easier to skip across a terrace than to roll along the foot of a step, and these molecules might become trapped in vacancies in an otherwise flat terrace. Diffusion may also be easier across one crystal face than another, and so the surface mobility depends on which lattice planes are exposed.

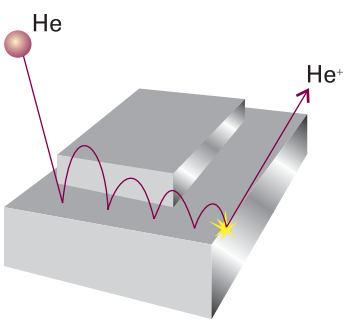

Fig. 25.24 The events leading to an FIM image of a surface. The He atom migrates across the surface until it is ionized at an exposed atom, when it is pulled off by the externally applied potential. (The bouncing motion is due to the intermolecular potential, not gravity!)

Diffusion characteristics of an adsorbate can be examined by using STM to follow the change in surface characteristics or by **field-ionization microscopy** (FIM), which portrays the electrical characteristics of a surface by using the ionization of noble gas atoms to probe the surface (Fig. 25.24). An individual atom is imaged, the temperature is raised, and then lowered after a definite interval. A new image is then recorded, and the new position of the atom measured (Fig. 25.25). A sequence of images shows

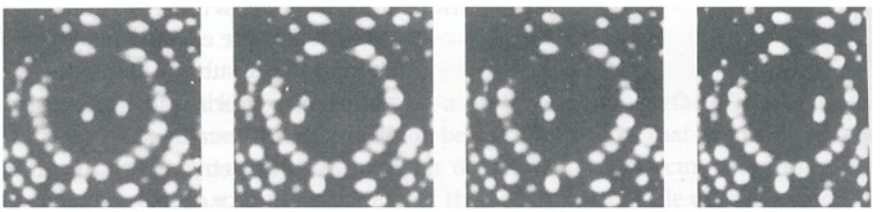

Fig. 25.25 FIM micrographs showing the migration of Re atoms on rhenium during 3 s intervals at 375 K. (Photographs provided by Professor G. Ehrlich.)

that the atom makes a random walk across the surface, and the diffusion coefficient, D, can be inferred from the mean distance, d, travelled in an interval τ by using the two-dimensional random walk expression $d = (D\tau)^{1/2}$. The value of D for different crystal planes at different temperatures can be determined directly in this way, and the activation energy for migration over each plane obtained from the Arrhenius-like expression

$$D = D_0 e^{-E_D/RT} \qquad (25.17)$$

where E_D is the activation energy for diffusion. Typical values for W atoms on tungsten have E_D in the range 57–87 kJ mol^{-1} and $D_0 \approx 3.8 \times 10^{-11}$ m^2 s^{-1}. For CO on tungsten, the activation energy falls from 144 kJ mol^{-1} at low surface coverage to 88 kJ mol^{-1} when the coverage is high.

IMPACT ON BIOCHEMISTRY

I25.1 Biosensor analysis

Biosensor analysis is a very sensitive and sophisticated optical technique that is now used routinely to measure the kinetics and thermodynamics of interactions between biopolymers. A biosensor detects changes in the optical properties of a surface in contact with a biopolymer.

The mobility of delocalized valence electrons accounts for the electrical conductivity of metals and these mobile electrons form a **plasma**, a dense gas of charged particles. Bombardment of the plasma by light or an electron beam can cause transient changes in the distribution of electrons, with some regions becoming slightly more dense than others. Coulomb repulsion in the regions of high density causes electrons to move away from each other, so lowering their density. The resulting oscillations in electron density, called **plasmons**, can be excited both in the bulk and on the surface of a metal. Plasmons in the bulk may be visualized as waves that propagate through the solid. A surface plasmon also propagates away from the surface, but the amplitude of the wave, also called an **evanescent wave**, decreases sharply with distance from the surface.

Biosensor analysis is based on the phenomenon of **surface plasmon resonance** (SPR), the absorption of energy from an incident beam of electromagnetic radiation by surface plasmons. Absorption, or 'resonance', can be observed with appropriate choice of the wavelength and angle of incidence of the excitation beam. It is common practice to use a monochromatic beam and to vary the angle of incidence θ (Fig. 25.26). The beam passes through a prism that strikes one side of a thin film of gold or silver. The angle corresponding to light absorption depends on the refractive index of the medium in direct contact with the opposing side of the metallic film. This variation of the resonance angle with the state of the surface arises from the ability of the evanescent wave to interact with material a short distance away from the surface.

As an illustration of biosensor analysis, we consider the association of two polymers, A and B. In a typical experiment, a stream of solution containing a known concentration of A flows above the surface to which B is chemisorbed. Figure 25.27 shows that the kinetics of binding of A to B may be followed by monitoring the time dependence

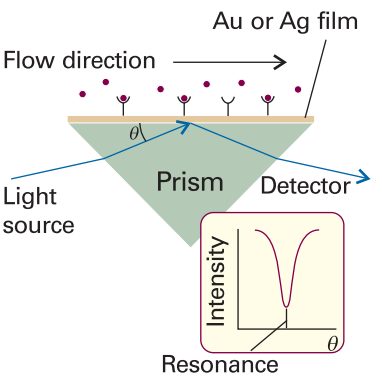

Fig. 25.26 The experimental arrangement for the observation of surface plasmon resonance, as explained in the text.

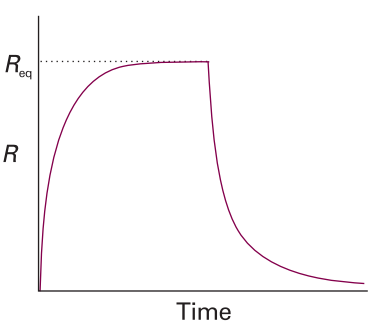

Fig. 25.27 The time dependence of a surface plasmon resonance signal, R, showing the effect of binding of a ligand to a biopolymer adsorbed on to a surface. Binding leads to an increase in R until an equilibrium value, R_{eq}, is obtained. Passing a solution containing no ligand over the surface leads to dissociation and decrease in R.

of the SPR signal, denoted by R, which is typically the shift in resonance angle. The system is normally allowed to reach equilibrium, which is denoted by the plateau in Fig. 25.27. Then, a solution containing no A is flowed above the surface and the AB complex dissociates. Again, analysis of the decay of the SPR signal reveals the kinetics of dissociation of the AB complex.

The equilibrium constant for formation of the AB complex can be measured directly from data of the type displayed in Fig. 25.27. Consider the equilibrium

$$\mathrm{A} + \mathrm{B} \rightleftharpoons \mathrm{AB} \qquad K = \frac{k_{\mathrm{on}}}{k_{\mathrm{off}}}$$

where k_{on} and k_{off} are the rate constants for formation and dissociation of the AB complex, and K is the equilibrium constant for formation of the AB complex. It follows that

$$\frac{\mathrm{d}[\mathrm{AB}]}{\mathrm{d}t} = k_{\mathrm{on}}[\mathrm{A}][\mathrm{B}] - k_{\mathrm{off}}[\mathrm{AB}] \tag{25.18}$$

In a typical experiment, the flow rate of A is sufficiently high that $[\mathrm{A}] = a_0$ is essentially constant. We can also write $[\mathrm{B}] = b_0 - [\mathrm{AB}]$ from mass-balance considerations, where b_0 is the total concentration of B. Finally, the SPR signal is often observed to be proportional to [AB]. The maximum value that R can have is $R_{\mathrm{max}} \propto b_0$, which would be measured if all B molecules were ligated to A. We may then write

$$\frac{\mathrm{d}R}{\mathrm{d}t} = k_{\mathrm{on}}a_0(R_{\mathrm{max}} - R) - k_{\mathrm{off}}R = k_{\mathrm{on}}a_0R_{\mathrm{max}} - (k_{\mathrm{on}}a_0 + k_{\mathrm{off}})R \tag{25.19}$$

At equilibrium $R = R_{\mathrm{eq}}$ and $\mathrm{d}R/\mathrm{d}t = 0$. It follows that (after some algebra)

$$R_{\mathrm{eq}} = R_{\mathrm{max}}\left(\frac{a_0K}{a_0K + 1}\right) \tag{25.20}$$

Hence, the value of K can be obtained from measurements of R_{eq} for a series of a_0.

Biosensor analysis has been used in the study of thin films, metal–electrolyte surfaces, Langmuir–Blodgett films, and a number of biopolymer interactions, such as antibody–antigen and protein–DNA interactions. The most important advantage of the technique is its sensitivity; it is possible to measure the adsorption of nanograms of material on to a surface. For biological studies, the main disadvantage is the requirement for immobilization of at least one of the components of the system under study.

Heterogeneous catalysis

A catalyst acts by providing an alternative reaction path with a lower activation energy (Table 25.3). It does not disturb the final equilibrium composition of the system, only the rate at which that equilibrium is approached. In this section we consider heterogeneous catalysis, in which (as mentioned in the introduction to Section 23.5) the catalyst and the reagents are in different phases. For simplicity, we consider only gas/solid systems.

Many catalysts depend on **co-adsorption**, the adsorption of two or more species. One consequence of the presence of a second species may be the modification of the electronic structure at the surface of a metal. For instance, partial coverage of *d*-metal surfaces by alkali metals has a pronounced effect on the electron distribution and reduces the work function of the metal. Such modifiers can act as promoters (to enhance the action of catalysts) or as poisons (to inhibit catalytic action).

Synoptic table 25.3* Activation energies of catalysed reactions

Reaction	Catalyst	E_a/(kJ mol^{-1})
$2\,\mathrm{HI} \rightarrow \mathrm{H_2} + \mathrm{I_2}$	None	184
	Au	105
	Pt	59
$2\,\mathrm{NH_3} \rightarrow$	None	350
$\mathrm{N_2} + 3\,\mathrm{H_2}$	W	162

* More values are given in the *Data section*.

25.6 Mechanisms of heterogeneous catalysis

Heterogeneous catalysis normally depends on at least one reactant being adsorbed (usually chemisorbed) and modified to a form in which it readily undergoes reaction. This modification often takes the form of a fragmentation of the reactant molecules. In practice, the active phase is dispersed as very small particles of linear dimension less than 2 nm on a porous oxide support. **Shape-selective catalysts**, such as the zeolites (*Impact* I25.2), which have a pore size that can distinguish shapes and sizes at a molecular scale, have high internal specific surface areas, in the range of 100–500 $m^2\ g^{-1}$.

The decomposition of phosphine (PH_3) on tungsten is first-order at low pressures and zeroth-order at high pressures. To account for these observations, we write down a plausible rate law in terms of an adsorption isotherm and explore its form in the limits of high and low pressure. If the rate is supposed to be proportional to the surface coverage and we suppose that θ is given by the Langmuir isotherm, we would write

$$v = k\theta = \frac{kKp}{1 + Kp} \tag{25.21}$$

where p is the pressure of phosphine. When the pressure is so low that $Kp \ll 1$, we can neglect Kp in the denominator and obtain

$$v = kKp \tag{25.22a}$$

and the decomposition is first-order. When $Kp \gg 1$, we can neglect the 1 in the denominator, whereupon the Kp terms cancel and we are left with

$$v = k \tag{25.22b}$$

and the decomposition is zeroth-order.

Self-test 25.4 Suggest the form of the rate law for the deuteration of NH_3 in which D_2 adsorbs dissociatively but not extensively (that is, $Kp \ll 1$, with p the partial pressure of D_2), and NH_3 (with partial pressure p') adsorbs at different sites.
$[v = k(Kp)^{1/2}K'p'/(1 + K'p')]$

In the **Langmuir–Hinshelwood mechanism** (LH mechanism) of surface-catalysed reactions, the reaction takes place by encounters between molecular fragments and atoms adsorbed on the surface. We therefore expect the rate law to be second-order in the extent of surface coverage:

$$A + B \rightarrow P \qquad v = k\theta_A\theta_B \tag{25.23}$$

Insertion of the appropriate isotherms for A and B then gives the reaction rate in terms of the partial pressures of the reactants. For example, if A and B follow Langmuir isotherms, and adsorb without dissociation, so that

$$\theta_A = \frac{K_A p_A}{1 + K_A p_A + K_B p_B} \qquad \theta_B = \frac{K_B p_B}{1 + K_A p_A + K_B p_B} \tag{25.24}$$

then it follows that the rate law is

$$v = \frac{kK_A K_B p_A p_B}{(1 + K_A p_A + K_B p_B)^2} \tag{25.25}$$

The parameters K in the isotherms and the rate constant k are all temperature-dependent, so the overall temperature dependence of the rate may be strongly non-Arrhenius (in the sense that the reaction rate is unlikely to be proportional to $e^{-E_a/RT}$).

The Langmuir–Hinshelwood mechanism is dominant for the catalytic oxidation of CO to CO_2.

In the **Eley–Rideal mechanism** (ER mechanism) of a surface-catalysed reaction, a gas-phase molecule collides with another molecule already adsorbed on the surface. The rate of formation of product is expected to be proportional to the partial pressure, p_B, of the non-adsorbed gas B and the extent of surface coverage, θ_A, of the adsorbed gas A. It follows that the rate law should be

$$A + B \rightarrow P \qquad v = kp_B\theta_A \tag{25.26}$$

The rate constant, k, might be much larger than for the uncatalysed gas-phase reaction because the reaction on the surface has a low activation energy and the adsorption itself is often not activated.

If we know the adsorption isotherm for A, we can express the rate law in terms of its partial pressure, p_A. For example, if the adsorption of A follows a Langmuir isotherm in the pressure range of interest, then the rate law would be

$$v = \frac{kKp_Ap_B}{1 + Kp_A} \tag{25.27}$$

If A were a diatomic molecule that adsorbed as atoms, we would substitute the isotherm given in eqn 25.6 instead.

According to eqn 25.27, when the partial pressure of A is high (in the sense $Kp_A \gg 1$) there is almost complete surface coverage, and the rate is equal to kp_B. Now the rate-determining step is the collision of B with the adsorbed fragments. When the pressure of A is low ($Kp_A \ll 1$), perhaps because of its reaction, the rate is equal to kKp_Ap_B; now the extent of surface coverage is important in the determination of the rate.

Almost all thermal surface-catalysed reactions are thought to take place by the LH mechanism, but a number of reactions with an ER mechanism have also been identified from molecular beam investigations. For example, the reaction between H(g) and D(ad) to form HD(g) is thought to be by an ER mechanism involving the direct collision and pick-up of the adsorbed D atom by the incident H atom. However, the two mechanisms should really be thought of as ideal limits, and all reactions lie somewhere between the two and show features of each one.

25.7 Catalytic activity at surfaces

Molecular beam reactive scattering (MBRS) studies are able to provide detailed information about catalysed reactions. It has become possible to investigate how the catalytic activity of a surface depends on its structure as well as its composition. For instance, the cleavage of C—H and H—H bonds appears to depend on the presence of steps and kinks, and a terrace often has only minimal catalytic activity. The reaction $H_2 + D_2 \rightarrow 2\,HD$ has been studied in detail. For this reaction, terrace sites are inactive but one molecule in ten reacts when it strikes a step. Although the step itself might be the important feature, it may be that the presence of the step merely exposes a more reactive crystal face (the step face itself). Likewise, the dehydrogenation of hexane to hexene depends strongly on the kink density, and it appears that kinks are needed to cleave C—C bonds. These observations suggest a reason why even small amounts of impurities may poison a catalyst: they are likely to attach to step and kink sites, and so impair the activity of the catalyst entirely. A constructive outcome is that the extent of dehydrogenation may be controlled relative to other types of reactions by seeking impurities that adsorb at kinks and act as specific poisons.

Molecular beam studies can also be used to investigate the details of the reaction process, particularly by using **pulsed beams**, in which the beam is chopped into short

Table 25.4 Chemisorption abilities*

	O_2	C_2H_2	C_2H_4	CO	H_2	CO_2	N_2
Ti, Cr, Mo, Fe	+	+	+	+	+	+	+
Ni, Co	+	+	+	+	+	+	–
Pd, Pt	+	+	+	+	+	–	–
Mn, Cu	+	+	+	+	±	–	–
Al, Au	+	+	+	+	–	–	–
Li, Na, K	+	+	–	–	–	–	–
Mg, Ag, Zn, Pb	+	–	–	–	–	–	–

* +, Strong chemisorption; ±, chemisorption; –, no chemisorption.

slugs. The angular distribution of the products, for instance, can be used to assess the length of time that a species remains on the surface during the reaction, for a long residence time will result in a loss of memory of the incident beam direction.

The activity of a catalyst depends on the strength of chemisorption as indicated by the 'volcano' curve in Fig. 25.28 (which is so-called on account of its general shape). To be active, the catalyst should be extensively covered by adsorbate, which is the case if chemisorption is strong. On the other hand, if the strength of the substrate–adsorbate bond becomes too great, the activity declines either because the other reactant molecules cannot react with the adsorbate or because the adsorbate molecules are immobilized on the surface. This pattern of behaviour suggests that the activity of a catalyst should initially increase with strength of adsorption (as measured, for instance, by the enthalpy of adsorption) and then decline, and that the most active catalysts should be those lying near the summit of the volcano. Most active metals are those that lie close to the middle of the *d* block.

Many metals are suitable for adsorbing gases, and the general order of adsorption strengths decreases along the series O_2, C_2H_2, C_2H_4, CO, H_2, CO_2, N_2. Some of these molecules adsorb dissociatively (for example, H_2). Elements from the *d* block, such as iron, vanadium, and chromium, show a strong activity towards all these gases, but manganese and copper are unable to adsorb N_2 and CO_2. Metals towards the left of the periodic table (for example, magnesium and lithium) can adsorb (and, in fact, react with) only the most active gas (O_2). These trends are summarized in Table 25.4.

IMPACT ON TECHNOLOGY

I25.2 Catalysis in the chemical industry

Almost the whole of modern chemical industry depends on the development, selection, and application of catalysts (Table 25.5). All we can hope to do in this section is to give a brief indication of some of the problems involved. Other than the ones we consider, these problems include the danger of the catalyst being poisoned by by-products or impurities, and economic considerations relating to cost and lifetime.

An example of catalytic action is found in the hydrogenation of alkenes. The alkene (**2**) adsorbs by forming two bonds with the surface (**3**), and on the same surface there may be adsorbed H atoms. When an encounter occurs, one of the alkene–surface bonds is broken (forming **4** or **5**) and later an encounter with a second H atom releases the fully hydrogenated hydrocarbon, which is the thermodynamically more stable species. The evidence for a two-stage reaction is the appearance of different isomeric alkenes in the mixture. The formation of isomers comes about because, while the hydrocarbon chain is waving about over the surface of the metal, an atom in the chain

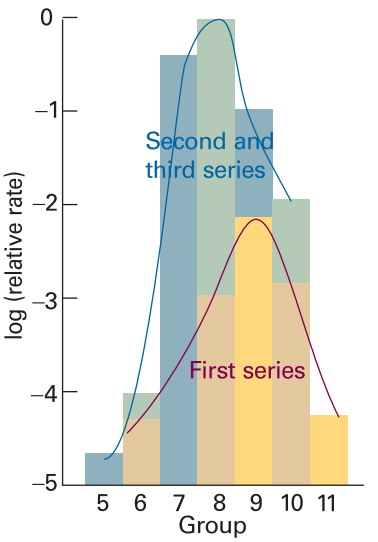

Fig. 25.28 A volcano curve of catalytic activity arises because, although the reactants must adsorb reasonably strongly, they must not adsorb so strongly that they are immobilized. The lower curve refers to the first series of *d*-block metals, the upper curve to the second and third series *d*-block metals. The group numbers relate to the periodic table inside the back cover.

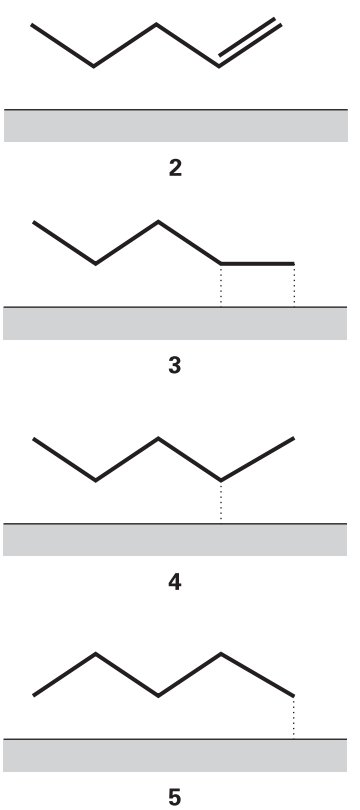

Table 25.5 Properties of catalysts

Catalyst	Function	Examples
Metals	Hydrogenation Dehydrogenation	Fe, Ni, Pt, Ag
Semiconducting oxides and sulfides	Oxidation Desulfurization	NiO, ZnO, MgO, Bi_2O_3/MoO_3, MoS_2
Insulating oxides	Dehydration	Al_2O_3, SiO_2, MgO
Acids	Polymerization Isomerization Cracking Alkylation	H_3PO_4, H_2SO_4, SiO_3/Al_2O_3, zeolites

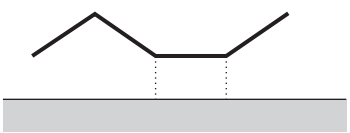

6

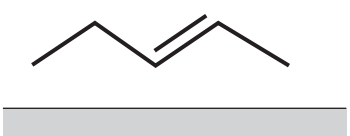

7

might chemisorb again to form (**6**) and then desorb to (**7**), an isomer of the original molecule. The new alkene would not be formed if the two hydrogen atoms attached simultaneously.

A major industrial application of catalytic hydrogenation is to the formation of edible fats from vegetable and animal oils. Raw oils obtained from sources such as the soya bean have the structure $CH_2(OOCR)CH(OOCR')CH_2(OOCR'')$, where R, R′, and R″ are long-chain hydrocarbons with several double bonds. One disadvantage of the presence of many double bonds is that the oils are susceptible to atmospheric oxidation, and therefore are liable to become rancid. The geometrical configuration of the chains is responsible for the liquid nature of the oil, and in many applications a solid fat is at least much better and often necessary. Controlled partial hydrogenation of an oil with a catalyst carefully selected so that hydrogenation is incomplete and so that the chains do not isomerize (finely divided nickel, in fact), is used on a wide scale to produce edible fats. The process, and the industry, is not made any easier by the seasonal variation of the number of double bonds in the oils.

Catalytic oxidation is also widely used in industry and in pollution control. Although in some cases it is desirable to achieve complete oxidation (as in the production of nitric acid from ammonia), in others partial oxidation is the aim. For example, the complete oxidation of propene to carbon dioxide and water is wasteful, but its partial oxidation to propenal (acrolein, $CH_2{=}CHCHO$) is the start of important industrial processes. Likewise, the controlled oxidations of ethene to ethanol, ethanal (acetaldehyde), and (in the presence of acetic acid or chlorine) to chloroethene (vinyl chloride, for the manufacture of PVC), are the initial stages of very important chemical industries.

Some of these oxidation reactions are catalysed by *d*-metal oxides of various kinds. The physical chemistry of oxide surfaces is very complex, as can be appreciated by considering what happens during the oxidation of propene to propenal on bismuth molybdate. The first stage is the adsorption of the propene molecule with loss of a hydrogen to form the propenyl (allyl) radical, $CH_2{=}CHCH_2$. An O atom in the surface can now transfer to this radical, leading to the formation of propenal and its desorption from the surface. The H atom also escapes with a surface O atom, and goes on to form H_2O, which leaves the surface. The surface is left with vacancies and metal ions in lower oxidation states. These vacancies are attacked by O_2 molecules in the overlying gas, which then chemisorb as O_2^- ions, so reforming the catalyst. This sequence of events, which is called the **Mars van Krevelen mechanism**, involves great upheavals of the surface, and some materials break up under the stress.

Many of the small organic molecules used in the preparation of all kinds of chemical products come from oil. These small building blocks of polymers, perfumes, and petrochemicals in general, are usually cut from the long-chain hydrocarbons drawn from the Earth as petroleum. The catalytically induced fragmentation of the

long-chain hydrocarbons is called **cracking**, and is often brought about on silica–alumina catalysts. These catalysts act by forming unstable carbocations, which dissociate and rearrange to more highly branched isomers. These branched isomers burn more smoothly and efficiently in internal combustion engines, and are used to produce higher octane fuels.

Catalytic **reforming** uses a dual-function catalyst, such as a dispersion of platinum and acidic alumina. The platinum provides the metal function, and brings about dehydrogenation and hydrogenation. The alumina provides the acidic function, being able to form carbocations from alkenes. The sequence of events in catalytic reforming shows up very clearly the complications that must be unravelled if a reaction as important as this is to be understood and improved. The first step is the attachment of the long-chain hydrocarbon by chemisorption to the platinum. In this process first one and then a second H atom is lost, and an alkene is formed. The alkene migrates to a Brønsted acid site, where it accepts a proton and attaches to the surface as a carbocation. This carbocation can undergo several different reactions. It can break into two, isomerize into a more highly branched form, or undergo varieties of ring-closure. Then the adsorbed molecule loses a proton, escapes from the surface, and migrates (possibly through the gas) as an alkene to a metal part of the catalyst where it is hydrogenated. We end up with a rich selection of smaller molecules which can be withdrawn, fractionated, and then used as raw materials for other products.

The concept of a solid surface has been extended with the availability of **microporous materials**, in which the surface effectively extends deep inside the solid. Zeolites are microporous aluminosilicates with the general formula $\{[M^{n+}]_{x/n}\cdot[H_2O]_m\}\{[AlO_2]_x[SiO_2]_y\}^{x-}$, where M^{n+} cations and H_2O molecules bind inside the cavities, or pores, of the Al—O—Si framework (Fig. 25.29). Small neutral molecules, such as CO_2, NH_3, and hydrocarbons (including aromatic compounds), can also adsorb to the internal surfaces and we shall see that this partially accounts for the utility of zeolites as catalysts.

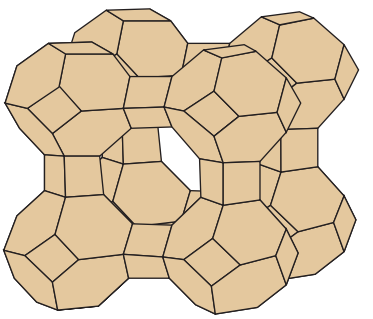

Fig. 25.29 A framework representation of the general layout of the Si, Al, and O atoms in a zeolite material. Each vertex corresponds to a Si or Al atom and each edge corresponds to the approximate location of a O atom. Note the large central pore, which can hold cations, water molecules, or other small molecules.

Some zeolites for which $M = H^+$ are very strong acids and catalyse a variety of reactions that are of particular importance to the petrochemical industry. Examples include the dehydration of methanol to form hydrocarbons such as gasoline and other fuels:

$$x\,CH_3OH \xrightarrow{\text{zeolite}} (CH_2)_x + x\,H_2O$$

and the isomerization of *m*-xylene (**8**) to *p*-xylene (**9**). The catalytically important form of these acidic zeolites may be either a Brønsted acid (**10**) or a Lewis acid (**11**). Like enzymes, a zeolite catalyst with a specific compostion and structure is very selective toward certain reactants and products because only molecules of certain sizes can enter

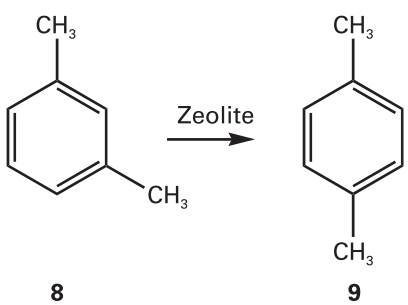

8 **9**

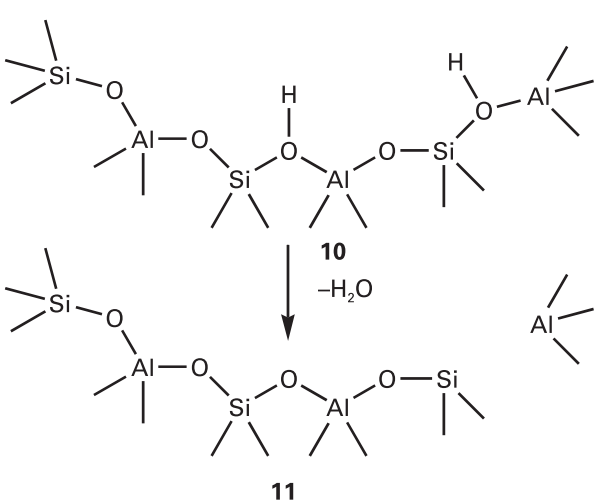

11

and exit the pores in which catalysis occurs. It is also possible that zeolites derive their selectivity from the ability to bind and to stabilize only transition states that fit properly in the pores. The analysis of the mechanism of zeolyte catalysis is greatly facilitated by computer simulation of microporous systems, which shows how molecules fit in the pores, migrate through the connecting tunnels, and react at the appropriate active sites.

Processes at electrodes

A special kind of surface is an electrode and the special kind of process that occurs there is the transfer of electrons. Detailed knowledge of the factors that determine the rate of electron transfer at electrodes leads to a better understanding of power production in batteries, and of electron conduction in metals, semiconductors, and nanometre-sized electronic devices. Indeed, the economic consequences of electron transfer reactions are almost incalculable. Most of the modern methods of generating electricity are inefficient, and the development of fuel cells could revolutionize our production and deployment of energy (*Impact* I25.3). Today we produce energy inefficiently to produce goods that then decay by corrosion. Each step of this wasteful sequence could be improved by discovering more about the kinetics of electrochemical processes. Similarly, the techniques of organic and inorganic electrosynthesis, where an electrode is an active component of an industrial process, depend on intimate understanding of the kinetics of electron transfer processes.

As for homogeneous systems (Chapter 24), electron transfer at the surface of an electrode involves electron tunnelling. However, the electrode possesses a nearly infinite number of closely spaced electronic energy levels rather than the small number of discrete levels of a typical complex. Furthermore, specific interactions with the electrode surface give the solute and solvent special properties that can be very different from those observed in the bulk of the solution. For this reason, we begin with a description of the electrode–solution interface. Then, we describe the kinetics of electrode processes by using a largely phenomenological (rather than strictly theoretical) approach that draws on the thermodynamic language inspired by transition state theory.

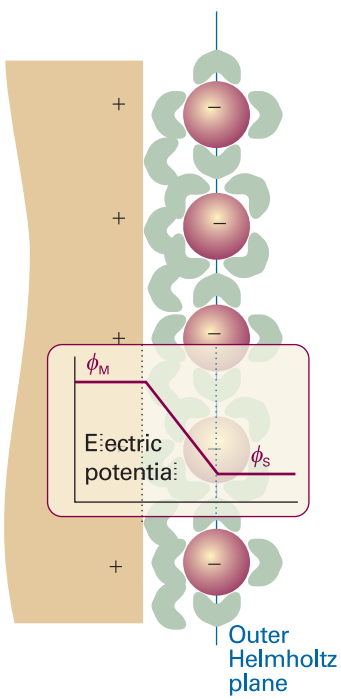

Fig. 25.30 A simple model of the electrode–solution interface treats it as two rigid planes of charge. One plane, the outer Helmholtz plane (OHP), is due to the ions with their solvating molecules and the other plane is that of the electrode itself. The plot shows the dependence of the electric potential with distance from the electrode surface according to this model. Between the electrode surface and the OHP, the potential varies linearly from φ_M, the value in the metal, to φ_S, the value in the bulk of the solution.

25.8 The electrode–solution interface

The most primitive model of the boundary between the solid and liquid phases is as an **electrical double layer**, which consists of a sheet of positive charge at the surface of the electrode and a sheet of negative charge next to it in the solution (or vice versa). We shall see that this arrangement creates an electrical potential difference, called the **Galvani potential difference**, between the bulk of the metal electrode and the bulk of the solution. More sophisticated models for the electrode–solution interface attempt to describe the gradual changes in the structure of the solution between two extremes: the charged electrode surface and the bulk of the solution.

(a) The structure of the interface

A more detailed picture of the interface can be constructed by speculating about the arrangement of ions and electric dipoles in the solution. In the **Helmholtz layer model** of the interface the solvated ions arrange themselves along the surface of the electrode but are held away from it by their hydration spheres (Fig. 25.30). The location of the sheet of ionic charge, which is called the **outer Helmholtz plane** (OHP), is identified as the plane running through the solvated ions. In this simple model, the electrical potential changes linearly within the layer bounded by the electrode surface on one side and the OHP on the other (see Exercise 25.15a). In a refinement of this

model, ions that have discarded their solvating molecules and have become attached to the electrode surface by chemical bonds are regarded as forming the **inner Helmholtz plane** (IHP). The Helmholtz layer model ignores the disrupting effect of thermal motion, which tends to break up and disperse the rigid outer plane of charge. In the **Gouy–Chapman model** of the **diffuse double layer**, the disordering effect of thermal motion is taken into account in much the same way as the Debye–Hückel model describes the ionic atmosphere of an ion (Section 5.9) with the latter's single central ion replaced by an infinite, plane electrode.

Figure 25.31 shows how the local concentrations of cations and anions differ in the Gouy–Chapman model from their bulk concentrations. Ions of opposite charge cluster close to the electrode and ions of the same charge are repelled from it. The modification of the local concentrations near an electrode implies that it might be misleading to use activity coefficients characteristic of the bulk to discuss the thermodynamic properties of ions near the interface. This is one of the reasons why measurements of the dynamics of electrode processes are almost always done using a large excess of supporting electrolyte (for example, a 1 M solution of a salt, an acid, or a base). Under such conditions, the activity coefficients are almost constant because the inert ions dominate the effects of local changes caused by any reactions taking place. The use of a concentrated solution also minimizes ion migration effects.

Neither the Helmholtz nor the Gouy–Chapman model is a very good representation of the structure of the double layer. The former overemphasizes the rigidity of the local solution; the latter underemphasizes its structure. The two are combined in the **Stern model**, in which the ions closest to the electrode are constrained into a rigid Helmholtz plane while outside that plane the ions are dispersed as in the Gouy–Chapman model (Fig. 25.32). Yet another level of sophistication is found in the **Grahame model**, which adds an inner Helmholtz plane to the Stern model.

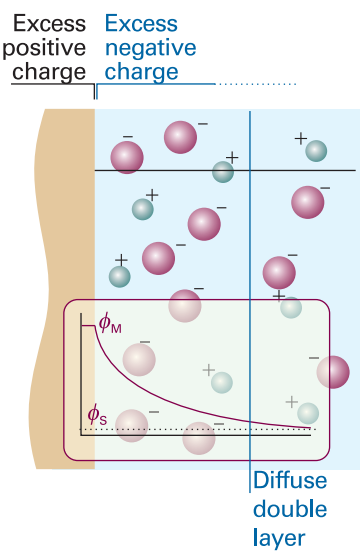

Fig. 25.31 The Gouy–Chapman model of the electrical double layer treats the outer region as an atmosphere of counter-charge, similar to the Debye–Hückel theory of ion atmospheres. The plot of electrical potential against distance from the electrode surface shows the meaning of the diffuse double layer (see text for details).

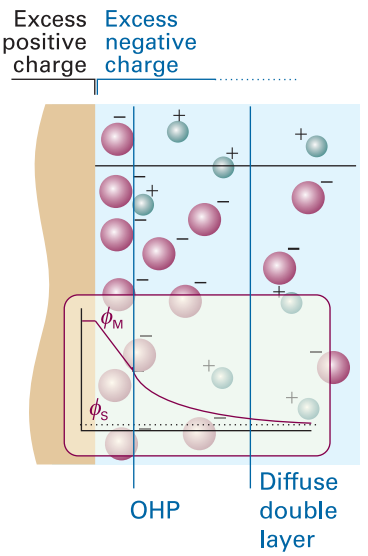

Fig. 25.32 A representation of the Stern model of the electrode–solution interface. The model incorporates the idea of an outer Helmholtz plane near the electrode surface and of a diffuse double layer further away from the surface.

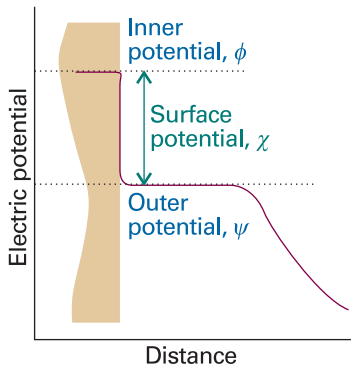

Fig. 25.33 The variation of potential with distance from an electrode that has been separated from the electrolyte solution without there being an adjustment of charge. A similar diagram applies to the separated solution.

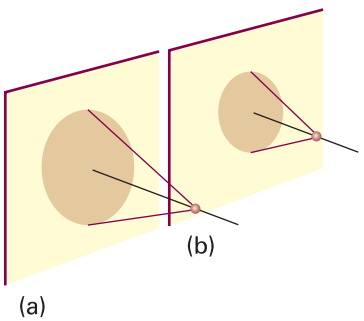

Fig. 25.34 The origin of the distance-independence of the outer potential. (a) Far from the electrode, a point charge experiences a potential arising from a wide area but each contribution is weak. (b) Close to the electrode, the point charge experiences a potential arising from a small area but each contribution is strong. Provided the point charge is in a certain range of values (and, specifically, where image charge effects can be ignored) the potential it experiences is largely independent of distance.

(b) The electric potential at the interface

The potential at the interface can be analysed by imagining the separation of the electrode from the solution, but with the charges of the metal and the solution frozen in position. A positive test charge at great distances from the isolated electrode experiences a Coulomb potential that varies inversely with distance (Fig. 25.33). As the test charge approaches the electrode, which can be a metal or membrane electrode, it enters a region where the potential varies more slowly. This change in behaviour can be traced to the fact that the surface charge is not point-like but is spread over an area. At about 100 nm from the surface the potential varies only slightly with distance because the closer the point of observation is to the surface, although the potential from a given region of charge is stronger, a smaller area of surface is sampled (Fig. 25.34). The potential in this region is called the **outer potential**, ψ. As the test charge is taken through the skin of electrons on the surface of the electrode, the potential it experiences changes until the probe reaches the inner, bulk metal environment, where the potential is called the **inner potential**, ϕ. The difference between the inner and outer potentials is called the **surface potential**, χ.

A similar sequence of changes of potential is observed as a positive test charge is brought up to and through the solution surface. The potential changes to its outer value as the charge approaches the charged medium, then to its inner value as the probe is taken into the bulk.

Now consider bringing the electrode and solution back together again but without any change of charge distribution. The potential difference between points in the bulk metal and the bulk solution is the Galvani potential difference, $\Delta\phi$. Apart from a constant, this Galvani potential difference is the electrode potential that was discussed in Chapter 7. We shall ignore the constant, which cannot be measured anyway, and identify changes in $\Delta\phi$ with changes in electrode potential (see *Further information* 25.1 for a quantitative treatment).

25.9 The rate of charge transfer

Because an electrode reaction is heterogeneous, it is natural to express its rate as the flux of products, the amount of material produced over a region of the electrode surface in an interval of time divided by the area of the region and the duration of the interval.

(a) The rate laws

A first-order heterogeneous rate law has the form

$$\text{Product flux} = k[\text{species}] \tag{25.28}$$

where [species] is the molar concentration of the relevant species in solution close to the electrode, just outside the double layer. The rate constant has dimensions of length/time (with units, for example, of centimetres per second, cm s^{-1}). If the molar concentrations of the oxidized and reduced materials outside the double layer are [Ox] and [Red], respectively, then the rate of reduction of Ox, v_{Ox}, is

$$v_{Ox} = k_c[Ox] \tag{25.29a}$$

and the rate of oxidation of Red, v_{Red}, is

$$v_{Red} = k_a[Red] \tag{25.29b}$$

(The notation k_c and k_a is justified below.)

Now consider a reaction at the electrode in which an ion is reduced by the transfer of a single electron in the rate-determining step. For instance, in the deposition of

cadmium only one electron is transferred in the rate-determining step even though overall the deposition involves the transfer of two electrons.

The net current density at the electrode is the difference between the current densities arising from the reduction of Ox and the oxidation of Red. Because the redox processes at the electrode involve the transfer of one electron per reaction event, the current densities, j, arising from the redox processes are the rates (as expressed above) multiplied by the charge transferred per mole of reaction, which is given by Faraday's constant. Therefore, there is a **cathodic current density** of magnitude

$$j_c = Fk_c[\text{Ox}] \qquad \text{for} \quad \text{Ox} + e^- \rightarrow \text{Red} \tag{25.30a}$$

arising from the reduction (because, as we saw in Chapter 7, the cathode is the site of reduction). There is also an opposing **anodic current density** of magnitude

$$j_a = Fk_a[\text{Red}] \qquad \text{for} \quad \text{Red} \rightarrow \text{Ox} + e^- \tag{25.30b}$$

arising from the oxidation (because the anode is the site of oxidation). The net current density at the electrode is the difference

$$j = j_a - j_c = Fk_a[\text{Red}] - Fk_c[\text{Ox}] \tag{25.30c}$$

Note that, when $j_a > j_c$, so that $j > 0$, the current is anodic (Fig. 25.35a); when $j_c > j_a$, so that $j < 0$, the current is cathodic (Fig. 25.35b).

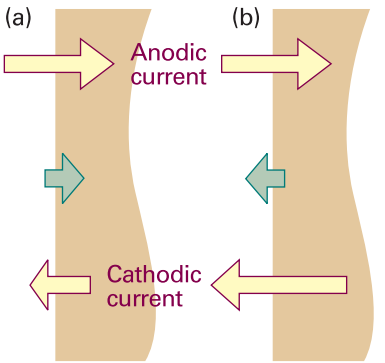

Fig. 25.35 The net current density is defined as the difference between the cathodic and anodic contributions. (a) When $j_a > j_c$, the net current is anodic, and there is a net oxidation of the species in solution. (b) When $j_c > j_a$, the net current is cathodic, and the net process is reduction.

(b) The activation Gibbs energy

If a species is to participate in reduction or oxidation at an electrode, it must discard any solvating molecules, migrate through the electrode–solution interface, and adjust its hydration sphere as it receives or discards electrons. Likewise, a species already at the inner plane must be detached and migrate into the bulk. Because both processes are activated, we can expect to write their rate constants in the form suggested by transition state theory (Section 24.4) as

$$k = Be^{-\Delta^{\ddagger}G/RT} \tag{25.31}$$

where $\Delta^{\ddagger}G$ is the activation Gibbs energy and B is a constant with the same dimensions as k.

When eqn 25.31 is inserted into eqn 25.30 we obtain

$$j = FB_a[\text{Red}]e^{-\Delta^{\ddagger}G_a/RT} - FB_c[\text{Ox}]e^{-\Delta^{\ddagger}G_c/RT} \tag{25.32}$$

This expression allows the activation Gibbs energies to be different for the cathodic and anodic processes. That they are different is the central feature of the remaining discussion.

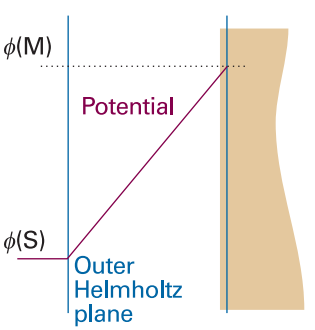

Fig. 25.36 The potential, ϕ, varies linearly between two plane parallel sheets of charge, and its effect on the Gibbs energy of the transition state depends on the extent to which the latter resembles the species at the inner or outer planes.

(c) The Butler–Volmer equation

Now we relate j to the Galvani potential difference, which varies across the electrode–solution interface as shown schematically in Fig. 25.36.

Consider the reduction reaction, $\text{Ox} + e^- \rightarrow \text{Red}$, and the corresponding reaction profile. If the transition state of the activated complex is product-like (as represented by the peak of the reaction profile being close to the electrode in Fig. 25.37), the activation Gibbs energy is changed from $\Delta^{\ddagger}G_c(0)$, the value it has in the absence of a potential difference across the double layer, to

$$\Delta^{\ddagger}G_c = \Delta^{\ddagger}G_c(0) + F\Delta\phi \tag{25.33a}$$

Thus, if the electrode is more positive than the solution, $\Delta\phi > 0$, then more work has to be done to form an activated complex from Ox; in this case the activation Gibbs energy is increased. If the transition state is reactant-like (represented by the peak of

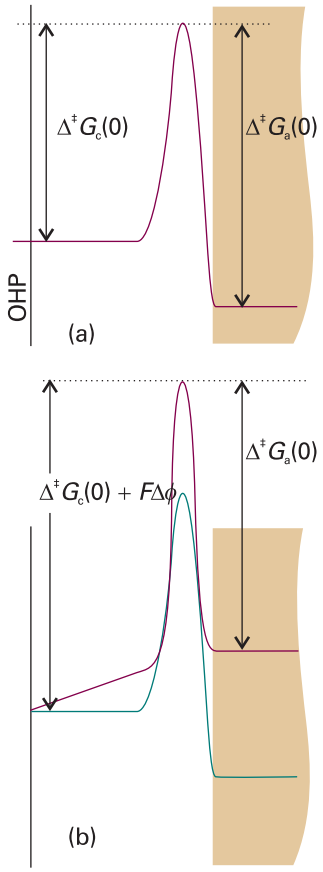

Fig. 25.37 When the transition state resembles a species that has undergone reduction, the activation Gibbs energy for the anodic current is almost unchanged, but the full effect applies to the cathodic current. (a) Zero potential difference; (b) nonzero potential difference.

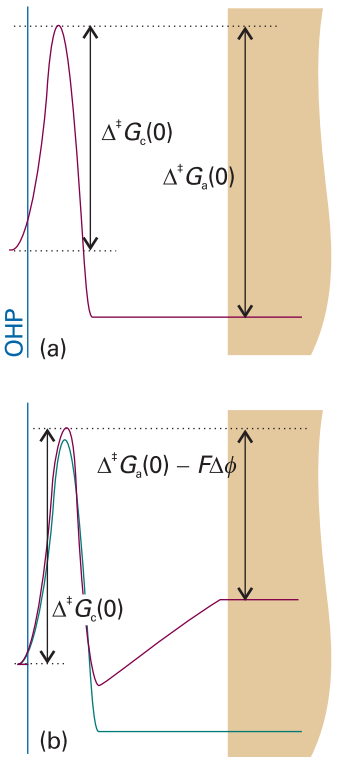

Fig. 25.38 When the transition state resembles a species that has undergone oxidation, the activation Gibbs energy for the cathodic current is almost unchanged but the activation Gibbs energy for the anodic current is strongly affected. (a) Zero potential difference; (b) nonzero potential difference.

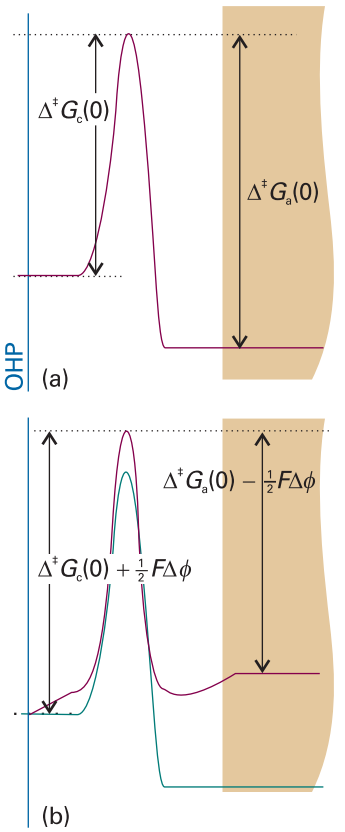

Fig. 25.39 When the transition state is intermediate in its resemblance to reduced and oxidized species, as represented here by a peak located at an intermediate position as measured by α (with $0 < \alpha < 1$), both activation Gibbs energies are affected; here, $\alpha \approx 0.5$. (a) Zero potential difference; (b) nonzero potential difference.

the reaction profile being close to the outer plane of the double-layer in Fig. 25.38), then $\Delta^{\ddagger}G_c$ is independent of $\Delta\phi$. In a real system, the transition state has an intermediate resemblance to these extremes (Fig. 25.39) and the activation Gibbs energy for reduction may be written as

$$\Delta^{\ddagger}G_c = \Delta^{\ddagger}G_c(0) + \alpha F\Delta\phi \qquad (25.33b)$$

The parameter α is called the (cathodic) **transfer coefficient**, and lies in the range 0 to 1. Experimentally, α is often found to be about 0.5.

Now consider the oxidation reaction, Red + e^- → Ox and its reaction profile. Similar remarks apply. In this case, Red discards an electron to the electrode, so the extra work is zero if the transition state is reactant-like (represented by a peak close to the electrode). The extra work is the full $-F\Delta\phi$ if it resembles the product (the peak close to the outer plane). In general, the activation Gibbs energy for this anodic process is

$$\Delta^{\ddagger}G_a = \Delta^{\ddagger}G_a(0) - (1-\alpha)F\Delta\phi \qquad (25.34)$$

The two activation Gibbs energies can now be inserted in place of the values used in eqn 25.32 with the result that

$$j = FB_a[\text{Red}]e^{-\Delta^{\ddagger}G_a(0)/RT}e^{(1-\alpha)F\Delta\phi/RT} - FB_c[\text{Ox}]e^{-\Delta^{\ddagger}G_c(0)/RT}e^{-\alpha F\Delta\phi/RT} \quad (25.35)$$

This is an explicit, if complicated, expression for the net current density in terms of the potential difference.

The appearance of eqn 25.35 can be simplified. First, in a purely cosmetic step we write

$$f = \frac{F}{RT} \quad [25.36]$$

Next, we identify the individual cathodic and anodic current densities:

$$\left.\begin{aligned} j_a &= FB_a[\text{Red}]e^{-\Delta^{\ddagger}G_a(0)/RT}e^{(1-\alpha)f\Delta\phi} \\ j_c &= FB_c[\text{Ox}]e^{-\Delta^{\ddagger}G_c(0)/RT}e^{-\alpha f\Delta\phi} \end{aligned}\right\} j = j_a - j_c \quad (25.37)$$

Illustration 25.1 *Calculating the current density 1*

To calculate the change in cathodic current density at an electrode when the potential difference changes from $\Delta\phi'$ and $\Delta\phi$, we use eqn 25.37 to express the ratio of cathodic current densities j_c' and j_c

$$\frac{j_c'}{j_c} = e^{-\alpha f(\Delta\phi' - \Delta\phi)}$$

When $\Delta\phi' - \Delta\phi = 1.0$ V, $T = 298$ K, and $\alpha = \frac{1}{2}$ (a typical value), we obtain

$$\alpha f \times (\Delta\phi' - \Delta\phi) = \frac{\frac{1}{2} \times (9.6485 \times 10^4 \text{ C mol}^{-1}) \times (1.0 \text{ V})}{(8.3145 \text{ J K}^{-1} \text{ mol}^{-1}) \times (298 \text{ K})} = \frac{9.6485 \times 10^4 \times 1.0}{2 \times 8.3145 \times 298}$$

Hence (after using 1 J = 1 VC),

$$\frac{j_c'}{j_c} = e^{-\frac{9.6485\times10^4\times1.0}{2\times8.3145\times298}} = 4 \times 10^{-9}$$

This huge change in current density, by a factor of a billion, occurs for a very mild and easily applied change of conditions. We can appreciate why the change is so great by realizing that a change of potential difference by 1 V changes the activation Gibbs energy by (1 V) × F, or about 50 kJ mol^{-1}, which has an enormous effect on the rates.

Self-test 25.5 Calculate the change in anodic current density under the same circumstances. $[j_a'/j_a = 3 \times 10^8]$

If the cell is balanced against an external source, the Galvani potential difference, $\Delta\phi$, can be identified as the (zero-current) electrode potential, E, and we can write

$$\begin{aligned} j_a &= FB_a[\text{Red}]e^{-\Delta^{\ddagger}G_a(0)/RT}e^{(1-\alpha)fE} \\ j_c &= FB_c[\text{Ox}]e^{-\Delta^{\ddagger}G_c(0)/RT}e^{-\alpha fE} \end{aligned} \quad (25.38)$$

When these equations apply, there is no net current at the electrode (as the cell is balanced), so the two current densities must be equal. From now on we denote them both as j_0, which is called the **exchange current density**.

When the cell is producing current (that is, when a load is connected between the electrode being studied and a second counter electrode) the electrode potential changes

Comment 25.1
Here we are assuming that we can identify the Galvani potential difference and the zero-current electrode potential. As explained earlier, they differ by a constant amount, which may be regarded as absorbed into the constant B.

from its zero-current value, E, to a new value, E', and the difference is the electrode's **overpotential**, η:

$$\eta = E' - E \qquad [25.39]$$

Hence, $\Delta\phi$ changes to $\Delta\phi = E + \eta$ and the two current densities become

$$j_a = j_0 e^{(1-\alpha)f\eta} \qquad j_c = j_0 e^{-\alpha f\eta} \qquad (25.40)$$

Then from eqn 25.32 we obtain the **Butler–Volmer equation**:

$$j = j_0\{e^{(1-\alpha)f\eta} - e^{-\alpha f\eta}\} \qquad (25.41)$$

This equation is the basis of all that follows.

(d) The low overpotential limit

When the overpotential is so small that $f\eta \ll 1$ (in practice, η less than about 0.01 V) the exponentials in eqn 25.41 can be expanded by using $e^x = 1 + x + \cdots$ to give

$$j = j_0\{1 + (1-\alpha)f\eta + \cdots - (1 - \alpha f\eta + \cdots)\} \approx j_0 f\eta \qquad (25.42)$$

This equation shows that the current density is proportional to the overpotential, so at low overpotentials the interface behaves like a conductor that obeys Ohm's law. When there is a small positive overpotential the current is anodic ($j > 0$ when $\eta > 0$), and when the overpotential is small and negative the current is cathodic ($j < 0$ when $\eta < 0$). The relation can also be reversed to calculate the potential difference that must exist if a current density j has been established by some external circuit:

$$\eta = \frac{RTj}{Fj_0} \qquad (25.43)$$

The importance of this interpretation will become clear below.

Illustration 25.2 *Calculating the current density 2*

The exchange current density of a $Pt(s)|H_2(g)|H^+(aq)$ electrode at 298 K is 0.79 mA cm^{-2}. Therefore, the current density when the overpotential is +5.0 mV is obtained by using eqn 25.42 and $f = F/RT = 1/(25.69\text{ mV})$:

$$j = j_0 f\eta = \frac{(0.79\text{ mA cm}^{-2}) \times (5.0\text{ mV})}{25.69\text{ mV}} = 0.15\text{ mA cm}^{-2}$$

The current through an electrode of total area 5.0 cm^2 is therefore 0.75 mA.

Self-test 25.6 What would be the current at pH = 2.0, the other conditions being the same? [−18 mA (cathodic)]

(e) The high overpotential limit

When the overpotential is large and positive (in practice, $\eta \geq 0.12$ V), corresponding to the electrode being the anode in electrolysis, the second exponential in eqn 25.41 is much smaller than the first, and may be neglected. Then

$$j = j_0 e^{(1-\alpha)f\eta} \qquad (25.44)$$

so

$$\ln j = \ln j_0 + (1-\alpha)f\eta \qquad (25.45)$$

When the overpotential is large but negative (in practice, $\eta \leq -0.12$ V), corresponding to the cathode in electrolysis, the first exponential in eqn 25.41 may be neglected. Then

$$j = -j_0 e^{-\alpha f \eta} \tag{25.46}$$

so

$$\ln(-j) = \ln j_0 - \alpha f \eta \tag{25.47}$$

The plot of the logarithm of the current density against the overpotential is called a **Tafel plot**. The slope gives the value of α and the intercept at $\eta = 0$ gives the exchange current density.

The experimental arrangement used for a Tafel plot is shown in Fig. 25.40. A similar arrangement is typical of all kinds of electrochemical rate measurements. The current-carrying electrodes are the **working electrode**, the electrode of interest, and the **counter electrode**, which is necessary to complete the electrical circuit. The current flowing through them is controlled externally. If the area of the working electrode is A and the current is I, the current density across its surface is I/A. The potential difference across the interface cannot be measured directly, but the potential of the working electrode relative to a third electrode, the **reference electrode**, can be measured with a high impedance voltmeter, and no current flows in that half of the circuit. The reference electrode is in contact with the solution close to the working electrode through a 'Luggin capillary', which helps to eliminate any ohmic potential difference that might arise accidentally. Changing the current flowing through the working circuit causes a change of potential of the working electrode, and that change is measured with the voltmeter. The overpotential is then obtained by taking the difference between the potentials measured with and without a flow of current through the working circuit.

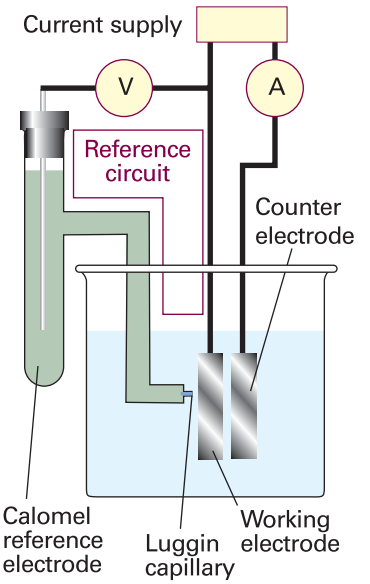

Fig. 25.40 The general arrangement for electrochemical rate measurements. The external source establishes a current between the working electrode and the counter electrode, and its effect on the potential difference of either of them relative to the reference electrode is observed. No current flows in the reference circuit.

Example 25.4 *Interpreting a Tafel plot*

The data below refer to the anodic current through a platinum electrode of area 2.0 cm^2 in contact with an Fe^{3+},Fe^{2+} aqueous solution at 298 K. Calculate the exchange current density and the transfer coefficient for the electrode process.

η/mV	50	100	150	200	250
I/mA	8.8	25.0	58.0	131	298

Method The anodic process is the oxidation $Fe^{2+}(aq) \rightarrow Fe^{3+}(aq) + e^-$. To analyse the data, we make a Tafel plot (of $\ln j$ against η) using the anodic form (eqn 25.45). The intercept at $\eta = 0$ is $\ln j_0$ and the slope is $(1 - \alpha)f$.

Answer Draw up the following table:

η/mV	50	100	150	200	250
j/(mA cm^{-2})	4.4	12.5	29.0	65.5	149
$\ln(j/(\text{mA cm}^{-2}))$	1.48	2.53	3.37	4.18	5.00

The points are plotted in Fig. 25.41. The high overpotential region gives a straight line of intercept 0.88 and slope 0.0165. From the former it follows that $\ln(j_0/(\text{mA cm}^{-2})) = 0.88$, so $j_0 = 2.4$ mA cm^{-2}. From the latter,

$$(1 - \alpha)\frac{F}{RT} = 0.0165 \text{ mV}^{-1}$$

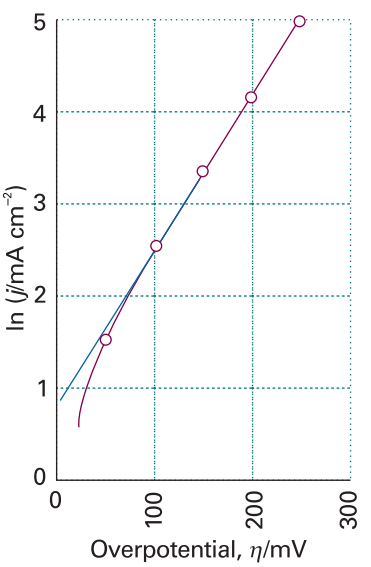

Fig. 25.41 A Tafel plot is used to measure the exchange current density (given by the extrapolated intercept at $\eta = 0$) and the transfer coefficient (from the slope). The data are from Example 25.4.

so $\alpha = 0.58$. Note that the Tafel plot is nonlinear for $\eta < 100$ mV; in this region $\alpha f\eta = 2.3$ and the approximation that $\alpha f\eta \gg 1$ fails.

Self-test 25.7 Repeat the analysis using the following cathodic current data:

η/mV	−50	−100	−150	−200	−250	−300
I/mA	−0.3	−1.5	−6.4	−27.6	−118.6	−510

[$\alpha = 0.75$, $j_0 = 0.041$ mA cm^{-2}]

Some experimental values for the Butler–Volmer parameters are given in Table 25.6. From them we can see that exchange current densities vary over a very wide range. For example, the N_2,N_3^- couple on platinum has $j_0 = 10^{-76}$ A cm^{-2}, whereas the H^+,H_2 couple on platinum has $j_0 = 8 \times 10^{-4}$ A cm^{-2}, a difference of 73 orders of magnitude. Exchange currents are generally large when the redox process involves no bond breaking (as in the $[Fe(CN)_6]^{3-}$,$[Fe(CN)_6]^{4-}$ couple) or if only weak bonds are broken (as in Cl_2,Cl^-). They are generally small when more than one electron needs to be transferred, or when multiple or strong bonds are broken, as in the N_2,N_3^- couple and in redox reactions of organic compounds.

25.10 Voltammetry

The kinetics of electrode processes can be studied by **voltammetry**, in which the current is monitored as the potential of the electrode is changed, and by **chronopotentiometry**, in which the potential is monitored as the current flow is changed. Voltammetry may also be used to identify species present in solution and to determine their concentration.

Before we describe voltammetry in detail, we need to understand how electrode potentials vary with current. Electrodes with potentials that change only slightly when a current passes through them are classified as **non-polarizable**. Those with strongly current-dependent potentials are classified as **polarizable**. From the linearized equation (eqn 25.43) it is clear that the criterion for low polarizability is high exchange current density (so η may be small even though j is large). The calomel and H_2/Pt electrodes are both highly non-polarizable, which is one reason why they are so extensively used as reference electrodes in electrochemistry.

(a) Concentration polarization

One of the assumptions in the derivation of the Butler–Volmer equation is the negligible conversion of the electroactive species at low current densities, resulting in uniformity of concentration near the electrode. This assumption fails at high current

Synoptic table 25.6* Exchange current densities and transfer coefficients at 298 K

Reaction	Electrode	j_0/(A cm^{-2})	α
$2\,H^+ + 2\,e^- \rightarrow H_2$	Pt	7.9×10^{-4}	
	Ni	6.3×10^{-6}	0.58
	Pb	5.0×10^{-12}	
$Fe^{3+} + e^- \rightarrow Fe^{2+}$	Pt	2.5×10^{-3}	0.58

* More values are given in the *Data section*.

densities because the consumption of electroactive species close to the electrode results in a concentration gradient; diffusion of the species towards the electrode from the bulk is slow and may become rate-determining. A larger overpotential is then needed to produce a given current. This effect is called **concentration polarization** and its contribution to the total overpotential is called the **polarization overpotential**, η^c.

Consider a case for which the concentration polarization dominates all the rate processes and a redox couple of the type M^{z+},M with the reduction $M^{z+} + z\,e^- \rightarrow M$. Under zero-current conditions, when the net current density is zero, the electrode potential is related to the activity, a, of the ions in the solution by the Nernst equation (eqn 7.29):

$$E = E^{\ominus} + \frac{RT}{zF} \ln a \tag{25.48}$$

As remarked earlier, electrode kinetics are normally studied using a large excess of support electrolyte so as to keep the mean activity coefficients approximately constant. Therefore, the constant activity coefficient in $a = \gamma c$ may be absorbed into E, and we write the **formal potential**, $E°$, of the electrode as

$$E° = E^{\ominus} + \frac{RT}{zF} \ln \gamma \tag{25.49}$$

Then the electrode potential is

$$E = E° + \frac{RT}{zF} \ln c \tag{25.50}$$

When the cell is producing current, the active ion concentration at the OHP changes to c' and the electrode potential changes to

$$E' = E° + \frac{RT}{zF} \ln c' \tag{25.51}$$

The concentration overpotential is therefore

$$\eta^c = E' + E = \frac{RT}{zF} \ln\left(\frac{c'}{c}\right) \tag{25.52}$$

We now suppose that the solution has its bulk concentration, c, up to a distance δ from the outer Helmholtz plane, and then falls linearly to c' at the plane itself. This **Nernst diffusion layer** is illustrated in Fig. 25.42. The thickness of the Nernst layer (which is typically 0.1 mm, and strongly dependent on the condition of hydrodynamic flow due to any stirring or convective effects) is quite different from that of the electric double layer (which is typically less than 1 nm, and unaffected by stirring). The concentration gradient through the Nernst layer is

$$\frac{dc}{dx} = \frac{c' - c}{\delta} \tag{25.53}$$

This gradient gives rise to a flux of ions towards the electrode, which replenishes the cations as they are reduced. The (molar) flux, J, is proportional to the concentration gradient, and according to Fick's first law (Section 21.4)

$$J = -D\left(\frac{\partial c}{\partial x}\right) \tag{25.54}$$

Therefore, the particle flux towards the electrode is

$$J = D\frac{c - c'}{\delta} \tag{25.55}$$

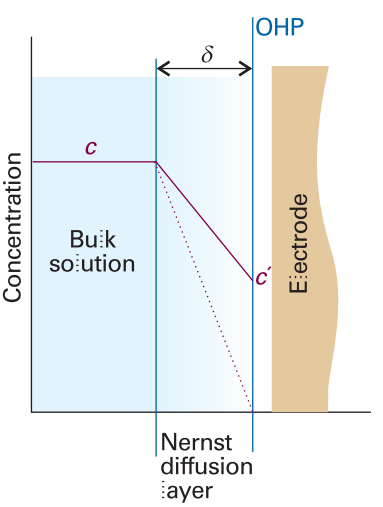

Fig. 25.42 In a simple model of the Nernst diffusion layer there is a linear variation in concentration between the bulk and the outer Helmholtz plane; the thickness of the layer depends strongly on the state of flow of the fluid. Note that the diffusion layer is much thicker relative to the OHP than shown here.

The cathodic current density towards the electrode is the product of the particle flux and the charge transferred per mole of ions, zF:

$$j = zFJ = zFD\frac{c - c'}{\delta} \tag{25.56}$$

For instance, for the couple $[Fe(CN)_6]^{2-}/[Fe(CN)_6]^{3-}$, $z = 1$, but for Fe^{3+}/Fe, $z = 3$. The maximum rate of diffusion across the Nernst layer occurs when the gradient is steepest, which is when $c' = 0$. This concentration occurs when an electron from an ion that diffuses across the layer is snapped over the activation barrier and on to the electrode. No flow of current can exceed the **limiting current density**, j_{lim}, which is given by

$$j_{lim} = zFJ_{lim} = \frac{zFDc}{\delta} \tag{25.57a}$$

By using the Nernst–Einstein equation (eqn 21.65, written as $D = RT\lambda/z^2F^2$), we can express j_{lim} in terms of the ionic conductivity λ:

$$j_{lim} = \frac{cRT\lambda}{zF\delta} \tag{25.57b}$$

Illustration 25.3 *Estimating the limiting current density*

Consider an electrode in a 0.10 M $Cu^{2+}(aq)$ unstirred solution in which the thickness of the diffusion layer is about 0.3 mm. With $\lambda = 107$ S cm^2 mol^{-1} (Table 21.4), $\delta = 0.3$ mm, $c = 0.10$ mol dm^{-3}, $z = 2$, and $T = 298$ K, it follows from eqn 25.57b that $j_{lim} = 5$ mA cm^{-2}. The result implies that the current towards an electrode of area 1 cm^2 electrode cannot exceed 5 mA in this (unstirred) solution.

Self-test 25.8 Evaluate the limiting current density for an $Ag(s)|Ag^+(aq)$ electrode in 0.010 mol dm^{-3} $Ag^+(aq)$ at 298 K. Take $\delta = 0.03$ mm. [5 mA cm^{-2}]

It follows from eqn 25.56 that the concentration c' is related to the current density at the double layer by

$$c' = c - \frac{j\delta}{zFD} \tag{25.58}$$

Hence, as the current density is increased, the concentration falls below the bulk value. However, this decline in concentration is small when the diffusion constant is large, for then the ions are very mobile and can quickly replenish any ions that have been removed.

Finally, we substitute eqn 25.58 into eqn 25.52 and obtain the following expressions for the overpotential in terms of the current density, and vice versa:

$$\eta^c = \frac{RT}{zF}\ln\left(1 - \frac{j\delta}{zcFD}\right) \tag{25.59a}$$

$$j = \frac{zcFD}{\delta}(1 - e^{zf\eta^c}) \tag{25.59b}$$

(b) Experimental techniques

The kind of output from **linear-sweep voltammetry** is illustrated in Fig. 25.43. Initially, the absolute value of the potential is low, and the cathodic current is due to the

migration of ions in the solution. However, as the potential approaches the reduction potential of the reducible solute, the cathodic current grows. Soon after the potential exceeds the reduction potential the current rises and reaches a maximum value (as specified in eqn 25.57). This maximum current is proportional to the molar concentration of the species, so that concentration can be determined from the peak height after subtraction of an extrapolated baseline. In **differential pulse voltammetry** the current is monitored before and after a pulse of potential is applied, and the processed output is the slope of a curve like that obtained by linear-sweep voltammetry (Fig. 25.44). The area under the curve (in effect, the integral of the derivative displayed in the illustration) is proportional to the concentration of the species.

In **cyclic voltammetry** the potential is applied in a sawtooth manner to the working electrode and the current is monitored. A typical cyclic voltammogram is shown in Fig. 25.45. The shape of the curve is initially like that of a linear sweep experiment, but after reversal of the sweep there is a rapid change in current on account of the high concentration of oxidizable species close to the electrode that were generated on the reductive sweep. When the potential is close to the value required to oxidize the reduced species, there is a substantial anodic current until all the oxidation is complete, and the current returns to zero.

When the reduction reaction at the electrode can be reversed, as in the case of the $[Fe(CN)_6]^{3-}/[Fe(CN)_6]^{4-}$ couple, the cyclic voltammogram is broadly symmetric about the standard potential of the couple (as in Fig. 25.45b). The scan is initiated with $[Fe(CN)_6]^{3-}$ present in solution and, as the potential approaches $E^\ominus$ for the couple, the $[Fe(CN)_6]^{3-}$ near the electrode is reduced and current begins to flow. As the potential continues to change, the cathodic current begins to decline again because all

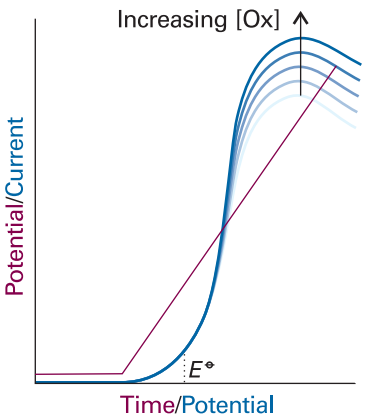

Fig. 25.43 The change of potential with time and the resulting current/potential curve in a voltammetry experiment. The peak value of the current density is proportional to the concentration of electroactive species (for instance, [Ox]) in solution.

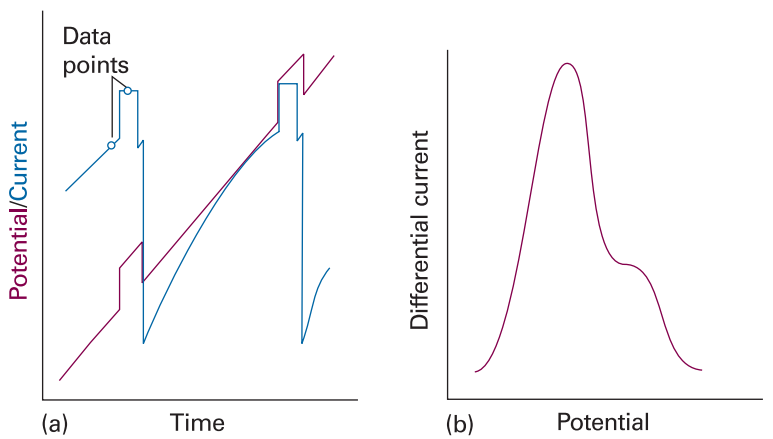

Fig. 25.44 A differential pulse voltammetry experiment. (a) The potential is swept linearly as a mercury droplet grows on the end of a capillary dipping into the sample and then pulsed as shown by the purple line. The resulting current is shown as the blue line and is sampled at the two points shown. (b) The data output is obtained as the difference of the currents at the two sampled points.

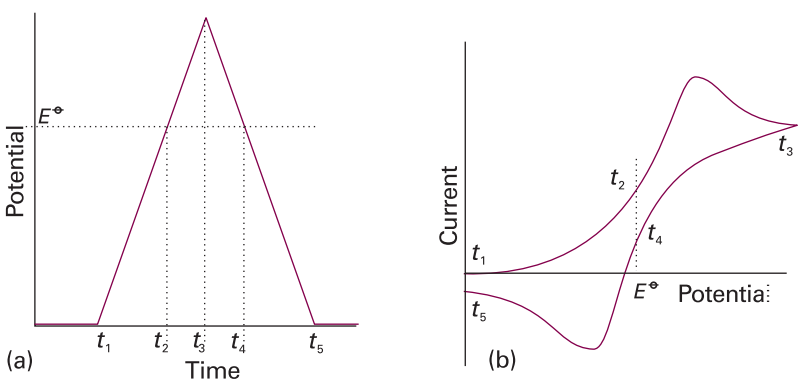

Fig. 25.45 (a) The change of potential with time and (b) the resulting current/potential curve in a cyclic voltammetry experiment.

the $[Fe(CN)_6]^{3-}$ near the electrode has been reduced and the current reaches its limiting value. The potential is now returned linearly to its initial value, and the reverse series of events occurs with the $[Fe(CN)_6]^{4-}$ produced during the forward scan now undergoing oxidation. The peak of current lies on the other side of $E^{\ominus}$, so the species present and its standard potential can be identified, as indicated in the illustration, by noting the locations of the two peaks.

The overall shape of the curve gives details of the kinetics of the electrode process and the change in shape as the rate of change of potential is altered gives information on the rates of the processes involved. For example, the matching peak on the return phase of the sawtooth change of potential may be missing, which indicates that the oxidation (or reduction) is irreversible. The appearance of the curve may also depend on the timescale of the sweep for, if the sweep is too fast, some processes might not have time to occur. This style of analysis is illustrated in the following example.

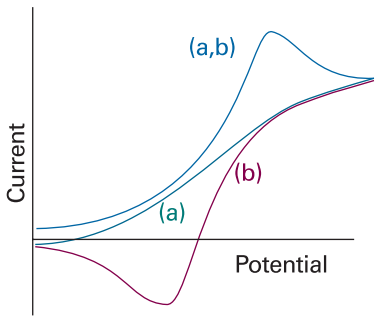

Fig. 25.46 (a) When a non-reversible step in a reaction mechanism has time to occur, the cyclic voltammogram may not show the reverse oxidation or reduction peak. (b) However, if the rate of sweep is increased, the return step may be caused to occur before the irreversible step has had time to intervene, and a typical 'reversible' voltammogram is obtained.

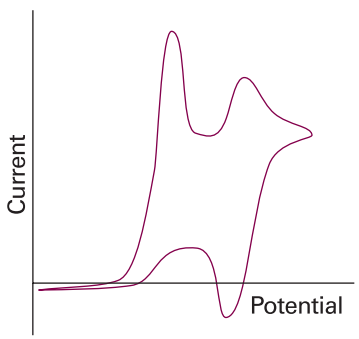

Fig. 25.47 The cyclic voltammogram referred to in Self-test 25.9.

Example 25.5 *Analysing a cyclic voltammetry experiment*

The electroreduction of *p*-bromonitrobenzene in liquid ammonia is believed to occur by the following mechanism:

$$BrC_6H_4NO_2 + e^- \rightarrow BrC_6H_4NO_2^-$$
$$BrC_6H_4NO_2^- \rightarrow \cdot C_6H_4NO_2 + Br^-$$
$$\cdot C_6H_4NO_2 + e^- \rightarrow C_6H_4NO_2^-$$
$$C_6H_4NO_2^- + H^+ \rightarrow C_6H_5NO_2$$

Suggest the likely form of the cyclic voltammogram expected on the basis of this mechanism.

Method Decide which steps are likely to be reversible on the timescale of the potential sweep: such processes will give symmetrical voltammograms. Irreversible processes will give unsymmetrical shapes because reduction (or oxidation) might not occur. However, at fast sweep rates, an intermediate might not have time to react, and a reversible shape will be observed.

Answer At slow sweep rates, the second reaction has time to occur, and a curve typical of a two-electron reduction will be observed, but there will be no oxidation peak on the second half of the cycle because the product, $C_6H_5NO_2$, cannot be oxidized (Fig. 25.46a). At fast sweep rates, the second reaction does not have time to take place before oxidation of the $BrC_6H_4NO_2^-$ intermediate starts to occur during the reverse scan, so the voltammogram will be typical of a reversible one-electron reduction (Fig. 25.46b).

Self-test 25.9 Suggest an interpretation of the cyclic voltammogram shown in Fig. 25.47. The electroactive material is ClC_6H_4CN in acid solution; after reduction to $ClC_6H_4CN^-$, the radical anion may form C_6H_5CN irreversibly.

$$[ClC_6H_4CN + e^- \rightleftharpoons ClC_6H_4CN^-,$$
$$ClC_6H_4CN^- + H^+ + e^- \rightarrow C_6H_5CN + Cl^-,\ C_6H_5CN + e^- \rightleftharpoons C_6H_5CN^-]$$

25.11 Electrolysis

To induce current to flow through an electrolytic cell and bring about a nonspontaneous cell reaction, the applied potential difference must exceed the zero-current potential by at least the **cell overpotential**. The cell overpotential is the sum of the overpotentials at the two electrodes and the ohmic drop (IR_s, where R_s is the internal

resistance of the cell) due to the current through the electrolyte. The additional potential needed to achieve a detectable rate of reaction may need to be large when the exchange current density at the electrodes is small. For similar reasons, a working galvanic cell generates a smaller potential than under zero-current conditions. In this section we see how to cope with both aspects of the overpotential.

The relative rates of gas evolution or metal deposition during electrolysis can be estimated from the Butler–Volmer equation and tables of exchange current densities. From eqn 25.46 and assuming equal transfer coefficients, we write the ratio of the cathodic currents as

$$\frac{j'}{j} = \frac{j'_0}{j_0} e^{(\eta - \eta')\alpha f} \tag{25.60}$$

where j' is the current density for electrodeposition and j is that for gas evolution, and j'_0 and j_0 are the corresponding exchange current densities. This equation shows that metal deposition is favoured by a large exchange current density and relatively high gas evolution overpotential (so $\eta - \eta'$ is positive and large). Note that $\eta < 0$ for a cathodic process, so $-\eta' > 0$.

The exchange current density depends strongly on the nature of the electrode surface, and changes in the course of the electrodeposition of one metal on another. A very crude criterion is that significant evolution or deposition occurs only if the overpotential exceeds about 0.6 V.

Self-test 25.10 Deduce an expression for the ratio when the hydrogen evolution is limited by transport across a diffusion layer. $[j'/j = (\delta j'_0/cFD)e^{-\alpha\eta' f}]$

A glance at Table 25.6 shows the wide range of exchange current densities for a metal/hydrogen electrode. The most sluggish exchange currents occur for lead and mercury, and the value of 1 pA cm^{-2} corresponds to a monolayer of atoms being replaced in about 5 years. For such systems, a high overpotential is needed to induce significant hydrogen evolution. In contrast, the value for platinum (1 mA cm^{-2}) corresponds to a monolayer being replaced in 0.1 s, so gas evolution occurs for a much lower overpotential.

The exchange current density also depends on the crystal face exposed. For the deposition of copper on copper, the (100) face has $j_0 = 1$ mA cm^{-2}, so for the same overpotential the (100) face grows at 2.5 times the rate of the (111) face, for which $j_0 = 0.4$ mA cm^{-2}.

25.12 Working galvanic cells

In working galvanic cells (those not balanced against an external potential), the overpotential leads to a smaller potential than under zero-current conditions. Furthermore, we expect the cell potential to decrease as current is generated because it is then no longer working reversibly and can therefore do less than maximum work.

We shall consider the cell $M|M^+(aq)\|M'^+(aq)|M'$ and ignore all the complications arising from liquid junctions. The potential of the cell is $E' = \Delta\phi_R - \Delta\phi_L$. Because the cell potential differences differ from their zero-current values by overpotentials, we can write $\Delta\phi_X = E_X + \eta_X$, where X is L or R for the left or right electrode, respectively. The cell potential is therefore

$$E' = E + \eta_R - \eta_L \tag{25.61a}$$

To avoid confusion about signs (η_R is negative, η_L is positive) and to emphasize that a working cell has a lower potential than a zero-current cell, we shall write this expression as

$$E' = E - |\eta_R| - |\eta_L| \tag{25.61b}$$

with E the cell emf. We should also subtract the ohmic potential difference IR_s, where R_s is the cell's internal resistance:

$$E' = E - |\eta_R| - |\eta_L| - IR_s \tag{25.61c}$$

The ohmic term is a contribution to the cell's irreversibility—it is a thermal dissipation term—so the sign of IR_s is always such as to reduce the potential in the direction of zero.

The overpotentials in eqn 25.61 can be calculated from the Butler–Volmer equation for a given current, I, being drawn. We shall simplify the equations by supposing that the areas, A, of the electrodes are the same, that only one electron is transferred in the rate-determining steps at the electrodes, that the transfer coefficients are both $\frac{1}{2}$, and that the high-overpotential limit of the Butler–Volmer equation may be used. Then from eqns 25.46 and 25.61c we find

$$E' = E - IR_s - \frac{4RT}{F}\ln\left(\frac{I}{A\bar{j}}\right) \qquad \bar{j} = (j_{0L}j_{0R})^{1/2} \tag{25.62}$$

where j_{0L} and j_{0R} are the exchange current densities for the two electrodes.

The concentration overpotential also reduces the cell potential. If we use the Nernst diffusion layer model for each electrode, the total change of potential arising from concentration polarization is given by eqn 25.59 as

$$E' = E - \frac{RT}{zF}\ln\left\{\left(1 - \frac{I}{Aj_{\text{lim,L}}}\right)\left(1 - \frac{I}{Aj_{\text{lim,R}}}\right)\right\} \tag{25.63}$$

This contribution can be added to the one in eqn 25.62 to obtain a full (but still very approximate) expression for the cell potential when a current I is being drawn:

$$E' = E - IR_s - \frac{2RT}{zF}\ln g(I) \tag{25.64a}$$

with

$$g(I) = \left(\frac{I}{A\bar{j}}\right)^{2z}\left\{\left(1 - \frac{I}{Aj_{\text{lim,L}}}\right)\left(1 - \frac{I}{Aj_{\text{lim,R}}}\right)\right\}^{1/2} \tag{25.64b}$$

This equation depends on a lot of parameters, but an example of its general form is given in Fig. 25.48. Notice the very steep decline of working potential when the current is high and close to the limiting value for one of the electrodes.

Because the power, P, supplied by a galvanic cell is IE', from eqn 25.64 we can write

$$P = IE - I^2R_s - \frac{2IRT}{zF}\ln g(I) \tag{25.65}$$

The first term on the right is the power that would be produced if the cell retained its zero-current potential when delivering current. The second term is the power generated uselessly as heat as a result of the resistance of the electrolyte. The third term is the reduction of the potential at the electrodes as a result of drawing current.

The general dependence of power output on the current drawn is shown in Fig. 25.48 as the purple line. Notice how maximum power is achieved just before the concentration polarization quenches the cell's performance. Information of this kind is essential if the optimum conditions for operating electrochemical devices are to be found and their performance improved.

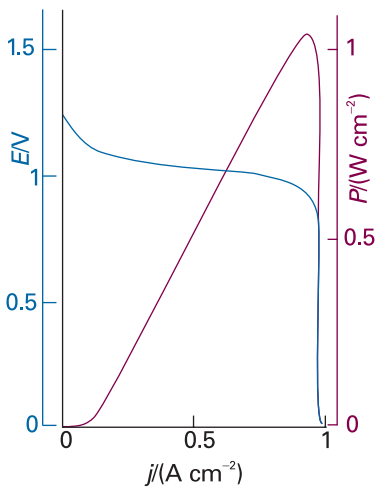

Fig. 25.48 The dependence of the potential of a working galvanic cell on the current density being drawn (blue line) and the corresponding power output (purple line) calculated by using eqns 25.64 and 25.65, respectively. Notice the sharp decline in power just after the maximum.

Exploration Using mathematical software, and electronic spreadsheet, or the interactive applets found in the *Living graphs* section of the text's web site, confirm that the sharp decline in potential and power observed in Fig. 25.48 is true for any value of R_s.

Electric storage cells operate as galvanic cells while they are producing electricity but as electrolytic cells while they are being charged by an external supply. The lead–acid battery is an old device, but one well suited to the job of starting cars (and the only one available). During charging the cathode reaction is the reduction of Pb^{2+} and its deposition as lead on the lead electrode. Deposition occurs instead of the reduction of the acid to hydrogen because the latter has a low exchange current density on lead. The anode reaction during charging is the oxidation of Pb(II) to Pb(IV), which is deposited as the oxide PbO_2. On discharge, the two reactions run in reverse. Because they have such high exchange current densities the discharge can occur rapidly, which is why the lead battery can produce large currents on demand.

IMPACT ON TECHNOLOGY

I25.3 Fuel cells

A fuel cell operates like a conventional galvanic cell with the exception that the reactants are supplied from outside rather than forming an integral part of its construction. A fundamental and important example of a fuel cell is the hydrogen/oxygen cell, such as the ones used in space missions (Fig. 25.49). One of the electrolytes used is concentrated aqueous potassium hydroxide maintained at 200°C and 20–40 atm; the electrodes may be porous nickel in the form of sheets of compressed powder. The cathode reaction is the reduction

$$O_2(g) + 2\,H_2O(l) + 4\,e^- \rightarrow 4\,OH^-(aq) \qquad E^\ominus = +0.40\ V$$

and the anode reaction is the oxidation

$$H_2(g) + 2\,OH^-(aq) \rightarrow 2\,H_2O(l) + 2\,e^-$$

For the corresponding reduction, $E^\ominus = -0.83$ V. Because the overall reaction

$$2\,H_2(g) + O_2(g) \rightarrow 2\,H_2O(l) \qquad E^\ominus = +1.23\ V$$

is exothermic as well as spontaneous, it is less favourable thermodynamically at 200°C than at 25°C, so the cell potential is lower at the higher temperature. However, the increased pressure compensates for the increased temperature, and $E \approx +1.2$ V at 200°C and 40 atm.

One advantage of the hydrogen/oxygen system is the large exchange current density of the hydrogen reaction. Unfortunately, the oxygen reaction has an exchange current density of only about 0.1 nA cm^{-2}, which limits the current available from the cell. One way round the difficulty is to use a catalytic surface (to increase j_0) with a large surface area. One type of highly developed fuel cell has phosphoric acid as the electrolyte and operates with hydrogen and air at about 200°C; the hydrogen is obtained from a reforming reaction on natural gas:

Anode: $2\,H_2(g) \rightarrow 4\,H^+(aq) + 4\,e^-$

Cathode: $O_2(g) + 4\,H^+(aq) + 4\,e^- \rightarrow 2\,H_2O(l)$

This fuel cell has shown promise for *combined heat and power systems* (CHP systems). In such systems, the waste heat is used to heat buildings or to do work. Efficiency in a CHP plant can reach 80 per cent. The power output of batteries of such cells has reached the order of 10 MW. Although hydrogen gas is an attractive fuel, it has disadvantages for mobile applications: it is difficult to store and dangerous to handle. One possibility for portable fuel cells is to store the hydrogen in carbon nanotubes (*Impact* 20.2). It has been shown that carbon nanofibres in herringbone patterns can store huge amounts of hydrogen and result in an energy density (the magnitude of the released energy divided by the volume of the material) twice that of gasoline.

Cells with molten carbonate electrolytes at about 600°C can make use of natural gas directly. Solid-state electrolytes are also used. They include one version in which the

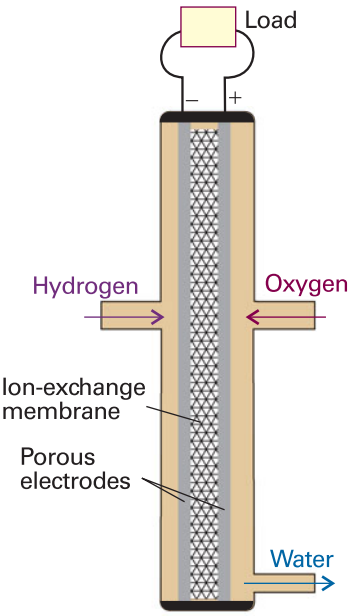

Fig. 25.49 A single cell of a hydrogen/oxygen fuel cell. In practice, a stack of many cells is used.

electrolyte is a solid polymeric ionic conductor at about 100°C, but in current versions it requires very pure hydrogen to operate successfully. Solid ionic conducting oxide cells operate at about 1000°C and can use hydrocarbons directly as fuel. Until these materials have been developed, one attractive fuel is methanol, which is easy to handle and is rich in hydrogen atoms:

Anode: $CH_3OH(l) + 6\ OH^-(aq) \rightarrow 5\ H_2O(l) + CO_2(g) + 6\ e^-$

Cathode: $O_2(g) + 4\ e^- + 2\ H_2O(l) \rightarrow 4\ OH^-(aq)$

One disadvantage of methanol, however, is the phenomenon of 'electro-osmotic drag' in which protons moving through the polymer electrolyte membrane separating the anode and cathode carry water and methanol with them into the cathode compartment where the potential is sufficient to oxidize CH_3OH to CO_2, so reducing the efficiency of the cell. Solid ionic conducting oxide cells operate at about 1000°C and can use hydrocarbons directly as fuel.

A *biofuel cell* is like a conventional fuel cell but in place of a platinum catalyst it uses enzymes or even whole organisms. The electricity will be extracted through organic molecules that can support the transfer of electrons. One application will be as the power source for medical implants, such as pacemakers, perhaps using the glucose present in the bloodstream as the fuel.

25.13 Corrosion

A thermodynamic warning of the likelihood of corrosion is obtained by comparing the standard potentials of the metal reduction, such as

$$Fe^{2+}(aq) + 2\ e^- \rightarrow Fe(s) \qquad E^\ominus = -0.44\ V$$

with the values for one of the following half-reactions:

In acidic solution:

(a) $2\ H^+(aq) + 2\ e^- \rightarrow H_2(g)$ $\qquad E^\ominus = 0$

(b) $4\ H^+(aq) + O_2(g) + 4\ e^- \rightarrow 2\ H_2O(l)$ $\qquad E^\ominus = +1.23\ V$

In basic solution:

(c) $2\ H_2O(l) + O_2(g) + 4\ e^- \rightarrow 4\ OH^-(aq)$ $\qquad E^\ominus = +0.40\ V$

Because all three redox couples have standard potentials more positive than $E^\ominus(Fe^{2+}/Fe)$, all three can drive the oxidation of iron to iron(II). The electrode potentials we have quoted are standard values, and they change with the pH of the medium. For the first two:

$$E(a) = E^\ominus(a) + (RT/F)\ln a(H^+) = -(0.059\ V)pH$$

$$E(b) = E^\ominus(b) + (RT/F)\ln a(H^+) = 1.23\ V - (0.059\ V)pH$$

These expressions let us judge at what pH the iron will have a tendency to oxidize (see Chapter 7). A thermodynamic discussion of corrosion, however, only indicates whether a tendency to corrode exists. If there is a thermodynamic tendency, we must examine the kinetics of the processes involved to see whether the process occurs at a significant rate.

A model of a corrosion system is shown in Fig. 25.50a. It can be taken to be a drop of slightly acidic (or basic) water containing some dissolved oxygen in contact with the metal. The oxygen at the edges of the droplet, where the O_2 concentration is higher, is reduced by electrons donated by the iron over an area A. Those electrons are replaced by others released elsewhere as $Fe \rightarrow Fe^{2+} + 2\ e^-$. This oxidative release occurs over an area A' under the oxygen-deficient inner region of the droplet. The droplet acts as a short-circuited galvanic cell (Fig. 25.50b).

The rate of corrosion is measured by the current of metal ions leaving the metal surface in the anodic region. This flux of ions gives rise to the **corrosion current**, I_{corr}, which can be identified with the anodic current, I_a. We show in the justification below that the corrosion current is related to the cell potential of the corrosion couple by

$$I_{corr} = \bar{j}_0 \bar{A} e^{fE/4} \qquad \bar{j}_0 = (j_0 j_0')^{1/2} \qquad \bar{A} = (AA')^{1/2} \tag{25.66}$$

Justification 25.1 *The corrosion current*

Because any current emerging from the anodic region must find its way to the cathodic region, the cathodic current, I_c, and the anodic current, I_a, must both be equal to the corrosion current. In terms of the current densities at the oxidation and reduction sites, j and j', respectively, we can write

$$I_{corr} = jA = j'A' = (jj'AA')^{1/2} = \bar{j}\bar{A} \qquad \bar{j} = (jj')^{1/2} \qquad \bar{A} = (AA')^{1/2} \tag{25.67}$$

The Butler–Volmer equation is now used to express the current densities in terms of overpotentials. For simplicity we assume that the overpotentials are large enough for the high-overpotential limit (eqn 25.46, $j = -j_0 e^{-\alpha f\eta}$) to apply, that polarization overpotential can be neglected, that the rate-determining step is the transfer of a single electron, and that the transfer coefficients are $\frac{1}{2}$. We also assume that, since the droplet is so small, there is negligible potential difference between the cathode and anode regions of the solution. Moreover, because it is short-circuited by the metal, the potential of the metal is the same in both regions, and so the potential difference between the metal and the solution is the same in both regions too; it is denoted $\Delta\phi_{corr}$. The overpotentials in the two regions are therefore $\eta = \Delta\phi_{corr} - \Delta\phi$ and $\eta' = \Delta\phi_{corr} - \Delta\phi'$, and the current densities are

$$j = j_0 e^{\eta f/2} = j_0 e^{f\Delta\phi_{corr}/2} e^{-f\Delta\phi/2} \qquad j' = j_0' e^{-\eta' f/2} = j_0' e^{-f\Delta\phi_{corr}/2} e^{f\Delta\phi'/2}$$

These expressions can be substituted into the expression for I_{corr} and $\Delta\phi' - \Delta\phi$ replaced by the difference of electrode potentials E to give eqn 25.66.

The effect of the exchange current density on the corrosion rate can be seen by considering the specific case of iron in contact with acidified water. Thermodynamically, either hydrogen or oxygen reduction reaction (a) or (b) on p. 946 is effective. However, the exchange current density of reaction (b) on iron is only about 10^{-14} A cm^{-2}, whereas for (a) it is 10^{-6} A cm^{-2}. The latter therefore dominates kinetically, and iron corrodes by hydrogen evolution in acidic solution.

For corrosion reactions with similar exchange current densities, eqn 25.66 predicts that the rate of corrosion is high when E is large. That is, rapid corrosion can be expected when the oxidizing and reducing couples have widely differing electrode potentials.

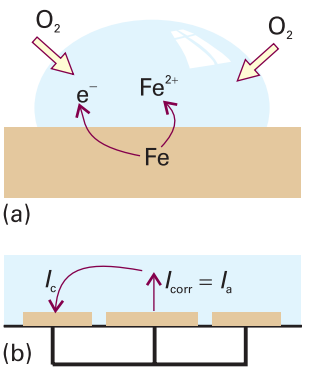

Fig. 25.50 (a) A simple version of the corrosion process is that of a droplet of water, which is oxygen rich near its boundary with air. The oxidation of the iron takes place in the region away from the oxygen because the electrons are transported through the metal. (b) The process may be modelled as a short-circuited electrochemical cell.

IMPACT ON TECHNOLOGY

I25.4 Protecting materials against corrosion

Several techniques for inhibiting corrosion are available. First, from eqn 25.66 we see that the rate of corrosion depends on the surfaces exposed: if either A or A' is zero, then the corrosion current is zero. This interpretation points to a trivial, yet often effective, method of slowing corrosion: cover the surface with some impermeable layer, such as paint, which prevents access of damp air. Paint also increases the effective solution resistance between the cathode and anode patches on the surface. Unfortunately, this protection fails disastrously if the paint becomes porous. The oxygen then has access to the exposed metal and corrosion continues beneath the paintwork. Another form of surface coating is provided by **galvanizing**, the coating of an iron object with zinc. Because the latter's standard potential is −0.76 V, which is more negative than that of the iron couple, the corrosion of zinc is thermodynamically

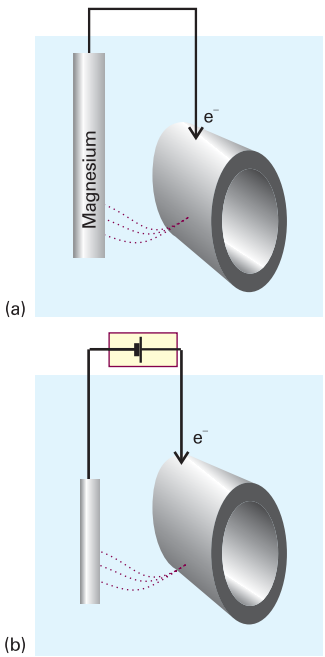

Fig. 25.51 (a) In cathodic protection an anode of a more strongly reducing metal is sacrificed to maintain the integrity of the protected object (for example, a pipeline, bridge, or boat). (b) In impressed-current cathodic protection electrons are supplied from an external cell so that the object itself is not oxidized. The broken lines depict the completed circuit through the soil.

favoured and the iron survives (the zinc survives because it is protected by a hydrated oxide layer). In contrast, tin plating leads to a very rapid corrosion of the iron once its surface is scratched and the iron exposed because the tin couple ($E^\ominus = -0.14$ V) oxidizes the iron couple ($E^\ominus = -0.44$ V). Some oxides are inert kinetically in the sense that they adhere to the metal surface and form an impermeable layer over a fairly wide pH range. This **passivation**, or kinetic protection, can be seen as a way of decreasing the exchange currents by sealing the surface. Thus, aluminium is inert in air even though its standard potential is strongly negative (−1.66 V).

Another method of protection is to change the electric potential of the object by pumping in electrons that can be used to satisfy the demands of the oxygen reduction without involving the oxidation of the metal. In **cathodic protection**, the object is connected to a metal with a more negative standard potential (such as magnesium, −2.36 V). The magnesium acts as a **sacrificial anode**, supplying its own electrons to the iron and becoming oxidized to Mg^{2+} in the process (Fig. 25.51a). A block of magnesium replaced occasionally is much cheaper than the ship, building, or pipeline for which it is being sacrificed. In **impressed-current cathodic protection** (Fig. 25.51b) an external cell supplies the electrons and eliminates the need for iron to transfer its own.

Table 25.7 Summary of acronyms

AES	Auger electron spectroscopy
AFM	Atomic force microscopy
BET isotherm	Brunauer–Emmett–Teller isotherm
EELS	Electron energy-loss spectroscopy
ER mechanism	Eley–Rideal mechanism
ESCA	Electron spectroscopy for chemical analysis
FIM	Field-ionization microscopy
HREELS	High-resolution electron energy-loss spectroscopy
IHP	Inner Helmholtz plane
LEED	Low-energy electron diffraction
LH mechanism	Langmuir–Hinshelwood mechanism
MBRS	Molecular beam reactive scattering
MBS	Molecular beam scattering
OHP	Outer Helmholtz plane
QCM	Quartz crystal microbalance
RAIRS	Reflection–absorption infrared spectroscopy
SAM	Scanning Auger electron microscopy
SAM	Self-assembled monolayer
SEM	Scanning electron microscopy
SERS	Surface-enhanced Raman scattering
SEXAFS	Surface-extended X-ray absorption fine structure spectroscopy
SHG	Second harmonic generation
SIMS	Secondary ion mass spectrometry
SPM	Scanning probe microscopy
SPR	Surface plasmon resonance
STM	Scanning tunnelling microscopy
TDS	Thermal desorption spectroscopy
TPD	Temperature programmed desorption
UHV	Ultra-high vacuum
UPS	Ultraviolet photoemission spectroscopy
XPS	X-ray photoemission spectroscopy

Checklist of key ideas

- ☐ 1. Adsorption is the attachment of molecules to a surface; the substance that adsorbs is the adsorbate and the underlying material is the adsorbent or substrate. The reverse of adsorption is desorption.
- ☐ 2. The collision flux, Z_W, of gas molecules bombarding a solid surface is related to the gas pressure by $Z_W = p/(2\pi mkT)^{1/2}$.
- ☐ 3. Techniques for studying surface composition and structure include scanning electron microscopy (SEM), scanning probe microscopy (STM), photoemission spectroscopy, sescondary-ion mass spectrometry, surface-enhanced Raman scattering (SERS), Auger electron spectroscopy (AES), low energy electron diffraction (LEED), and molecular beam scattering (MBS).
- ☐ 4. The fractional coverage, θ, is the ratio of the number of occupied sites to the number of available sites.
- ☐ 5. Techniques for studying the rates of surface processes include flash desorption, biosensor analysis, second harmonic generation (SHG), gravimetry by using a quartz crystal microbalance (QCM), and molecular beam reactive scattering (MRS).
- ☐ 6. Physisorption is adsorption by a van der Waals interaction; chemisorption is adsorption by formation of a chemical (usually covalent) bond.
- ☐ 7. The Langmuir isotherm is a relation between the fractional coverage and the partial pressure of the adsorbate: $\theta = Kp/(1 + Kp)$.
- ☐ 8. The isosteric enthalpy of adsorption is determined from a plot of $\ln K$ against $1/T$.
- ☐ 9. The BET isotherm is an isotherm applicable when multilayer adsorption is possible: $V/V_{mon} = cz/(1 - z)\{1 - (1 - c)z\}$, with $z = p/p^*$.
- ☐ 10. The sticking probability, s, is the proportion of collisions with the surface that successfully lead to adsorption.
- ☐ 11. Desorption is an activated process with half-life $t_{1/2} = \tau_0 e^{E_d/RT}$; the desorption activation energy is measured by temperature-programmed desorption (TPD) or thermal desorption spectroscopy (TDS).
- ☐ 12. In the Langmuir–Hinshelwood mechanism (LH mechanism) of surface-catalysed reactions, the reaction takes place by encounters between molecular fragments and atoms adsorbed on the surface.
- ☐ 13. In the Eley–Rideal mechanism (ER mechanism) of a surface-catalysed reaction, a gas-phase molecule collides with another molecule already adsorbed on the surface.
- ☐ 14. An electrical double layer consists of a sheet of positive charge at the surface of the electrode and a sheet of negative charge next to it in the solution (or vice versa).
- ☐ 15. The Galvani potential difference is the potential difference between the bulk of the metal electrode and the bulk of the solution.
- ☐ 16. Models of the double layer include the Helmholtz layer model and the Gouy–Chapman model.
- ☐ 17. The current density, j, at an electrode is expressed by the Butler–Volmer equation, $j = j_0\{e^{(1-\alpha)f\eta} - e^{-\alpha f\eta}\}$, where η is the overpotential, $\eta = E' - E$, α is the transfer coefficient, and j_0 is the exchange-current density.
- ☐ 18. A Tafel plot is a plot of the logarithm of the current density against the overpotential: the slope gives the value of α and the intercept at $\eta = 0$ gives the exchange-current density.
- ☐ 19. Voltammetry is the study of the current through an electrode as a function of the applied potential difference. Experimental techniques include linear-sweep voltammetry, differential pulse voltammetry, and cyclic voltammetry.
- ☐ 20. To induce current to flow through an electrolytic cell and bring about a nonspontaneous cell reaction, the applied potential difference must exceed the cell emf by at least the cell overpotential.
- ☐ 21. The corrosion current is a current proportional to the rate at which metal ions leave a metal surface in the anodic region during corrosion.

Further reading

Articles and texts

A.W. Adamson and A. Gast, *Physical chemistry of surfaces*. Wiley, New York (1997).

A.J. Bard and L.R. Faulkner, *Electrochemical methods: fundamentals and applications*. Wiley, New York (2000).

J.O'M. Bockris, R.E. White, and B.E. Conway (ed.), *Modern aspects of electrochemistry*. Vol. 33. Plenum, New York (1999).

G. Ertl, H. Knözinger, and J. Weitkamp, *Handbook of heterogeneous catalysis*. VCH, Weinheim (1997).

M.G. Fontanna and R.W. Staehle (ed.), *Advances in corrosion science and technology*. Plenum, New York (1980).

C.H. Hamann, W. Vielstich, and A. Hammett, *Electrochemistry*. Wiley–VCH, New York (1998).

J.C. Lindon, G.E. Tranter, and J.L. Holmes (ed.), *Encyclopedia of spectroscopy and spectrometry*. Academic Press, San Diego (2000).

N. Mizuno and M. Misono, Heterogeneous catalysis. *Chem. Rev.* **98**, 199 (1998).

G.A. Somorjai, Modern surface science and surface technologies: an introduction. *Chem. Rev.* **96**, 1223 (1996).

C.D.S. Tuck, *Modern battery construction*. Ellis Horwood, New York (1991).

J. Vickerman, *Surface analysis: techniques and applications*. Wiley, New York (1997).

Sources of data and information

C.M.A. Brett and A.M.O. Brett, *Electrode potentials*. Oxford Chemistry Primers, Oxford University Press (1998).

D. Linden (ed.), *Handbook of batteries and cells*. McGraw-Hill, New York (1984).

Further information

Further information 25.1 *The relation between electrode potential and the Galvani potential*

To demonstrate the relation between $\Delta\phi$ and E, consider the cell $Pt|H_2(g)|H^+(g)||M^+(aq)|M(s)$ and the half-reactions

$$M^+(aq) + e^- \rightarrow M(s) \qquad H^+(aq) + e^- \rightarrow \tfrac{1}{2}\,H_2(g)$$

The Gibbs energies of these two half-reactions can be expressed in terms of the chemical potentials, μ, of all the species. However, we must take into account the fact that the species are present in phases with different electric potentials. Thus, a cation in a region of positive potential has a higher chemical potential (is chemically more active in a thermodynamic sense) than in a region of zero potential.

The contribution of an electric potential to the chemical potential is calculated by noting that the electrical work of adding a charge ze to a region where the potential is ϕ is $ze\phi$, and therefore that the work per mole is $zF\phi$, where F is Faraday's constant. Because at constant temperature and pressure the maximum electrical work can be identified with the change in Gibbs energy (Section 7.7), the difference in chemical potential of an ion with and without the electrical potential present is $zF\phi$. The chemical potential of an ion in the presence of an electric potential is called its **electrochemical potential**, $\bar{\mu}$. It follows that

$$\bar{\mu} = \mu + zF\phi \qquad [25.68]$$

where μ is the chemical potential of the species when the electrical potential is zero. When $z = 0$ (a neutral species), the electrochemical potential is equal to the chemical potential.

To express the Gibbs energy for the half-reactions in terms of the electrochemical potentials of the species we note that the cations M^+ are in the solution where the inner potential is ϕ_S and the electrons are in the electrode where it is ϕ_M. It follows that

$$\begin{aligned}\Delta_r G_R &= \bar{\mu}(M) - \{\bar{\mu}(M^+) + \bar{\mu}(e^-)\}\\ &= \mu(M) - \{\mu(M^+) + F\phi_S + \mu(e^-) - F\phi_M\}\\ &= \mu(M) - \mu(M^+) - \mu(e^-) + F\Delta\phi_R\end{aligned}$$

where $\Delta\phi_R = \phi_M - \phi_S$ is the Galvani potential difference at the right-hand electrode. Likewise, in the hydrogen half-reaction, the electrons are in the platinum electrode at a potential ϕ_{Pt} and the H^+ ions are in the solution where the potential is ϕ_S:

$$\begin{aligned}\Delta_r G_L &= \tfrac{1}{2}\bar{\mu}(H_2) - \{\bar{\mu}(H^+) + \bar{\mu}(e^-)\}\\ &= \tfrac{1}{2}\mu(H_2) - \mu(H^+) - \mu(e^-) + F\Delta\phi_L\end{aligned}$$

where $\Delta\phi_L = \phi_{Pt} - \phi_S$ is the Galvani potential difference at the left-hand electrode.

The overall reaction Gibbs energy is

$$\begin{aligned}\Delta_r G_R - \Delta_r G_L &= \mu(M) + \mu(H^+) - \mu(M^+) - \tfrac{1}{2}\mu(H_2) + F(\Delta\phi_R - \Delta\phi_L)\\ &= \Delta_r G + F(\Delta\phi_R - \Delta\phi_L)\end{aligned}$$

where $\Delta_r G$ is the Gibbs energy of the cell reaction. When the cell is balanced against an external source of potential the entire system is at equilibrium. The overall reaction Gibbs energy is then zero (because its tendency to change is balanced against the external source of potential and overall there is stalemate), and the last equation becomes

$$0 = \Delta_r G + F(\Delta\phi_R - \Delta\phi_L)$$

which rearranges to

$$\Delta_r G = -F(\Delta\phi_R - \Delta\phi_L) \qquad (25.69)$$

If we compare this with the result established in Section 7.7 that $\Delta_r G = -FE$ and $E = E_R - E_L$, we can conclude that (ignoring the effects of any metal–platinum and liquid junction potentials that may be present in an actual cell)

$$E_R - E_L = \Delta\phi_R - \Delta\phi_L \qquad (25.70)$$

This is the result we wanted to show, for it implies that the Galvani potential difference at each electrode can differ from the electrode potential by a constant at most; that constant cancels when the difference is taken.

Discussion questions

25.1 (a) Distinguish between a step and a terrace. (b) Describe how steps and terraces can be formed by dislocations.

25.2 (a) Describe the advantages and limitations of each of the spectroscopic techniques designated by the acronyms AES, EELS, HREELS, RAIRS, SERS, SEXAFS, SHG, UPS, and XPS. (b) Describe the advantages and limitations of each of the microscopy, diffraction, and scattering techniques designated by the acronyms AFM, FIM, LEED, MBRS, MBS, SAM, SEM, and STM.

25.3 Distinguish between the following adsorption isotherms: Langmuir, BET, Temkin, and Freundlich.

25.4 Consider the analysis of surface plasmon resonance data (as in biosensor analysis) and discuss how a plot of a_0/R_{eq} against a_0 may be used to evaluate R_{max} and K.

25.5 Describe the essential features of the Langmuir–Hinshelwood, Eley–Rideal, and Mars van Krevelen mechanisms for surface-catalysed reactions.

25.6 Account for the dependence of catalytic activity of a surface on the strength of chemisorption, as shown in Fig. 25.28.

25.7 Discuss the unique physical and chemical properties of zeolites that make them useful heterogeneous catalysts.

25.8 (a) Discuss the main structural features of the electrical double layer. (b) Distinguish between the electrical double layer and the Nernst diffusion layer.

25.9 Define the terms in and limit the generality of the following expressions: (a) $j = j_0 f\eta$, (b) $j = j_0 e^{(1-\alpha)f\eta}$, and (c) $j = -j_0 e^{-\alpha f\eta}$.

25.10 Discuss the technique of cyclic voltammetry and account for the characteristic shape of a cyclic voltammogram, such as those shown in Figs. 25.45 and 25.46.

25.11 Discuss the principles of operation of a fuel cell.

25.12 Discuss the chemical origins of corrosion and useful strategies for preventing it.

Exercises

25.1a Calculate the frequency of molecular collisions per square centimetre of surface in a vessel containing (a) hydrogen, (b) propane at 25°C when the pressure is (i) 100 Pa, (ii) 0.10 μTorr.

25.1b Calculate the frequency of molecular collisions per square centimetre of surface in a vessel containing (a) nitrogen, (b) methane at 25°C when the pressure is (i) 10.0 Pa, (ii) 0.150 μTorr.

25.2a What pressure of argon gas is required to produce a collision rate of $4.5 \times 10^{20}\ s^{-1}$ at 425 K on a circular surface of diameter 1.5 mm?

25.2b What pressure of nitrogen gas is required to produce a collision rate of $5.00 \times 10^{19}\ s^{-1}$ at 525 K on a circular surface of diameter 2.0 mm?

25.3a Calculate the average rate at which He atoms strike a Cu atom in a surface formed by exposing a (100) plane in metallic copper to helium gas at 80 K and a pressure of 35 Pa. Crystals of copper are face-centred cubic with a cell edge of 361 pm.

25.3b Calculate the average rate at which He atoms strike an iron atom in a surface formed by exposing a (100) plane in metallic iron to helium gas at 100 K and a pressure of 24 Pa. Crystals of iron are body-centred cubic with a cell edge of 145 pm.

25.4a A monolayer of N_2 molecules (effective area 0.165 nm^2) is adsorbed on the surface of 1.00 g of an Fe/Al_2O_3 catalyst at 77 K, the boiling point of liquid nitrogen. Upon warming, the nitrogen occupies 2.86 cm^3 at 0°C and 760 Torr. What is the surface area of the catalyst?

25.4b A monolayer of CO molecules (effective area 0.165 nm^2) is adsorbed on the surface of 1.00 g of an Fe/Al_2O_3 catalyst at 77 K, the boiling point of liquid nitrogen. Upon warming, the carbon monoxide occupies 4.25 cm^3 at 0°C and 1.00 bar. What is the surface area of the catalyst?

25.5a The volume of oxygen gas at 0°C and 101 kPa adsorbed on the surface of 1.00 g of a sample of silica at 0°C was 0.284 cm^3 at 142.4 Torr and 1.430 cm^3 at 760 Torr. What is the value of V_{mon}?

25.5b The volume of gas at 20°C and 1.00 bar adsorbed on the surface of 1.50 g of a sample of silica at 0°C was 1.60 cm^3 at 52.4 kPa and 2.73 cm^3 at 104 kPa. What is the value of V_{mon}?

25.6a The enthalpy of adsorption of CO on a surface is found to be −120 kJ mol^{-1}. Estimate the mean lifetime of a CO molecule on the surface at 400 K.

25.6b The enthalpy of adsorption of ammonia on a nickel surface is found to be −155 kJ mol^{-1}. Estimate the mean lifetime of an NH_3 molecule on the surface at 500 K.

25.7a The average time for which an oxygen atom remains adsorbed to a tungsten surface is 0.36 s at 2548 K and 3.49 s at 2362 K. Find the activation energy for desorption. What is the pre-exponential factor for these tightly chemisorbed atoms?

25.7b The chemisorption of hydrogen on manganese is activated, but only weakly so. Careful measurements have shown that it proceeds 35 per cent faster at 1000 K than at 600 K. What is the activation energy for chemisorption?

25.8a The adsorption of a gas is described by the Langmuir isotherm with $K = 0.85\ kPa^{-1}$ at 25°C. Calculate the pressure at which the fractional surface coverage is (a) 0.15, (b) 0.95.

25.8b The adsorption of a gas is described by the Langmuir isotherm with $K = 0.777\ kPa^{-1}$ at 25°C. Calculate the pressure at which the fractional surface coverage is (a) 0.20, (b) 0.75.

25.9a A certain solid sample adsorbs 0.44 mg of CO when the pressure of the gas is 26.0 kPa and the temperature is 300 K. The mass of gas adsorbed when the pressure is 3.0 kPa and the temperature is 300 K is 0.19 mg. The Langmuir isotherm is known to describe the adsorption. Find the fractional coverage of the surface at the two pressures.

25.9b A certain solid sample adsorbs 0.63 mg of CO when the pressure of the gas is 36.0 kPa and the temperature is 300 K. The mass of gas adsorbed when the pressure is 4.0 kPa and the temperature is 300 K is 0.21 mg. The Langmuir isotherm is known to describe the adsorption. Find the fractional coverage of the surface at the two pressures.

25.10a For how long on average would an H atom remain on a surface at 298 K if its desorption activation energy were (a) 15 kJ mol^{-1}, (b) 150 kJ mol^{-1}? Take $\tau_0 = 0.10$ ps. For how long on average would the same atoms remain at 1000 K?

25.10b For how long on average would an atom remain on a surface at 400 K if its desorption activation energy were (a) 20 kJ mol^{-1}, (b) 200 kJ mol^{-1}? Take $\tau_0 = 0.12$ ps. For how long on average would the same atoms remain at 800 K?

25.11a A solid in contact with a gas at 12 kPa and 25°C adsorbs 2.5 mg of the gas and obeys the Langmuir isotherm. The enthalpy change when 1.00 mmol of the adsorbed gas is desorbed is +10.2 J. What is the equilibrium pressure for the adsorption of 2.5 mg of gas at 40°C?

25.11b A solid in contact with a gas at 8.86 kPa and 25°C adsorbs 4.67 mg of the gas and obeys the Langmuir isotherm. The enthalpy change when 1.00 mmol of the adsorbed gas is desorbed is +12.2 J. What is the equilibrium pressure for the adsorption of the same mass of gas at 45°C?

25.12a Hydrogen iodide is very strongly adsorbed on gold but only slightly adsorbed on platinum. Assume the adsorption follows the Langmuir isotherm and predict the order of the HI decomposition reaction on each of the two metal surfaces.

25.12b Suppose it is known that ozone adsorbs on a particular surface in accord with a Langmuir isotherm. How could you use the pressure dependence of the fractional coverage to distinguish between adsorption (a) without dissociation, (b) with dissociation into $O + O_2$, (c) with dissociation into O + O + O?

25.13a Nitrogen gas adsorbed on charcoal to the extent of 0.921 $cm^3\ g^{-1}$ at 490 kPa and 190 K, but at 250 K the same amount of adsorption was achieved only when the pressure was increased to 3.2 MPa. What is the enthalpy of adsorption of nitrogen on charcoal?

25.13b Nitrogen gas adsorbed on a surface to the extent of 1.242 $cm^3\ g^{-1}$ at 350 kPa and 180 K, but at 240 K the same amount of adsorption was achieved only when the pressure was increased to 1.02 MPa. What is the enthalpy of adsorption of nitrogen on the surface?

25.14a In an experiment on the adsorption of oxygen on tungsten it was found that the same volume of oxygen was desorbed in 27 min at 1856 K and 2.0 min at 1978 K. What is the activation energy of desorption? How long would it take for the same amount to desorb at (a) 298 K, (b) 3000 K?

25.14b In an experiment on the adsorption of ethene on iron it was found that the same volume of the gas was desorbed in 1856 s at 873 K and 8.44 s at 1012 K. What is the activation energy of desorption? How long would it take for the same amount of ethene to desorb at (a) 298 K, (b) 1500 K?

25.15a The Helmholtz model of the electric double layer is equivalent to a parallel plate capacitor. Hence the potential difference across the double layer is given by $\Delta\varphi = \sigma d/\varepsilon$, where d is the distance between the plates and σ is the surface charge density. Assuming that this model holds for concentrated salt solutions calculate the magnitude of the electric field at the surface of silica in 5.0 M NaCl(aq) if the surface charge density is 0.10 C m^{-2}.

25.15b Refer to the preceding exercise. Calculate the magnitude of the electric field at the surface of silica in 4.5 M NaCl(aq) if the surface charge density is 0.12 C m^{-2}.

25.16a The transfer coefficient of a certain electrode in contact with M^{3+} and M^{4+} in aqueous solution at 25°C is 0.39. The current density is found to be 55.0 mA cm^{-2} when the overvoltage is 125 mV. What is the overvoltage required for a current density of 75 mA cm^{-2}?

25.16b The transfer coefficient of a certain electrode in contact with M^{2+} and M^{3+} in aqueous solution at 25°C is 0.42. The current density is found to be 17.0 mA cm^{-2} when the overvoltage is 105 mV. What is the overvoltage required for a current density of 72 mA cm^{-2}?

25.17a Determine the exchange current density from the information given in Exercise 25.16a.

25.17b Determine the exchange current density from the information given in Exercise 25.16b.

25.18a To a first approximation, significant evolution or deposition occurs in electrolysis only if the overpotential exceeds about 0.6 V. To illustrate this criterion determine the effect that increasing the overpotential from 0.40 V to 0.60 V has on the current density in the electrolysis of 1.0 M NaOH(aq), which is 1.0 mA cm^{-2} at 0.4 V and 25°C. Take $\alpha = 0.5$.

25.18b Determine the effect that increasing the overpotential from 0.50 V to 0.60 V has on the current density in the electrolysis of 1.0 M NaOH(aq), which is 1.22 mA cm^{-2} at 0.50 V and 25°C. Take $\alpha = 0.50$.

25.19a Use the data in Table 25.6 for the exchange current density and transfer coefficient for the reaction $2\ H^+ + 2\ e^- \rightarrow H_2$ on nickel at 25°C to determine what current density would be needed to obtain an overpotential of 0.20 V as calculated from (a) the Butler–Volmer equation, and (b) the Tafel equation. Is the validity of the Tafel approximation affected at higher overpotentials (of 0.4 V and more)?

25.19b Use the data in Table 25.6 for the exchange current density and transfer coefficient for the reaction $Fe^{3+} + e^- \rightarrow Fe^{2+}$ on platinum at 25°C to determine what current density would be needed to obtain an overpotential of 0.30 V as calculated from (a) the Butler–Volmer equation, and (b) the Tafel equation. Is the validity of the Tafel approximation affected at higher overpotentials (of 0.4 V and more)?

25.20a Estimate the limiting current density at an electrode in which the concentration of Ag^+ ions is 2.5 mmol dm^{-3} at 25°C. The thickness of the Nernst diffusion layer is 0.40 mm. The ionic conductivity of Ag^+ at infinite dilution and 25°C is 6.19 mS $m^2\ mol^{-1}$.

25.20b Estimate the limiting current density at an electrode in which the concentration of Mg^{2+} ions is 1.5 mmol dm^{-3} at 25°C. The thickness of the Nernst diffusion layer is 0.32 mm. The ionic conductivity of Mg^{2+} at infinite dilution and 25°C is 10.60 mS $m^2\ mol^{-1}$.

25.21a A 0.10 M $CdSO_4$(aq) solution is electrolysed between a cadmium cathode and a platinum anode with a current density of 1.00 mA cm^{-2}. The hydrogen overpotential is 0.60 V. What will be the concentration of Cd^{2+} ions when evolution of H_2 just begins at the cathode? Assume all activity coefficients are unity.

25.21b A 0.10 M $FeSO_4$(aq) solution is electrolysed between a magnesium cathode and a platinum anode with a current density of 1.50 mA cm^{-2}. The hydrogen overpotential is 0.60 V. What will be the concentration of Fe^{2+} ions when evolution of H_2 just begins at the cathode? Assume all activity coefficients are unity.

25.22a A typical exchange current density, that for H^+ discharge at platinum, is 0.79 mA cm^{-2} at 25°C. What is the current density at an electrode when its overpotential is (a) 10 mV, (b) 100 mV, (c) −5.0 V? Take $\alpha = 0.5$.

25.22b The exchange current density for a $Pt|Fe^{3+},Fe^{2+}$ electrode is 2.5 mA cm^{-2}. The standard potential of the electrode is +0.77 V. Calculate the current flowing through an electrode of surface area 1.0 cm^2 as a function of the potential of the electrode. Take unit activity for both ions.

25.23a Suppose that the electrode potential is set at 1.00 V. The exchange current density is 6.0×10^{-4} A cm^{-2} and $\alpha = 0.50$. Calculate the current density for the ratio of activities $a(Fe^{3+})/a(Fe^{2+})$ in the range 0.1 to 10.0 and at 25°C.

25.23b Suppose that the electrode potential is set at 0.50 V. Calculate the current density for the ratio of activities $a(Cr^{3+})/a(Cr^{2+})$ in the range 0.1 to 10.0 and at 25°C.

25.24a What overpotential is needed to sustain a current of 20 mA at a $Pt|Fe^{3+},Fe^{2+}$ electrode in which both ions are at a mean activity $a = 0.10$? The surface area of the electrode is 1.0 cm^2.

25.24b What overpotential is needed to sustain a current of 15 mA at a $Pt|Ce^{4+},Ce^{3+}$ electrode in which both ions are at a mean activity $a = 0.010$?

25.25a How many electrons or protons are transported through the double layer in each second when the $Pt,H_2|H^+$, $Pt|Fe^{3+},Fe^{2+}$, and $Pb,H_2|H^+$ electrodes are at equilibrium at 25°C? Take the area as 1.0 cm^2 in each case. Estimate the number of times each second a single atom on the surface takes part in a electron transfer event, assuming an electrode atom occupies about $(280\ pm)^2$ of the surface.

25.25b How many electrons or protons are transported through the double layer in each second when the $Cu,H_2|H^+$ and $Pt|Ce^{4+},Ce^{3+}$ electrodes are at equilibrium at 25°C? Take the area as 1.0 cm^2 in each case. Estimate the number of times each second a single atom on the surface takes part in a electron transfer event, assuming an electrode atom occupies about $(260\ pm)^2$ of the surface.

25.26a What is the effective resistance at 25°C of an electrode interface when the overpotential is small? Evaluate it for 1.0 cm^2 (a) $Pt,H_2|H^+$, (b) $Hg,H_2|H^+$ electrodes.

25.26b Evaluate the effective resistance at 25°C of an electrode interface for 1.0 cm^2 (a) $Pb,H_2|H^+$, (b) $Pt|Fe^{2+},Fe^{3+}$ electrodes.

25.27a State what happens when a platinum electrode in an aqueous solution containing both Cu^{2+} and Zn^{2+} ions at unit activity is made the cathode of an electrolysis cell.

25.27b State what happens when a platinum electrode in an aqueous solution containing both Fe^{2+} and Ni^{2+} ions at unit activity is made the cathode of an electrolysis cell.

25.28a What are the conditions that allow a metal to be deposited from aqueous acidic solution before hydrogen evolution occurs significantly at 293 K? Why may silver be deposited from aqueous silver nitrate?

25.28b The overpotential for hydrogen evolution on cadmium is about 1 V at current densities of 1 mA cm^{-2}. Why may cadmium be deposited from aqueous cadmium sulfate?

25.29a The exchange current density for H^+ discharge at zinc is about 50 pA cm^{-2}. Can zinc be deposited from a unit activity aqueous solution of a zinc salt?

25.29b The standard potential of the $Zn^{2+}|Zn$ electrode is –0.76 V at 25°C. The exchange current density for H^+ discharge at platinum is 0.79 mA cm^{-2}. Can zinc be plated on to platinum at that temperature? (Take unit activities.)

25.30a Can magnesium be deposited on a zinc electrode from a unit activity acid solution at 25°C?

25.30b Can iron be deposited on a copper electrode from a unit activity acid solution at 25°C?

25.31a Calculate the maximum (zero-current) potential difference of a nickel–cadmium cell, and the maximum possible power output when 100 mA is drawn at 25°C.

25.31b Calculate the maximum (zero-current) potential difference of a lead–acid cell, and the maximum possible power output when 100 mA is drawn at 25°C.

25.32a The corrosion current density j_{corr} at an iron anode is 1.0 A m^{-2}. What is the corrosion rate in millimetres per year? Assume uniform corrosion.

25.32b The corrosion current density j_{corr} at a zinc anode is 2.0 A m^{-2}. What is the corrosion rate in millimetres per year? Assume uniform corrosion.

Problems*

Numerical problems

25.1 The movement of atoms and ions on a surface depends on their ability to leave one position and stick to another, and therefore on the energy changes that occur. As an illustration, consider a two-dimensional square lattice of univalent positive and negative ions separated by 200 pm, and consider a cation on the upper terrace of this array. Calculate, by direct summation, its Coulombic interaction when it is in an empty lattice point directly above an anion. Now consider a high step in the same lattice, and let the cation move into the corner formed by the step and the terrace. Calculate the Coulombic energy for this position, and decide on the likely settling point for the cation.

25.2 In a study of the catalytic properties of a titanium surface it was necessary to maintain the surface free from contamination. Calculate the collision frequency per square centimetre of surface made by O_2 molecules at (a) 100 kPa, (b) 1.00 Pa and 300 K. Estimate the number of collisions made with a single surface atom in each second. The conclusions underline the importance of working at very low pressures (much lower than 1 Pa, in fact) in order to study the properties of uncontaminated surfaces. Take the nearest-neighbour distance as 291 pm.

25.3 Nickel is face-centred cubic with a unit cell of side 352 pm. What is the number of atoms per square centimetre exposed on a surface formed by (a) (100), (b) (110), (c) (111) planes? Calculate the frequency of molecular collisions per surface atom in a vessel containing (a) hydrogen, (b) propane at 25°C when the pressure is (i) 100 Pa, (ii) 0.10 μTorr.

25.4 The data below are for the chemisorption of hydrogen on copper powder at 25°C. Confirm that they fit the Langmuir isotherm at low coverages. Then find the value of K for the adsorption equilibrium and the adsorption volume corresponding to complete coverage.

p/Pa	25	129	253	540	1000	1593
V/cm^3	0.042	0.163	0.221	0.321	0.411	0.471

25.5 The data for the adsorption of ammonia on barium fluoride are reported below. Confirm that they fit a BET isotherm and find values of c and V_{mon}.

(a) $\theta = 0$°C, $p^* = 429.6$ kPa:

p/kPa	14.0	37.6	65.6	79.2	82.7	100.7	106.4
V/cm^3	11.1	13.5	14.9	16.0	15.5	17.3	16.5

(b) $\theta = 18.6$°C, $p^* = 819.7$ kPa:

p/kPa	5.3	8.4	14.4	29.2	62.1	74.0	80.1	102.0
V/cm^3	9.2	9.8	10.3	11.3	12.9	13.1	13.4	14.1

25.6 The following data have been obtained for the adsorption of H_2 on the surface of 1.00 g of copper at 0°C. The volume of H_2 below is the volume that the gas would occupy at STP (0°C and 1 atm).

p/atm	0.050	0.100	0.150	0.200	0.250
V/cm^3	1.22	1.33	1.31	1.36	1.40

Determine the volume of H_2 necessary to form a monolayer and estimate the surface area of the copper sample. The density of liquid hydrogen is 0.708 g cm^{-3}.

25.7 The adsorption of solutes on solids from liquids often follows a Freundlich isotherm. Check the applicability of this isotherm to the following data for the adsorption of acetic acid on charcoal at 25°C and find the values of the parameters c_1 and c_2.

[acid]/(mol dm^{-3})	0.05	0.10	0.50	1.0	1.5
w_a/g	0.04	0.06	0.12	0.16	0.19

w_a is the mass adsorbed per unit mass of charcoal.

25.8 In some catalytic reactions the products may adsorb more strongly than the reacting gas. This is the case, for instance, in the catalytic decomposition of ammonia on platinum at 1000°C. As a first step in examining the kinetics of

* Problems denoted with the symbol ‡ were supplied by Charles Trapp, Carmen Giunta, and Marshall Cady.

this type of process, show that the rate of ammonia decomposition should follow

$$\frac{dp_{NH_3}}{dt} = -k_c \frac{p_{NH_3}}{p_{H_2}}$$

in the limit of very strong adsorption of hydrogen. Start by showing that, when a gas J adsorbs very strongly, and its pressure is p_J, the fraction of uncovered sites is approximately $1/Kp_J$. Solve the rate equation for the catalytic decomposition of NH_3 on platinum and show that a plot of $F(t) = (1/t)\ln(p/p_0)$ against $G(t) = (p - p_0)/t$, where p is the pressure of ammonia, should give a straight line from which k_c can be determined. Check the rate law on the basis of the data below, and find k_c for the reaction.

t/s	0	30	60	100	160	200	250
p/kPa	13.3	11.7	11.2	10.7	10.3	9.9	9.6

25.9‡ A. Akgerman and M. Zardkoohi (*J. Chem. Eng. Data* **41**, 185 (1996)) examined the adsorption of phenol from aqueous solution on to fly ash at 20°C. They fitted their observations to a Freundlich isotherm of the form $c_{ads} = Kc_{sol}^{1/n}$, where c_{ads} is the concentration of adsorbed phenol and c_{sol} is the concentration of aqueous phenol. Among the data reported are the following:

c_{sol}/(mg g^{-1})	8.26	15.65	25.43	31.74	40.00
c_{ads}/(mg g^{-1})	4.4	19.2	35.2	52.0	67.2

Determine the constants K and n. What further information would be necessary in order to express the data in terms of fractional coverage, θ?

25.10‡ C. Huang and W.P. Cheng (*J. Colloid Interface Sci.* **188**, 270 (1997)) examined the adsorption of the hexacyanoferrate(III) ion, $[Fe(CN)_6]^{3-}$, on γ-Al_2O_3 from aqueous solution. They modelled the adsorption with a modified Langmuir isotherm, obtaining the following values of K at pH = 6.5:

T/K	283	298	308	318
$10^{-11}K$	2.642	2.078	1.286	1.085

Determine the isosteric enthalpy of adsorption, $\Delta_{ads}H^\ominus$, at this pH. The researchers also reported $\Delta_{ads}S^\ominus = +146$ J mol^{-1} K^{-1} under these conditions. Determine $\Delta_{ads}G^\ominus$.

25.11‡ M.-G. Olivier and R. Jadot (*J. Chem. Eng. Data* **42**, 230 (1997)) studied the adsorption of butane on silica gel. They report the following amounts of absorption (in moles per kilogram of silica gel) at 303 K:

p/kPa	31.00	38.22	53.03	76.38	101.97
n/(mol kg^{-1})	1.00	1.17	1.54	2.04	2.49
p/kPa	130.47	165.06	182.41	205.75	219.91
n/(mol kg^{-1})	2.90	3.22	3.30	3.35	3.36

Fit these data to a Langmuir isotherm, and determine the value of n that corresponds to complete coverage and the constant K.

25.12‡ The following data were obtained for the extent of adsorption, s, of acetone on charcoal from an aqueous solution of molar concentration, c, at 18°C.

c/(mmol dm^{-3})	15.0	23.0	42.0	84.0	165	390	800
s/(mmol acetone/g charcoal)	0.60	0.75	1.05	1.50	2.15	3.50	5.10

Which isotherm fits this data best, Langmuir, Freundlich, or Temkin?

25.13 In an experiment on the $Pt|H_2|H^+$ electrode in dilute H_2SO_4 the following current densities were observed at 25°C. Evaluate α and j_0 for the electrode.

η/mV	50	100	150	200	250
j/(mA cm^{-2})	2.66	8.91	29.9	100	335

How would the current density at this electrode depend on the overpotential of the same set of magnitudes but of opposite sign?

25.14 The standard potentials of lead and tin are −126 mV and −136 mV respectively at 25°C, and the overvoltage for their deposition are close to zero. What should their relative activities be in order to ensure simultaneous deposition from a mixture?

25.15 The limiting current density for the reaction $I_3^- + 2\,e^- \rightarrow 3\,I^-$ at a platinum electrode is 28.9 μA cm^{-2} when the concentration of KI is 6.6×10^{-4} mol dm^{-3} and the temperature 25°C. The diffusion coefficient of I_3^- is 1.14×10^{-9} m^2 s^{-3}. What is the thickness of the diffusion layer?

25.16 Estimating the power output and potential of a cell under operating conditions is very difficult, but eqn 25.65 summarizes, in an approximate way, some of the parameters involved. As a first step in manipulating this expression, identify all the quantities that depend on the ionic concentrations. Express E in terms of the concentration and conductivities of the ions present in the cell. Estimate the parameters for $Zn(s)|ZnSO_4(aq)||CuSO_4(aq)|Cu(s)$. Take electrodes of area 5 cm^2 separated by 5 cm. Ignore both potential differences and resistance of the liquid junction. Take the concentration as 1 mol dm^{-3}, the temperature 25°C, and neglect activity coefficients. Plot E as a function of the current drawn. On the same graph, plot the power output of the cell. What current corresponds to maximum power?

25.17 Consider a cell in which the current is activation-controlled. Show that the current for maximum power can be estimated by plotting $\log(I/I_0)$ and $c_1 - c_2 I$ against I (where $I_0 = A^2 j_0 j_0'$ and c_1 and c_2 are constants), and looking for the point of intersection of the curves. Carry through this analysis for the cell in Problem 25.16 ignoring all concentration overpotentials.

25.18‡ The rate of deposition of iron, v, on the surface of an iron electrode from an aqueous solution of Fe^{2+} has been studied as a function of potential, E, relative to the standard hydrogen electrode, by J. Kanya (*J. Electroanal. Chem.* **84**, 83 (1977)). The values in the table below are based on the data obtained with an electrode of surface area 9.1 cm^2 in contact with a solution of concentration 1.70 μmol dm^{-3} in Fe^{2+}. (a) Assuming unit activity coefficients, calculate the zero current potential of the Fe^{2+}/Fe cathode and the overpotential at each value of the working potential. (b) Calculate the cathodic current density, j_c, from the rate of deposition of Fe^{2+} for each value of E. (c) Examine the extent to which the data fit the Tafel equation and calculate the exchange current density.

v/(pmol s^{-1})	1.47	2.18	3.11	7.26
$-E$/mV	702	727	752	812

25.19‡ The thickness of the diffuse double layer according to the Gouy–Chapman model is given by eqn 19.46. Use this equation to calculate and plot the thickness as a function of concentration and electrolyte type at 25°C. For examples, choose aqueous solutions of NaCl and Na_2SO_4 ranging in concentration from 0.1 to 100 mmol dm^{-3}.

25.20‡ V.V. Losev and A.P. Pchel'nikov (*Soviet Electrochem.* **6**, 34 (1970)) obtained the following current–voltage data for an indium anode relative to a standard hydrogen electrode at 293 K:

$-E$/V	0.388	0.365	0.350	0.335
j/(A m^{-2})	0	0.590	1.438	3.507

Use these data to calculate the transfer coefficient and the exchange current density. What is the cathodic current density when the potential is 0.365 V?

25.21‡ The redox reactions of quinones have been the subject of many studies over the years and they continue to be of interest to electrochemists. In a study of methone (1,1-dimethyl-3,5-cyclohexanedione) by E. Kariv, J. Hermolin, and E. Gileadi (*Electrochim. Acta* **16**, 1437 (1971)), the following current–voltage data were obtained for the reduction of the quinone in anhydrous butanol on a mercury electrode:

$-E$/V	1.50	1.58	1.63	1.72	1.87	1.98	≥2.10
j/(A m^{-2})	10	30	50	100	200	250	290

(a) How well do these data fit the empirical Tafel equation? (b) The authors postulate that the reduction product is the dimer HMMH formed by the following mechanism (where the quinone is denoted M):

(1) $M(sol) \rightleftharpoons M(ads)$

(2) $M(ads) + H^+ + e^- \rightarrow MH(ads)$

(3) $MH(ads) + MH(ads) \rightleftharpoons HMMH$

The affixes sol and ads refer to species in solution and on the surface of the electrode, respectively. Does this mechanism help to explain the current–voltage data?

25.22‡ An early study of the hydrogen overpotential is that of H. Bowden and T. Rideal (*Proc. Roy. Soc.* **A120**, 59 (1928)), who measured the overpotential for H_2 evolution with a mercury electrode in dilute aqueous solutions of H_2SO_4 at 25°C. Determine the exchange current density and transfer coefficient, α, from their data:

$j/(\text{mA m}^{-2})$	2.9	6.3	28	100	250	630	1650	3300
η/V	0.60	0.65	0.73	0.79	0.84	0.89	0.93	0.96

Explain any deviations from the result expected from the Tafel equation.

Theoretical problems

25.23 Although the attractive van der Waals interaction between individual molecules varies as R^{-6}, the interaction of a molecule with a nearby solid (a homogeneous collection of molecules) varies as R^{-3}, where R is its vertical distance above the surface. Confirm this assertion. Calculate the interaction energy between an Ar atom and the surface of solid argon on the basis of a Lennard-Jones (6,12)-potential. Estimate the equilibrium distance of an atom above the surface.

25.24 Use the Gibbs adsorption isotherm (another name for eqn 19.50), to show that the volume adsorbed per unit area of solid, V_a/σ, is related to the pressure of the gas by $V_a = -(\sigma/RT)(\mathrm{d}\mu/\mathrm{d}\ln p)$, where μ is the chemical potential of the adsorbed gas.

25.25 If the dependence of the chemical potential of the gas on the extent of surface coverage is known, the Gibbs adsorption isotherm, eqn 19.50, can be integrated to give a relation between V_a and p, as in a normal adsorption isotherm. For instance, suppose that the change in the chemical potential of a gas when it adsorbs is of the form $\mathrm{d}\mu = -c_2(RT/\sigma)\mathrm{d}V_a$, where c_2 is a constant of proportionality: show that the Gibbs isotherm leads to the Freundlich isotherm in this case.

25.26 Finally we come full circle and return to the Langmuir isotherm. Find the form of $\mathrm{d}\mu$ that, when inserted in the Gibbs adsorption isotherm, leads to the Langmuir isotherm.

25.27 Show that, for the association part of the surface plasmon resonance experiment in Fig. 25.27, $R(t) = R_{eq}(1 - e^{-k_{obs}t})$ and write an expression for k_{obs}. Then, derive an expression for $R(t)$ that applies to the dissociation part of the surface plasmon resonance experiment in Fig. 25.27.

25.28 If $\alpha = \frac{1}{2}$, an electrode interface is unable to rectify alternating current because the current density curve is symmetrical about $\eta = 0$. When $\alpha \neq \frac{1}{2}$, the magnitude of the current density depends on the sign of the overpotential, and so some degree of 'faradaic rectification' may be obtained. Suppose that the overpotential varies as $\eta = \eta_0 \cos \omega t$. Derive an expression for the mean flow of current (averaged over a cycle) for general α, and confirm that the mean current is zero when $\alpha = \frac{1}{2}$. In each case work in the limit of small η_0 but to second order in $\eta_0 F/RT$. Calculate the mean direct current at 25°C for a 1.0 cm^2 hydrogen–platinum electrode with $\alpha = 0.38$ when the overpotential varies between ±10 mV at 50 Hz.

25.29 Now suppose that the overpotential is in the high overpotential region at all times even though it is oscillating. What waveform will the current across the interface show if it varies linearly and periodically (as a sawtooth waveform) between η_- and η_+ around η_0? Take $\alpha = \frac{1}{2}$.

25.30 Derive an expression for the current density at an electrode where the rate process is diffusion-controlled and η_c is known. Sketch the form of j/j_L as a function of η_c. What changes occur if anion currents are involved?

Applications: to chemical engineering and environmental science

25.31 The designers of a new industrial plant wanted to use a catalyst code-named CR-1 in a step involving the fluorination of butadiene. As a first step in the investigation they determined the form of the adsorption isotherm. The volume of butadiene adsorbed per gram of CR-1 at 15°C varied with pressure as given below. Is the Langmuir isotherm suitable at this pressure?

p/kPa	13.3	26.7	40.0	53.3	66.7	80.0
V/cm^3	17.9	33.0	47.0	60.8	75.3	91.3

Investigate whether the BET isotherm gives a better description of the adsorption of butadiene on CR-1. At 15°C, $p^\star$(butadiene) = 200 kPa. Find V_{mon} and c.

25.32‡ In a study relevant to automobile catalytic converters, C.E. Wartnaby, A. Stuck, Y.Y. Yeo, and D.A. King (*J. Phys. Chem.* **100**, 12483 (1996)) measured the enthalpy of adsorption of CO, NO, and O_2 on initially clean platinum 110 surfaces. They report $\Delta_{ads}H^\ominus$ for NO to be −160 kJ mol^{-1}. How much more strongly adsorbed is NO at 500°C than at 400°C?

25.33‡ The removal or recovery of volatile organic compounds (VOCs) from exhaust gas streams is an important process in environmental engineering. Activated carbon has long been used as an adsorbent in this process, but the presence of moisture in the stream reduces its effectiveness. M.-S. Chou and J.-H. Chiou (*J. Envir. Engrg.* ASCE, **123**, 437(1997)) have studied the effect of moisture content on the adsorption capacities of granular activated carbon (GAC) for normal hexane and cyclohexane in air streams. From their data for dry streams containing cyclohexane, shown in the table below, they conclude that GAC obeys a Langmuir type model in which $q_{VOC,RH=0} = abc_{VOC}/(1 + bc_{VOC})$, where $q = m_{VOC}/m_{GAC}$, RH denotes relative humidity, a the maximum adsorption capacity, b is an affinity parameter, and c is the abundance in parts per million (ppm). The following table gives values of $q_{VOC,RH=0}$ for cyclohexane:

c/ppm	33.6°C	41.5°C	57.4°C	76.4°C	99°C
200	0.080	0.069	0.052	0.042	0.027
500	0.093	0.083	0.072	0.056	0.042
1000	0.101	0.088	0.076	0.063	0.045
2000	0.105	0.092	0.083	0.068	0.052
3000	0.112	0.102	0.087	0.072	0.058

(a) By linear regression of $1/q_{VOC,\,RH=0}$ against $1/c_{VOC}$, test the goodness of fit and determine values of a and b. (b) The parameters a and b can be related to $\Delta_{ads}H$, the enthalpy of adsorption, and $\Delta_b H$, the difference in activation energy for adsorption and desorption of the VOC molecules, through Arrhenius type equations of the form $a = k_a \exp(-\Delta_{ads}H/RT)$ and $b = k_b \exp(-\Delta_b H/RT)$. Test the goodness of fit of the data to these equations and obtain values for k_a, k_b, $\Delta_{ads}H$, and $\Delta_b H$. (c) What interpretation might you give to k_a and k_b?

25.34‡ M.-S. Chou and J.-H. Chiou (*J. Envir. Engrg.*, ASCE, **123**, 437(1997)) have studied the effect of moisture content on the adsorption capacities of granular activated carbon (GAC, Norit PK 1–3) for the volatile organic compounds (VOCs) normal hexane and cyclohexane in air streams. The following table shows the adsorption capacities ($q_{water} = m_{water}/m_{GAC}$) of GAC for pure water from moist air streams as a function of relative humidity (RH) in the absence of VOCs at 41.5°C.

RH	0.00	0.26	0.49	0.57	0.80	1.00
q_{water}	0.00	0.026	0.072	0.091	0.161	0.229

The authors conclude that the data at this and other temperatures obey a Freundlich type isotherm, $q_{water} = k(RH)^{1/n}$. (a) Test this hypothesis for their data at 41.5°C and determine the constants k and n. (b) Why might VOCs obey the Langmuir model, but water the Freundlich model? (c) When both water vapour and cyclohexane were present in the stream the values given in the table below were determined for the ratio $r_{VOC} = q_{VOC}/q_{VOC,\,RH=0}$ at 41.5°C.

RH	0.00	0.10	0.25	0.40	0.53	0.76	0.81
r_{VOC}	1.00	0.98	0.91	0.84	0.79	0.67	0.61

The authors propose that these data fit the equation $r_{VOC} = 1 - q_{water}$. Test their proposal and determine values for k and n and compare to those obtained in part (b) for pure water. Suggest reasons for any differences.

25.35‡ The release of petroleum products by leaky underground storage tanks is a serious threat to clean ground water. BTEX compounds (benzene, toluene, ethylbenzene, and xylenes) are of primary concern due to their ability to cause health problems at low concentrations. D.S. Kershaw, B.C. Kulik, and S. Pamukcu (*J. Geotech. & Geoenvir. Engrg.* **123**, 324(1997)) have studied the ability of ground tyre rubber to sorb (adsorb and absorb) benzene and *o*-xylene. Though sorption involves more than surface interactions, sorption data are usually found to fit one of the adsorption isotherms. In this study, the authors have tested how well their data fit the linear ($q = Kc_{eq}$), Freundlich ($q = K_F c_{eq}^{1/n}$), and Langmuir ($q = K_L M c_{eq}/(1 + K_L c_{eq})$ type isotherms, where q is the mass of solvent sorbed per gram of ground rubber (in milligrams per gram), the Ks and M are empirical constants, and c_{eq} the equilibrium concentration of contaminant in solution (in milligrams per litre). (a) Determine the units of the empirical constants. (b) Determine which of the isotherms best fits the data in the table below for the sorption of benzene on ground rubber.

$c_{eq}/(\text{mg dm}^{-3})$	97.10	36.10	10.40	6.51	6.21	2.48
$q/(\text{mg g}^{-1})$	7.13	4.60	1.80	1.10	0.55	0.31

(c) Compare the sorption efficiency of ground rubber to that of granulated activated charcoal, which for benzene has been shown to obey the Freundlich isotherm in the form $q = 1.0c_{eq}^{1.6}$ with coefficient of determination $R^2 = 0.94$.

25.36 Calculate the thermodynamic limit to the zero-current potential of fuel cells operating on (a) hydrogen and oxygen, (b) methane and air, and (c) propane and air. Use the Gibbs energy information in the *Data section*, and take the species to be in their standard states at 25°C.

25.37 For each group below, determine which metal has a thermodynamic tendency to corrode in moist air at pH = 7. Take as a criterion of corrosion a metal ion concentration of at least 10^{-6} mol dm^{-3}.

(a) Fe, Cu, Pb, Al, Ag, Cr, Co

(b) Ni, Cd, Mg, Ti, Mn

25.38 Estimate the magnitude of the corrosion current for a patch of zinc of area 0.25 cm^2 in contact with a similar area of iron in an aqueous environment at 25°C. Take the exchange current densities as 1 μA cm^{-2} and the local ion concentrations as 1 μmol dm^{-3}.

25.39 The corrosion potential of iron immersed in a de-aerated acidic solution of pH = 3 is −0.720 V as measured at 25°C relative to the standard calomel electrode with potential 0.2802 V. A Tafel plot of cathodic current density against overpotential yields a slope of 18 V^{-1} and the hydrogen ion exchange current density $j_0 = 0.10$ μA cm^{-2}. Calculate the corrosion rate in milligrams of iron per square centimetre per day (mg cm^{-2} d^{-1}).